ELUCIDATION OF THE COBALT DETOXIFICATION MECHANISMS OF *GEOBACTER SULFURREDUCENS*

By

Michael Hunter Dulay

A DISSERTATION

Submitted to
Michigan State University
in partial fulfillment of the requirements
for the degree of

Microbiology and Molecular Genetics – Doctor of Philosophy

2023

ABSTRACT

The hallmark of the physiology of *Geobacter* bacteria is their ability to couple their oxidative metabolism to the respiration of a broad spectrum of metals, including Fe^{III} and Mn^{IV} oxide minerals. In nature, these metal oxides often coprecipitate with or adsorb various metal species such as the micronutrient Co. During the reductive dissolution of these metals by *Geobacter* cells, the divalent form of Co (Co^{II}) may be released into the environment. While most organisms require Co^{II} in the form of cobamide vitamins, the metal is toxic and is expected to exert a selective pressure on *Geobacter* and syntrophic partners to detoxify their local environment in order to remain viable and metabolically active. In this dissertation, I investigated the mechanisms that allow the model representative *Geobacter sulfurreducens* to tolerate Co^{II} exposure and the role that its complex respiratory chains have in the reductive detoxification of the metal.

Consistent with adaptation through regular exposure to Co^{II}, *G. sulfurreducens* expresses a complex network of detoxification pathways to mitigate metal intoxication. In chapter 2, I demonstrate that this transcriptional response enables *G. sulfurreducens* to survive Co^{II} concentrations typically used to enrich metal-resistant microorganisms. Among the most highly differentially expressed genes were cell envelope *c*-type cytochromes (CbcBA) that are involved in the reduction of low-potential electron acceptors. In concert with this, metal-stressed cells removed 25 μM of Co^{II} from culture supernatants and accumulated Co nanoparticles on the cell surface, suggesting that extracellular mineralization plays a role in the detoxification response.

In chapter 3, I investigated the role of CbcBA in Co^{II} detoxification using a mutant carrying a deletion in the *cbcBA* genes and a genetically complemented strain. CbcBA

was found to support acclimation of cells to Co^{II} stress, but compensatory effects were often observed that minimized the impact of the cytochrome defect in metal detoxification. Loss of the cytochrome pathway stimulated vesiculation, a phenotype associated with increased membrane fluidity and permeability. As a result, Co^{II} permeated into resting cells lacking the cytochrome pathway, impairing their growth recovery in fresh media. Hence, the CbcBA cytochrome pathway is part of a complex cellular response that contributes to Co^{II} detoxification in *G. sulfurreducens*. In addition, I describe the optimization of the resting cell assay in the appendix of this dissertation and demonstrate the need for careful formulation of buffers involved in metal reduction and tolerance studies.

Alternative to the numerous cytochromes for the extracellular reduction of metals, *G. sulfurreducens* also assembles conductive pili decorated with metal traps that can bind Co^{II} and reduce it to Co^{0} nanoparticles. In chapter 4, I investigated a biological role for the pili in Co^{II} detoxification via the extracellular reduction and precipitation of the metal. The study showed that cells that dynamically extend and retract their pili have a growth advantage in the presence of Co^{II} which may be related to accumulation of metal nanoparticles along the filaments. These results indicate that the conductive pili play a major role in the mineralization of Co^{II} and that this reaction is critical to avoid metal intoxication.

The last chapter summarizes the major conclusions of this work and describes future research directions that can expand our understanding of the adaptive responses used by *Geobacter* bacteria to respire metals as a cellular protective mechanism. The ecological impacts of these reactions and applications in biotechnology are discussed.

This dissertation is dedicated to my family, old and new.

ACKNOWLEDGEMENTS

I would first like to thank my two advisors, Dr. Gemma Reguera and Dr. Kaz Kashefi. I came to MSU with interest in your work as scientists but quickly found that your mentorship and friendship were equally as valuable. You have supported me through learning moments and victories alike and have been integral in developing my presentation and thinking skills. The wisdom you shared in the lab and the classroom will always stick with me. I have grown a lot since first arriving here and this development would not have been possible without your support. I hope to make you both proud as I journey out in pursuit of leading my own research.

I would also like to thank my lab mates who have helped make the lab feel like a home. Marcela Tabares trained me in the difficult ways of culturing *Geobacter* and worked with me on the first few cobalt growth curves during my rotation. Our coauthored paper became the backbone of my dissertation and without her expertise with RNA Seq, I would have been at a loss. I want to thank the third member of Team Geo, Morgen Clark, who trained me on the AFM and always been a source of good conversations about philosophy and how we do science. I've deeply appreciated our conversations about data analysis, metals and microbiology, fantasy books, and the next national park we want to go to. The lab always felt special when all three of us were there, and dancing and singing were never far away. I would also like to thank Dr. Kristin Jacob who was a mentor since my first day of interviews. Thank you for supporting my coffee drinking habits and for helping me sort out the stresses of pursuing a PhD. I would also like to thank our most recent lab member, Dr. Emily Greeson. You are truly a force of nature, both in the realm of running a research project and in making sure your family and friends are cared for.

I would like to thank my support at the microscope. The staff at the Center for Advanced Microscopy were instrumental in my training with an electron microscope. Thank you, Dr. Alicia Withrow for teaching me the in's and out's of the TEM. It was a joy working closely and learning from you. Thank you to the late Dr. Xudong Fan for your guidance in performing EDS analysis. And thank you to Dr. Reza Loloee for your support with the AFM, even when the AFM tried its best to halt our progress.

I must also thank my family who inspired me to pursue my love of science and learning and gave me the necessary background to make it through my PhD training. To my mom and dad, JoLynn Larsen and Michael Dulay, it was your encouragement of my potential that got me to where I am today. You showered me with love and support through difficult times in my youth and always reinforced that I could grow and become more. There was no goal too lofty or path too arduous for me in your eyes and I doubt I could have made it through my PhD training without the belief in myself that you fostered in me. To my brother Tanner Dulay, you have been my partner in all things imagination and mischief. You inspire me with your effort and passion, and I hope to collaborate in our shared love of science. To my brother Griffen Dulay and sister Peyton Dulay, it has been a joy to watch you grow up and learn about the world. Your insight on life has taught me to always take a fresh look at what I take for granted. To my grandmother, Carolyn Dulay, you were the rain and sunshine that began my growth as a scientist. You encouraged my early fascination with the world and went above and beyond as a grandparent and mentor. It was trips behind the scenes at the San Francisco Zoo to feed, watch, and care for the animals that instilled in me a sense of awe for the natural world.

Together, the Flying Dulays have been a source of love, encouragement, and joy that I will be forever grateful for. I could not have asked for a more amazing family.

It goes without saying that my success was deeply supported by my partner, Dr. Emily Gibson. Since meeting you in my first year of graduate school, we have grown together and made it through good times and bad. No matter the challenges we face, we are a team, a married couple, and always friends. Your excitement about the world is inspirational. You are gentle and empathetic in the face of strife, and righteous and passionate in the face of adversity. It was your personal care during long weeks of endless experiments that kept me energized and rested. It was your hugs and peptalks during bitter learning moments that kept me optimistic and bright. I am lucky, so lucky, to have found you in this world.

TABLE OF CONTENTS

Chapter 1: The Biogeochemistry of Cobalt

BIOLOGY AND THE REQUIREMENT FOR METALS AND METALLOENZYMES

Since the time of the last universal common ancestor, cells have used metals as catalytic centers for enzymatic activity. The metals predicted to be present in the early-Earth environment, such as Fe and Ni, could abiotically catalyze reactions such as H_2-oxidation coupled to C-fixation [1-3] and N_2-reduction [4,5]. Incorporation of these metal catalysts as prosthetic groups in enzymes allowed for a more controlled, efficient, and diverse set of biotic reactions to occur [6,7]. Indeed, geologically occurring Fe-S minerals and Fe-S catalytic centers of some metalloenzymes are highly similar in structure and facilitate critical activities for life [3,8,9]. This parallelism has led some to suggest that early cells took up free metals prior to the development of sophisticated chaperone pathways in order perform these reactions away from mineral surfaces [6,9]. Due to their ubiquity in biology, the distribution of various metals through geologic time is of key interest in understanding extant life and how it evolved to use specific metals as catalytic centers [10].

Transition metals such as Fe and Mn [11-13], Ni and Co [14-17], Mo [18,19], Cu [20,21], Mg [22], Zn [23] and V [24] are all part of prosthetic groups in metalloenzymes that drive many biological reactions [25]. All of these metals, with the exception of Zn, have a broad range of redox states that allow for the stabilization of the transition state of enzymatic reactions by either receiving or donating electrons with a substrate [25]. While many metal cofactors have similar properties and catalytic activities [10] there is variation in the biological requirements for specific metals between different organisms [16,26]. However, the essentiality of metal cofactors is clear as nearly half of all identified proteins to-date require at least one metal for proper functionality [27].

Cofactor selection by the metalloenzyme can be both highly selective and promiscuous. Briefly, specificity between a metal-binding site and the prosthetic group is driven by the electrochemical properties of the metal, such as its coordination geometry, charge radius, and position along the Irving-Williams series (binding affinities follow a trend of $Mn^{II} < Fe^{II} < Co^{II} < Ni^{II} < Cu^{II} > Zn^{II}$) [28]. But it can also be influenced by the chemical properties of the binding site, such as the flexibility of the ligand and the presence of specific amino acids or other biomolecules [29]. Greater thermodynamic specificity can be introduced through various metallochaperones, alterations to the metalloenzyme and modulation of the availability of metals to the metal-binding site [29]. And yet, many native metalloproteins bind more than one metal [30]. Replacement of the native metal with an alternative element can lead to changes in substrate specificity [31], rates of activity [32], and even the type of chemical reaction catalyzed by the enzyme [33].

Of all the metals within metalloenzymes, Mg is the most commonly used (16%), followed by Zn (9%), Fe (8%), Mn (6%), Ca (2%), Co (1%), Cu (1%) and V, Mo, W, Na, Ni, and K (all falling below 1%) [27]. Interestingly, the use of Cd as a cofactor has been reported in a single enzyme and suggests that nutrient limitations in various environments may drive the development of novel metal-enzyme interactions [34,35]. Collectively, all of these metals participate in reactions of the enzyme classes EC1 oxidoreductases, EC2 transferases, EC3 hydrolases, EC4 lyases, EC5 isomerases, and EC6 ligases [27]. While metalloenzymes often coordinate metal ions through sidechain interactions at the catalytic center, many metals assemble into large cofactors to which the metalloenzyme binds. Among the most common of these cofactors are those derived from bulky porphyrin rings including Fe-containing heme (~616 Da) and siroheme (~916 Da), Co-containing

cobamides (~1202-1578 Da), Mg-containing chlorophyll (~894-911 Da), and Ni-containing coenzyme F430 (~902 Da) [36-40].

THE COBAMIDE PROSTHETIC GROUP

While organisms can alter the structure of many prosthetic groups, selection for cobamide catalytic centers is highly dependent on structure and tightly regulated during biosynthesis and its secretion to support syntrophic partnerships [16,41-43]. The first steps in cobamide synthesis, which are shared with the pathways for the synthesis of other porphyrin rings, involve the conversion of two molecules of 5-aminolevulinate into one porphobilinogen by HemB (EC 4.2.1.24), the polymerization of four molecules of porphobilinogen into the ring-like hydroxymethylbilane by HemC (EC 2.5.1.61) and the closure of the ring by HemD (EC 4.2.1.75) to produce uroporphyrinogen III. This tetrapyrrole precursor is then split off the biosynthetic path of other porphyrins and converted into precorrin-2 by CysG/CobA (EC2.1.1.130). Precorrin-2 can then enter a multi-step process of corrin ring biosynthesis, for which an aerobic (CobIGJMFKLHBNST) and anaerobic (CbiKXLHFGDJTECA) pathway exists (Fig. 1.1). A key difference in these pathways is the chelation of the Co ion at the beginning of the anaerobic pathway (CbiK/CbiX, EC 4.99.1.3) as opposed to the end of the aerobic pathway (CobNST, EC 6.6.1.2). The insertion of the Co ion early in anaerobic biosynthesis assists in subsequent steps to contract the precorrin ring through oxidoreductase activities in the absence of O_2 [38]. The two pathways converge at cob(II)yrinic acid diamide which goes through adenosylation by BtuR/CobA/CobO (EC 2.5.1.17) and subsequent nucleotide loop assembly to produce a complete cobamide.

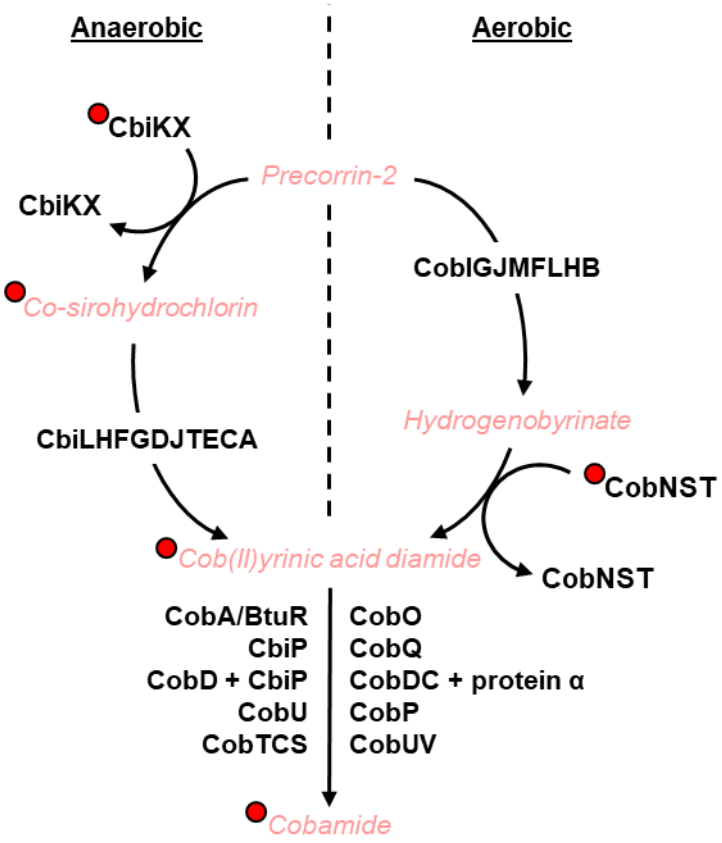

Figure 1.1 Abbreviated pathways for cobamide synthesis. Proteins (bold) involved in the anaerobic (left) and aerobic (right) contraction of the porphyrin ring are presented alongside key intermediate molecules (pink). Proteins involved in the final steps of cobamide synthesis follow below cob(II)yrinic acid diamide. Insertion of the Co ion is marked with a red circle.

A separate biosynthetic pathway is responsible for producing the lower ligand that attaches to the nucleotide loop. The identity of the ligand varies broadly and alters the accessibility of the cobamide to different organisms [16,41,42,44]. Indeed, many organisms specialize in using one type of cobamide over another and very few are able to alter the lower ligand once attached [16,43]. For example, coculture studies measuring the dechlorination activity of *Dehalococcoides mccartyi* found that cobamides with 5',6'-dimethylbenzimidazole, which are produced by *Geobacter lovleyi*, supported the growth of *D. mccartyi* via dechlorination [42]. By contrast, cobamides containing 5-

hydroxybenzimidazole, which are produced by *Geobacter sulfurreducens*, did not [42]. However, studies of *D. mccartyi* grown with cobamides alongside exogenous 5',6'-dimethylbenzimidazole revealed that these cells can remodel the prosthetic groups to contain the desired lower ligand, rescuing growth and dechlorination activity [45].

To this date, 15 cobamide-dependent functions have been identified that span a broad range of activities [14,16]. These activities include the catabolism of carbon (glycerol/propanediol, propionate) and nitrogen (ethanolamine, D-ornithine, glutamate, beta-lysine) [46,47], one-carbon metabolism in the Wood-Ljungdahl pathway (production of acetyl-CoA) [48] among other methyltransfer reactions, reduction of nucleotide di- and tri-phosphates to their respective deoxynucleotide states [49], tRNA synthesis (production of queosine) [50], synthesis of bacteriochlorophyll [51], methionine synthesis [46], mercury methylation [52], and, as noted above, reductive dehalogenation [47]. Bacterial genome analyses reveal that 86% of species have at least one cobamide-dependent enzyme though only 37% contain a complete cobamide biosynthesis pathway [16]. In the skin microbiome, only 1% of species synthesize cobamides *de novo* although 39% of the species contain at least one cobamide-dependent enzyme [41]. Thus, despite the ubiquitous nature of cobamide-dependent enzymes, there is a large disparity between cobamide producers and consumers in microbial communities. Notably, all cobamide producers require the prosthetic groups for their own metabolism and altruistic organisms (i.e., those that synthesize these metabolically costly prosthetic groups solely for others) are yet to be identified [16]. Mutualistic interactions between cobamide producers and syntrophic partners, however, are well documented [43,53,54]. While some cobamide-dependent enzymes reaction have counterparts that do not require the prosthetic group,

many species maintain both enzymes to broaden the range and efficiency of the desired reaction [16]. For example, cells requiring ribonucleotide reductases can overcome O_2 limitation associated with a requisite oxygen-dependent activation of the diiron enzyme through the alternative use of cobamide-dependent enzymes [55] and cobamide-dependent methionine synthase has a 100-fold greater turnover than the Zn-dependent form which can be more sensitive to oxidation and stress [56,57]. Taken together, the availability of cobamides, as well as free Co, in the environment is critical for many individual and community processes [16,43].

GEOLOGY AND GEOCHEMISTRY OF COBALT AND ITS LIMITATION IN THE ENVIRONMENT

Concentrations of Co can vary broadly across important geological landscapes. Spectroscopic measurements of the Sun predict the solar system abundance of Co to be ~10^5 atoms per 10^{12} atoms of H (less than 0.00001% or 0.1 ppm) [58]. On the other hand, concentrations in iron meteorites thought to represent the early Earth core suggest its enrichment (500-10,000 ppm) [58-60]. However, Co concentrations in Lunar basalt (20-45 ppm) [58] and the average Earth crust (25 ppm) [61] are notably lower. Concentrations of Co can be much higher locally in segregations of metal particles from Lunar regolith (>10,000 ppm) or igneous rock (2,500-44,000 ppm) [62] as well as those found in the Earth crust (<65% or 650,000 ppm) [63]. Notably, Co does not form a pure metal but instead is found in many S- and As-containing minerals (e.g., cobaltite, CoAsS) and regularly incorporates into Ni, Cu, Mn, and Fe minerals [58,63-65].

Weathering processes can often dictate the Co concentration in soils, sediments, and water ecosystems [58]. Parent rocks rich in Co, such as igneous ultramafic (100-200

ppm) and mafic (40 ppm) or metamorphic schists (40 ppm), can provide ecosystems with ample Co, whereas depleted rocks, such as shales (19 ppm), can produce ecosystems that are have limited availability of the micronutrient [58,63]. Indeed, sheep raised on pastures over Co-depleted granite rock, whose soil has <0.39 ppm Co content, developed vitamin B-12 anemia (i.e. cobalamin deficiency) as opposed to those raised on richer soils with 1.67 ppm [58,66]. Similar effects of Co-deficient soils on animal health have been reported in Kenyan animal reserves where lowland areas fall below a guideline 10 ppm Co for healthy soils as compared to highland areas that are less heavily flooded and grazed [58,67].

Concentrations in aquatic bodies are also modulated by rock weathering. Measurements of Co levels in large rivers typically range from 0.02-0.148 ppm [68] but contamination can increase the amount up to 2.028 ppm [69]. The relatively low concentrations of this metal in freshwater systems compared to soils are important for the viability of many aquatic organisms, as they are particularly susceptible to Co toxicity. Duckweed plants, for example, rapidly die at concentrations typically associated with healthy agricultural soils [70]. While many metals solubilized by weathering are precipitated by humic substances in water, Co is readily dissolved when bound by organic substances resulting in only 10% Co precipitation in some river waters [71]. As a result, near-shore buildups of Co have been reported that can raise the metal levels 30-fold compared to open ocean waters [58]. Oceans may also experience regional differences in Co concentrations, though on average metal levels are very low (0.0003 ppm or 0.3 ppb) and in the form of $CoSO_4$ and $CoCl_2$ salts [58]. In fact, open ocean levels of Co can fall low enough to limit biological activity. This is surprising because volcanism at ocean ridges

can release substantial amounts of Co into the waters but the metal accumulates locally in deep sea clays (12-16 ppm) [58] and in Mn-oxide minerals along deep seamounts (2,000 ppm) [72,73].

Although Co can be abundant in many environments, it is rapidly sequestered via co-precipitation with metal oxides and S-containing minerals such as pyrite (FeS_2) [58,65]. Adsorption of Co to the mineral phases may also occur and follows standard cationic behavior as a function of pH: adsorption can be insignificant below pH 4 but substantial at >pH 7 [65]. Once sequestered in Fe^{III} or Mn^{IV} oxides, Co is predicted to remain stably trapped [74]. Furthermore, the longer Co is sequestered in metal oxides, particularly Mn^{IV} oxides, the more difficult it becomes for desorption to occur [74]. Thus, despite its ubiquity and relative abundance in many environments, the bioavailability of Co has often been considered to be quite low.

METAL RESPIRATION AS A PART OF THE BIOGEOCHEMICAL CYCLE

For over a century, the ability of microbes to use extracellular metals as electron donors [75-77] and acceptors [78-80] for their metabolism has been of industrial [81,82], environmental [83,84] and astrobiological interest [6,85,86]. Metal-reducing microbes use oxidized metals as electron acceptors to gain energy from the establishment of a proton motive force across the inner membrane, similar to how O_2 is reduced by the respiratory chains of aerobic organisms. The ability of microbes to respire metals allows them to colonize a wide range of environments where stronger electron acceptors (e.g., O_2 and nitrate [NO_3^-]) may not be available, such as below the 1-cm crust of terrestrial soils, the ocean floor [87,88] and the subsurface [89]. The energy derived from metal reduction is dependent on the half- or reduction-potential of the metal species, making Mn^{IV} reduction to Mn^{II} (half-potential of

1.23 V) more favorable than Fe^{III} reduction to Fe^{II} (half-potential of 0.771 V), and so on [90].

Metal respiration can be facilitated through numerous mechanisms. In general, metal-reducing bacteria use NADH dehydrogenase enzymes to split protons and electrons at the membrane using reducing molecules (e.g., NADH) generated during their oxidative metabolism. The protons provide the gradient needed for ATP synthesis, while the electrons are transferred to the membrane menaquinone pool and from there to *c*-type cytochromes of the inner membrane (quinol oxidases) and, in Gram-negative bacteria, to periplasmic and outer membrane *c*-type cytochromes, which reduce the metal on the cell surface [21,91,92]. Metal-reducing bacteria in the genus *Geobacter* are unique in their ability to extend their redox-surface area via conductive protein appendages known as pili, which use tightly packed aromatic residues to discharge electrons from the periplasmic cytochromes onto terminal electron acceptors like Fe^{III} oxides [83,93,94]. Outer membrane cytochromes of *Geobacter* have also been reported to form conductive filaments in the extracellular matrix of biofilms [95] but planktonic cells, the most relevant state for metal reduction, primarily produce pili as nanowires [96]. Metal-reducing bacteria may also secrete soluble electron shuttles such as flavins to transfer electrons to the extracellular minerals [78]. All metal reducers may also stimulate their reductive activities with exogenous humic substances, which function as natural electron shuttles in environments where organic matter degradation is a significant process [97,98].

Collectively, metal-reducing microbes play important roles, whether directly or indirectly, in the biogeochemical cycling of many metals. The bioreduction of Fe^{III} and Mn^{IV} oxides dissolves the mineral phases and solubilizes the metals in their reduced

forms (Fe^{II}, Mn^{II}). Abiotic reactions between the free aqueous ions and the metal oxides may also occur concurrently, generating mixed valence metal minerals such as magnetite (Fe_3O_4) [93,99]. The reductive dissolution of the Fe^{III} and Mn^{IV} oxides supplies the essential metals to syntrophic partners for assimilation or for their use as electron donors (e.g. Fe^{II} oxidizers). The dissolution of the metal oxides also releases other metal species sequestered in the minerals such as Co [65,74]. Free Co^{III} is readily chelated by naturally-occurring organic molecules such as citric acid [65], providing a soluble electron acceptor for respiration via its reduction to Co^{II} [100,101]. But Co^{II} may also be sequestered from the metal oxides by the activities of metal-reducing microbes. As a result, Co^{II} concentrations may increase locally in environments where metal oxides are actively being reduced by microbes. This is expected to exert selective pressure on metal reducers to become resistant to the metal. In support of this proposal, metal cycling bacteria are the dominant genera in Co-containing deep-sea Mn nodules, such as those of the *Shewanella* and *Colwellia* genera [87] . Dissolution of the nodules by the bacterial activities releases Co into the environment [87] and provides a source of this micronutrient for cobamide-dependent members of the nodule community. Thus, Co resistance is critical for metal-reducing microbes to solubilize the Co pool sequestered in the mineral phases, making the metal available for the synthesis of cobamides. This behavior suggests that metal reducers are keystone members of cobamide-dependent communities, supporting the activity of the syntrophic partners in environments that would otherwise be limited in Co availability.

Given the important role of *Geobacter* bacteria in metal oxide reduction [102] and cobamide synthesis for syntrophic partners [42,103], I hypothesized that these microorganisms have evolved mechanisms for the efficient detoxification of Co released

during the reductive dissolution of Fe^{III} and Mn^{IV} oxides. In this dissertation, I describe studies that demonstrate the high resistance to Co^{II} of the model representative *Geobacter sulfurreducens*, the complex response that prevents fatal intoxication, and the role of respiratory chains have in the mineralization of the metal and detoxification.

REFERENCES

1 Varma, S. J., Muchowska, K. B., Chatelain, P. & Moran, J. Native iron reduces CO. *Nat Ecol Evol* **2**, 1019-1024 (2018). https://doi.org/10.1038/s41559-018-0542-2

2 Camprubi, E., Jordan, S. F., Vasiliadou, R. & Lane, N. Iron catalysis at the origin of life. *IUBMB Life* **69**, 373-381 (2017). https://doi.org/10.1002/iub.1632

3 Russell, M. J. & Martin, W. The rocky roots of the acetyl-CoA pathway. *Trends Biochem Sci* **29**, 358-363 (2004). https://doi.org/10.1016/j.tibs.2004.05.007

4 Dörr, M. *et al.* A possible prebiotic formation of ammonia from dinitrogen on iron sulfide surfaces. *Angew Chem Int Ed Engl* **42**, 1540-1543 (2003). https://doi.org/10.1002/anie.200250371

5 Smirnov, A., Hausner, D., Laffers, R., Strongin, D. R. & Schoonen, M. A. Abiotic ammonium formation in the presence of Ni-Fe metals and alloys and its implications for the Hadean nitrogen cycle. *Geochem Trans* **9**, 5 (2008). https://doi.org/10.1186/1467-4866-9-5

6 Spietz, R. L., Payne, D., Szilagyi, R. & Boyd, E. S. Reductive biomining of pyrite by methanogens. *Trends Microbiol* **30**, 1072-1083 (2022). https://doi.org/10.1016/j.tim.2022.05.005

7 Preiner, M. *et al.* Catalysts, autocatalysis and the origin of metabolism. *Interface Focus* **9**, 20190072 (2019). https://doi.org/10.1098/rsfs.2019.0072

8 Fuchs, G. Alternative pathways of carbon dioxide fixation: insights into the early evolution of life? *Annu Rev Microbiol* **65**, 631-658 (2011). https://doi.org/10.1146/annurev-micro-090110-102801

9 Boyd , E. S. *et al.* in *Iron-sulfur clusters in chemistry and biology* (ed Tracey Rouault) Ch. 23, 619-635 (de Gruyter, 2014).

10 Kacar, B., Garcia, A. K. & Anbar, A. D. Evolutionary History of Bioessential Elements Can Guide the Search for Life in the Universe. *Chembiochem* **22**, 114-119 (2021). https://doi.org/10.1002/cbic.202000500

11 Liu, J. *et al.* Metalloproteins containing cytochrome, iron-sulfur, or copper redox centers. *Chem Rev* **114**, 4366-4469 (2014). https://doi.org/10.1021/cr400479b

12 Valenti, R., Jabłońska, J. & Tawfik, D. S. Characterization of ancestral Fe/Mn superoxide dismutases indicates their cambialistic origin. *Protein Sci* **31**, e4423 (2022). https://doi.org/10.1002/pro.4423

13 Garcia, P. S. *et al.* An early origin of iron-sulfur cluster biosynthesis machineries before Earth oxygenation. *Nat Ecol Evol* **6**, 1564-1572 (2022). https://doi.org/10.1038/s41559-022-01857-1

14 Hausinger, R. P. & Zamble, D. B. in *Molecular Microbiology of Heavy Metals Microbiology Monographs* (eds Dietrich H. Nies & Simon Silver) (2007).

15 Alfano, M. & Cavazza, C. Structure, function, and biosynthesis of nickel-dependent enzymes. *Protein Sci* **29**, 1071-1089 (2020). https://doi.org/10.1002/pro.3836

16 Shelton, A. N. *et al.* Uneven distribution of cobamide biosynthesis and dependence in bacteria predicted by comparative genomics. *ISME J* **13**, 789-804 (2019). https://doi.org/10.1038/s41396-018-0304-9

17 Osman, D. *et al.* The requirement for cobalt in vitamin B. *Biochim Biophys Acta Mol Cell Res* **1868**, 118896 (2021). https://doi.org/10.1016/j.bbamcr.2020.118896

18 Mayr, S. J., Mendel, R. R. & Schwarz, G. Molybdenum cofactor biology, evolution and deficiency. *Biochim Biophys Acta Mol Cell Res* **1868**, 118883 (2021). https://doi.org/10.1016/j.bbamcr.2020.118883

19 Magalon, A. & Mendel, R. R. Biosynthesis and Insertion of the Molybdenum Cofactor. *EcoSal Plus* **6** (2015). https://doi.org/10.1128/ecosalplus.ESP-0006-2013

20 McGuirl, M. A. & Dooley, D. M. Copper-containing oxidases. *Current opinion in chemical biology* **3** (1999). https://doi.org/10.1016/S1367-5931(99)80025-8

21 Liu, Y. *et al.* A trans-outer membrane porin-cytochrome protein complex for extracellular electron transfer by Geobacter sulfurreducens PCA. *Environ Microbiol Rep* **6**, 776-785 (2014). https://doi.org/10.1111/1758-2229.12204

22 Perera, L., Beard, W. A., Pedersen, L. G. & Wilson, S. H. Hiding in plain sight: The bimetallic magnesium covalent bond in enzyme active sites. *Inorganic chemistry* **56** (2017). https://doi.org/10.1021/acs.inorgchem.6b02189

23 Maret, W. Zinc biochemistry: from a single zinc enzyme to a key element of life. *Advances in nutrition (Bethesda, Md.)* **4** (2013). https://doi.org/10.3945/an.112.003038

24 Tripathi, D., Mani, V. & Pal, R. P. Vanadium in biosphere and its role in biological processes. *Biological trace element research* **186** (2018). https://doi.org/10.1007/s12011-018-1289-y

25 Morowitz, H. J., Srinivasan, V. & Smith, E. Ligand field theory and the origin of life as an emergent feature of the periodic table of elements. *Biol Bull* **219**, 1-6 (2010). https://doi.org/10.1086/BBLv219n1p1

26 Zhang, Y. & Gladyshev, V. N. General trends in trace element utilization revealed by comparative genomic analyses of Co, Cu, Mo, Ni, and Se. *J Biol Chem* **285**, 3393-3405 (2010). https://doi.org/10.1074/jbc.M109.071746

27 Waldron, K. J., Rutherford, J. C., Ford, D. & Robinson, N. J. Metalloproteins and metal sensing. *Nature* **460**, 823-830 (2009). https://doi.org/10.1038/nature08300

28 Hill, H. A. O. & Sadler, P. J. Bringing inorganic chemistry to life with inspiration from R. J. P. Williams. *J. Biol. Inorg. Chem.* **21**, 5-12 (2016). https://doi.org/10.1007/s00775-016-1333-3

29 Kuchar, J. & Hausinger, R. P. Biosynthesis of metal sites. *Chem Rev* **104**, 509-525 (2004). https://doi.org/10.1021/cr020613p

30 Valdez, C. E., Smith, Q. A., Nechay, M. R. & Alexandrova, A. N. Mysteries of metals in metalloenzymes. *Acc Chem Res* **47**, 3110-3117 (2014). https://doi.org/10.1021/ar500227u

31 Lazcano, A., Fastag, J., Gariglio, P., Ramírez, C. & Oró, J. On the early evolution of RNA polymerase. *J Mol Evol* **27**, 365-376 (1988). https://doi.org/10.1007/BF02101199

32 Kogut, K. A. & Rowlett, R. S. A comparison of the mechanisms of CO2 hydration by native and Co2+-substituted carbonic anhydrase II. *J Biol Chem* **262**, 16417-16424 (1987).

33 Sparta, M., Valdez, C. E. & Alexandrova, A. N. Metal-dependent activity of Fe and Ni acireductone dioxygenases: how two electrons reroute the catalytic pathway. *J Mol Biol* **425**, 3007-3018 (2013). https://doi.org/10.1016/j.jmb.2013.05.001

34 Alterio, V., Langella, E., De Simone, G. & Monti, S. M. Cadmium-containing carbonic anhydrase CDCA1 in marine diatom Thalassiosira weissflogii. *Mar Drugs* **13**, 1688-1697 (2015). https://doi.org/10.3390/md13041688

35 Lane, T. W. *et al.* Biochemistry: a cadmium enzyme from a marine diatom. *Nature* **435**, 42 (2005). https://doi.org/10.1038/435042a

36 WITTENBERG, J. B. Formation of the porphyrin ring. *Nature* **184**, 876-878 (1959). https://doi.org/10.1038/184876a0

37 Layer, G., Reichelt, J., Jahn, D. & Heinz, D. W. Structure and function of enzymes in heme biosynthesis. *Protein Sci* **19**, 1137-1161 (2010). https://doi.org/10.1002/pro.405

38 Warren, M. J., Raux, E., Schubert, H. L. & Escalante-Semerena, J. C. The biosynthesis of adenosylcobalamin (vitamin B12). *Nat Prod Rep* **19**, 390-412 (2002). https://doi.org/10.1039/b108967f

39 Chew, A. G. & Bryant, D. A. Chlorophyll biosynthesis in bacteria: the origins of structural and functional diversity. *Annu Rev Microbiol* **61**, 113-129 (2007). https://doi.org/10.1146/annurev.micro.61.080706.093242

40 Thauer, R. K. & Bonacker, L. G. Biosynthesis of coenzyme F430, a nickel porphinoid involved in methanogenesis. *Ciba Found Symp* **180**, 210-222; discussion 222-217 (1994). https://doi.org/10.1002/9780470514535.ch12

41 Swaney, M. H., Sandstrom, S. & Kalan, L. R. Cobamide Sharing Is Predicted in the Human Skin Microbiome. *mSystems* **7**, e0067722 (2022). https://doi.org/10.1128/msystems.00677-22

42 Yan, J., Ritalahti, K. M., Wagner, D. D. & Löffler, F. E. Unexpected specificity of interspecies cobamide transfer from *Geobacter* spp. to organohalide-respiring *Dehalococcoides mccartyi* strains. *Appl Environ Microbiol* **78**, 6630-6636 (2012). https://doi.org/10.1128/aem.01535-12

43 Sokolovskaya, O. M., Shelton, A. N. & Taga, M. E. Sharing vitamins: Cobamides unveil microbial interactions. (2020). https://doi.org/10.1126/science.aba0165

44 Hazra, A. B. *et al.* Anaerobic biosynthesis of the lower ligand of vitamin B12. *Proc Natl Acad Sci USA* **112**, 10792-10797 (2015). https://doi.org/10.1073/pnas.1509132112

45 Yi, S. *et al.* Versatility in corrinoid salvaging and remodeling pathways supports corrinoid-dependent metabolism in *Dehalococcoides mccartyi*. *Appl Environ Microbiol* **78**, 7745-7752 (2012). https://doi.org/10.1128/AEM.02150-12

46 Roth, J. R., Lawrence, J. G. & Bobik, T. A. Cobalamin (coenzyme B12): synthesis and biological significance. *Annual review of microbiology* **50** (1996). https://doi.org/10.1146/annurev.micro.50.1.137

47 Banerjee, R. & Ragsdale, S. W. The many faces of vitamin B12: catalysis by cobalamin-dependent enzymes. *Annual review of biochemistry* **72** (2003). https://doi.org/10.1146/annurev.biochem.72.121801.161828

48 Ragsdale, S. W. & Pierce, E. Acetogenesis and the Wood-Ljungdahl pathway of CO(2) fixation. *Biochim Biophys Acta* **1784**, 1873-1898 (2008). https://doi.org/10.1016/j.bbapap.2008.08.012

49 Blakley, R. L. Cobamides and ribonucleotide reduction. I. Cobamide stimulation of ribonucleotide reduction in extracts of *Lactobacillus leichmanii*. *The Journal of Biological Chemistry* **240** (1965).

50 Frey, B., McCloskey, J., Kersten, W. & Kersten, H. New function of vitamin B12: cobamide-dependent reduction of epoxyqueuosine to queuosine in tRNAs of *Escherichia coli* and *Salmonella typhimurium*. *Journal of bacteriology* **170** (1988). https://doi.org/10.1128/jb.170.5.2078-2082.1988

51 Chen, G. E., Canniffe, D. P. & Hunter, C. N. Three classes of oxygen-dependent cyclase involved in chlorophyll and bacteriochlorophyll biosynthesis. (2017). https://doi.org/10.1073/pnas.1701687114

52 Choi, S. C. & Bartha, R. Cobalamin-mediated mercury methylation by Desulfovibrio desulfuricans LS. *Appl Environ Microbiol* **59**, 290-295 (1993). https://doi.org/10.1128/aem.59.1.290-295.1993

53 Croft, M. T., Lawrence, A. D., Raux-Deery, E., Warren, M. J. & Smith, A. G. Algae acquire vitamin B12 through a symbiotic relationship with bacteria. *Nature* **438** (2005). https://doi.org/10.1038/nature04056

54 Kazamia, E. *et al.* Mutualistic interactions between vitamin B12 -dependent algae and heterotrophic bacteria exhibit regulation. *Environmental microbiology* **14** (2012). https://doi.org/10.1111/j.1462-2920.2012.02733.x

55 Taga, M. E. & Walker, G. C. *Sinorhizobium meliloti* requires a cobalamin-dependent ribonucleotide reductase for symbiosis with its plant host. *Molecular plant-microbe interactions : MPMI* **23** (2010). https://doi.org/10.1094/MPMI-07-10-0151

56 González, J. C., Banerjee, R. V., Huang, S., Sumner, J. S. & Matthews, R. G. Comparison of cobalamin-independent and cobalamin-dependent methionine synthases from *Escherichia coli*: two solutions to the same chemical problem. *Biochemistry* **31** (1992). https://doi.org/10.1021/bi00141a013

57 ER, H. & RG, M. Oxidative stress inactivates cobalamin-independent methionine synthase (MetE) in Escherichia coli. *PLoS biology* **2** (2004). https://doi.org/10.1371/journal.pbio.0020336

58 Hamilton, E. I. The geobiochemistry of cobalt. *Sci Total Environ* **150**, 7-39 (1994). https://doi.org/10.1016/0048-9697(94)90126-0

59 Al Salhi, M. S. *et al.* Elemental composition and physical characteristics of the massive meteorite of the Saudi empty quarter. *Journal of King Saud University - Science* **33** (2021). https://doi.org/https://doi.org/10.1016/j.jksus.2021.101341

60 Mason, B. & Moore, C. B. *Principles of geochemistry*. 4th edn, (Wiley, 1982).

61 Taylor, S. R. Abundance of chemical elements in the continental crust: a new table. **28**, 1273-1285 (1964).

62 Wittmann, A. & Korotev, R. L. in *44th Lunar and Planetary Science Conference* (2013).

63 Dehaine, Q., Tijsseling, L. T., Glass, H. J., Tormanen, T. & Butcher, A. R. Geometallurgy of cobalt ores: A review. *Minerals Engineering* **160** (2021). https://doi.org/https://doi.org/10.1016/j.mineng.2020.106656

64 Moore, E. K. *et al.* Geological and Chemical Factors that Impacted the Biological Utilization of Cobalt in the Archean Eon - Moore - 2018 - Journal of Geophysical Research: Biogeosciences - Wiley Online Library. *JGR Biogeosciences* (2018). https://doi.org/10.1002/2017JG004067

65 Krupka, K. M. & Serne, R. J. (ed Pacific Northwest National Laboratory) (Washington, 2002).

66 Patterson, J. B. E. Cobalt, and Sheep Diseases. *Nature* (1937).

67 Maskall, J. & Thornton, I. Trace element geochemistry of soils and plants in Kenyan conservation areas and implications for wildlife nutrition. *Environ Geochem Health* **13**, 93-107 (1991). https://doi.org/10.1007/BF01734300

68 Gaillardet, J., Viers, J. & Dupre, B. Vol. 5 225-272 (Treatise on Geochemistry, 2003).

69 Canada, E. (ed Environment Canada) (2017).

70 Stubblefield, W. A. *et al.* Acute and Chronic Toxicity of Cobalt to Freshwater Organisms: Using a Species Sensitivity Distribution Approach to Establish International Water Quality Standards. *Environ Toxicol Chem* **39**, 799-811 (2020). https://doi.org/10.1002/etc.4662

71 Sholkovitz, E. R. & Copland, D. The coagulation, solubility and adsorption properties of Fe, Mn, Cu, Ni, Cd, Co and humic acids in a river water. *Geochimica et Cosmochimica Acta* **45**, 181-189 (1981). https://doi.org/10.1016/0016-7037(81)90161-7

72 Wegorzewski, A. V. & Kuhn, T. The influence of suboxic diagenesis on the formation of manganese nodules in the Clarion Clipperton nodule belt of the Pacific Ocean. *Marine Geology* **357**, 123-138 (2014). https://doi.org/10.1016/j.margeo.2014.07.004

73 Blöthe, M. *et al.* Manganese-cycling microbial communities inside deep-sea manganese nodules. *Environmental science & technology* **49** (2015). https://doi.org/10.1021/es504930v

74 Backes, C. A., McLaren, R. G., Rate, A. W. & Swift, R. S. Kinetics of cadmium and cobalt desorption from iron and manganese oxides. *Soil Sci. Soc. Am. J.* **59**, 778-785 (1995). https://doi.org/10.2136/sssaj1995.03615995005900030021x

75 Tyler, P. A. & Marshall, K. C. Microbial oxidation of manganese in hydro-electric pipelines. *Antonie van Leeuwenhoek* **33**, 171-183 (1967). https://doi.org/doi:10.1007/BF02045548

76 Beijerinck, M. Oxydation des mangancarbonates durch Bakterien und Schimmelpilze. *Folia Microbiol (Delft)* **2**, 123-134 (1913).

77 Ghiorse, W. C. in *Manganese in Soils and Plants: Proceedings of the International Symposium on 'Manganese in Soils and Plants' held at the Waite Agricultural Research Institute, The University of Adelaide, Glen Osmond, South Australia, August 22–26, 1988 as an Australian Bicentennial Event* (eds Robin D. Graham, Robert J. Hannam, & Nicholas C. Uren) 75-85 (Springer Netherlands, 1988).

78 Lovley, D. R., Holmes, D. E. & Nevin, K. P. Dissimilatory Fe(III) and Mn(IV) reduction. *Adv Microb Physiol* **49**, 219-286 (2004). https://doi.org/10.1016/S0065-2911(04)49005-5

79 Lovley, D. R. Electrotrophy: Other microbial species, iron, and electrodes as electron donors for microbial respirations. *Bioresource technology* **345** (2022). https://doi.org/10.1016/j.biortech.2021.126553

80 Nealson, K. H., Belz, A. & McKee, B. Breathing metals as a way of life: geobiology in action. *Antonie Van Leeuwenhoek* **81**, 215-222 (2002). https://doi.org/10.1023/a:1020518818647

81 Diep, P., Mahadevan, R. & Yakunin, A. F. Heavy Metal Removal by Bioaccumulation Using Genetically Engineered Microorganisms. *Front Bioeng Biotechnol* **6**, 157 (2018). https://doi.org/10.3389/fbioe.2018.00157

82 Cosert, K. M. & Reguera, G. Voltammetric study of conductive planar assemblies of Geobacter nanowire pilins unmasks their ability to bind and mineralize divalent cobalt. *J Ind Microbiol Biotechnol* **46**, 1239-1249 (2019). https://doi.org/10.1007/s10295-019-02167-5

83 Cologgi, D. L., Lampa-Pastirk, S., Speers, A. M., Kelly, S. D. & Reguera, G. Extracellular reduction of uranium via *Geobacter* conductive pili as a protective cellular mechanism. *Proc. Natl. Acad. Sci. USA* **108**, 15248-15252 (2011). https://doi.org/10.1073/pnas.1108616108

84 Gadd, G. M. Metals, minerals and microbes: geomicrobiology and bioremediation. *Microbiology (Reading)* **156**, 609-643 (2010). https://doi.org/10.1099/mic.0.037143-0

85 Nealson, K. & Cox, B. Microbial metal-ion reduction and Mars: extraterrestrial expectations? *Current opinion in microbiology* **5** (2002). https://doi.org/10.1016/s1369-5274(02)00326-0

86 Vargas, M., Kashefi, K., Blunt-Harris, E. L. & Lovley, D. R. Microbiological evidence for Fe(III) reduction on early Earth. *Nature* **395**, 65-67 (1998).

87 M, B. *et al.* Manganese-Cycling Microbial Communities Inside Deep-Sea Manganese Nodules. *Environmental science & technology* **49** (2015). https://doi.org/10.1021/es504930v

88 Kashefi, K. *et al.* Geoglobus ahangari gen. nov., sp. nov., a novel hyperthermophilic archaeon capable of oxidizing organic acids and growing autotrophically on hydrogen with Fe(III) serving as the sole electron acceptor. *Int J Syst Evol Microbiol* **52**, 719-728 (2002). https://doi.org/10.1099/00207713-52-3-719

89 Methé, B. A. *et al.* Genome of *Geobacter sulfurreducens*: metal reduction in subsurface environments. *Science (New York, N.Y.)* **302** (2003). https://doi.org/10.1126/science.1088727

90 Lovley, D. R. & Phillips, E. J. Novel mode of microbial energy metabolism: organic carbon oxidation coupled to dissimilatory reduction of iron or manganese. *Applied and environmental microbiology* **54** (1988). https://doi.org/10.1128/aem.54.6.1472-1480.1988

91 Bretschger, O. *et al.* Current production and metal oxide reduction by Shewanella oneidensis MR-1 wild type and mutants. *Appl Environ Microbiol* **73**, 7003-7012 (2007). https://doi.org/10.1128/AEM.01087-07

92 Reguera, G. Microbial nanowires and electroactive biofilms. *FEMS Microbiology Ecology* **94** (2018). https://doi.org/10.1093/femsec/fiy086

93 Reguera, G. *et al.* Extracellular electron transfer via microbial nanowires. *Nature* **435**, 1098-1101 (2005). https://doi.org/10.1038/nature03661

94 Reguera, G. Harnessing the power of microbial nanowires. *Microb. Biotechnol.* **11**, 979–994 (2018). https://doi.org/10.1111/1751-7915.13280

95 Wang, F. *et al.* Structure of *Geobacter* OmcZ filaments suggests extracellular cytochrome polymers evolved independently multiple times. *Elife* **11** (2022). https://doi.org/10.7554/eLife.81551

96 Liu, X., Walker, D. J. F., Nonnenmann, S. S., Sun, D. & Lovley, D. R. Direct Observation of Electrically Conductive Pili Emanating from. *mBio* **12**, e0220921 (2021). https://doi.org/10.1128/mBio.02209-21

97 Hobbie, S. N., Li, X., Basen, M., Stingl, U. & Brune, A. Humic substance-mediated Fe(III) reduction by a fermenting *Bacillus* strain from the alkaline gut of a humus-feeding scarab beetle larva. *Systematic and applied microbiology* **35** (2012). https://doi.org/10.1016/j.syapm.2012.03.003

98 Lovley, D. R. & Blunt-Harris, E. L. Role of humic-bound iron as an electron transfer agent in dissimilatory Fe(III) reduction. *Appl Environ Microbiol* **65**, 4252-4254 (1999). https://doi.org/10.1128/AEM.65.9.4252-4254.1999

99 Manzella, M. P., Reguera, G. & Kashefi, K. Extracellular electron transfer to Fe(III) oxides by the hyperthermophilic archaeon Geoglobus ahangari via a direct

contact mechanism. *Appl Environ Microbiol* **79**, 4694-4700 (2013). https://doi.org/10.1128/AEM.01566-13

100 Caccavo, F. *et al.* Geobacter sulfurreducens sp. nov., a hydrogen- and acetate-oxidizing dissimilatory metal-reducing microorganism. *Applied and environmental microbiology* **60** (1994). https://doi.org/10.1128/aem.60.10.3752-3759.1994

101 Hau, H. H., Gilbert, A., Coursolle, D. & Gralnick, J. A. Mechanism and consequences of anaerobic respiration of cobalt by *Shewanella oneidensis* strain MR-1. *Appl Environ Microbiol* **74**, 6880-6886 (2008). https://doi.org/10.1128/AEM.00840-08

102 Reguera, G. & Kashefi, K. The electrifying physiology of Geobacter bacteria, 30 years on. *Adv Microb Physiol* **74**, 1-96 (2019). https://doi.org/10.1016/bs.ampbs.2019.02.007

103 Berthomieu, R. *et al.* Mechanisms underlying Clostridium pasteurianum's metabolic shift when grown with Geobacter sulfurreducens. *Applied Microbiology and Biotechnology* **106**, 865-876 (2021). https://doi.org/doi:10.1007/s00253-021-11736-7

Chapter 2: Cobalt resistance via detoxification and mineralization in the iron-reducing bacterium *Geobacter sulfurreducens*

The material presented in this chapter has been adapted from the following, open access publication:

Dulay H[†], Tabares M[†], Kashefi K, Reguera G[*]. *Cobalt Resistance via Detoxification and Mineralization in the Iron-Reducing Bacterium* Geobacter sulfurreducens*.* Front Microbiol. 2020 Nov 26;11:600463. doi: 10.3389/fmicb.2020.600463. PMID: 33324382; PMCID: PMC7726332.

[†]Equal contribution

[*]Corresponding author

ABSTRACT

Bacteria in the genus *Geobacter* thrive in iron- and manganese-rich environments where the divalent cobalt cation (Co^{II}) accumulates to potentially toxic concentrations. Consistent with selective pressure from environmental exposure, the model laboratory representative *Geobacter sulfurreducens* grew with $CoCl_2$ concentrations (1 mM) typically used to enrich for metal-resistant bacteria from contaminated sites. We reconstructed from genomic data canonical pathways for Co^{II} import and assimilation into cofactors (cobamides) that support the growth of numerous syntrophic partners. We also identified several metal efflux pumps, including one that was specifically upregulated by Co^{II}. Cells acclimated to metal stress by downregulating non-essential proteins with metals and thiol groups that Co^{II} preferentially targets. They also activated sensory and regulatory proteins involved in detoxification as well as pathways for protein and DNA repair. In addition, *G. sulfurreducens* upregulated respiratory chains that could have contributed to the reductive mineralization of the metal on the cell surface. Transcriptomic evidence also revealed pathways for cell envelope modification that increased metal resistance and promoted cell-cell aggregation and biofilm formation in stationary phase. These complex adaptive responses confer on *Geobacter* a competitive advantage for growth in metal-rich environments that are essential to the sustainability of cobamide-dependent microbiomes and the sequestration of the metal in hitherto unknown biomineralization reactions.

INTRODUCTION

Metal micronutrients such as nickel (Ni^{II}), cobalt (Co^{II}), manganese (Mn^{II}) and iron (Fe^{II}) are essential for life yet toxic above relatively low concentrations [1]. Not surprisingly, microorganisms have evolved numerous adaptive responses to import the essential

metals from the environment while preventing their excessive intracellular accumulation and intoxication [2]. Metal homeostasis is primarily achieved by the antagonistic activities of metal importers and exporters [2]. Cells often use high affinity transporters to import the metals with specificity and rely on specialized proteins and chaperones to integrate them into pathways dedicated to the synthesis of metalloproteins and enzyme cofactors [1]. Collectively, biometals contribute to the synthesis of up to one third of the cell's proteome and to metabolic functions essential to the growth and survival of the cell [1]. Each of these metals must be available in just the right intracellular concentration (i.e., the cellular metal quota) to prevent intoxication [3]. Thus, dedicated metalloregulatory systems monitor the intracellular metal levels and modulate the expression of transporters and other proteins essential for metal homeostasis [2]. Metal exporters provide the primary mechanism to eliminate excess metal [2] but the cellular response to metal intoxication is often more extensive, as cells have to cope with the direct and indirect impacts of the reactive metals on proteins and DNA. For example, Co^{II} can bind and inactivate numerous proteins non-specifically, displace other metals (particularly, Fe^{II}) from prosthetic groups and metal-binding sites, and generate free radicals [4]. Its high affinity for thiol groups disrupts disulfide bonds in proteins, reduces the free thiol pool and can interfere with sulfur assimilation [5]. Hence, Co^{II} intoxication causes generalized damage in the cells, requiring extensive reprograming to cope with multiple stressors.

The essentiality yet toxicity of metal micronutrients such as Co^{II} exerts selective pressure on microorganisms to tune their metabolism to the fluctuating availability of the metal species from geochemical sources. Yet, many aspects of the biological cycling of metal micronutrients remain relatively obscure. This is particularly true for Co^{II}, a metal

micronutrient that some microorganisms assimilate to produce enzyme cofactors (cobamides) in the cobalamin (vitamin B_{12}) family that catalyze metabolic reactions essential to all living cells [6]. Genes encoding cobamide-dependent enzymes are widespread in prokaryotes but only a fraction of surveyed genomes have complete pathways for *de novo* cobamide synthesis [6,7]. As a result, most microorganisms need to salvage cobamides from the environment, a nutritional dependency that drives syntrophic interactions with cobamide producers [8]. Cobamide-dependent microbiomes depend on the ability of cobamide producers to import and assimilate the soluble Co^{II} cation. The divalent species, however, readily oxidizes to Co^{III} on the surface of Mn^{IV} oxide particles [9,10]. Co^{II} mobility in soil and sediment systems is also limited by the tendency of the metal to coprecipitate with Fe^{III} and Mn^{IV} oxide minerals [11]. Additionally, Fe^{III} and Mn^{IV} oxides sorb large amounts of the metal cation, sequestering it in solid phases that reduce its bioavailability [12].

The absorption and co-precipitation of most of the available Co^{II} into Fe^{III} and Mn^{IV} minerals gives Fe^{III} and Mn^{IV}-reducing bacteria, such as those in the genus *Geobacter*, a competitive advantage for growth in cobamide-dependent microbiomes (Fig. 1). These bacteria gain energy for growth from the reductive dissolution of the metal oxides, which are reactions that could solubilize Fe^{II} and Mn^{II} and could remobilize Co^{II} and Co^{III} [13]. *Geobacter* species are also important drivers of organic matter degradation, a process that generates organic chelators with affinity for Co^{III}. This keeps the trivalent species in solution and available for use as an electron acceptor [13]. The dissimilatory reduction of chelated forms of Co^{III} by *Geobacter* reduces Co^{III} to Co^{II} [13]. The low reduction potential of the divalent species (− 0.28 V versus standard hydrogen electrode, SHE) and its

toxicity to bacteria at relatively low concentrations have been assumed to prevent its biological reduction to Co^0 [14,15]. Yet, *Geobacter* species, including the model laboratory strain *Geobacter sulfurreducens*, assimilate Co^{II} to synthesize cobamides, which they secrete to sustain several syntrophic partners [16] (Fig. 2.1). These syntrophic interactions are favored in local epigenetic zones enriched in Fe^{III} and Mn^{IV} oxides, which are the regions where Co^{II} preferentially accumulates [17]. This raises yet unexplored questions about the cellular tolerance of *Geobacter* species for Co^{II} and the mechanisms that allow these microorganisms to survive and even thrive in Co^{II}-rich environments.

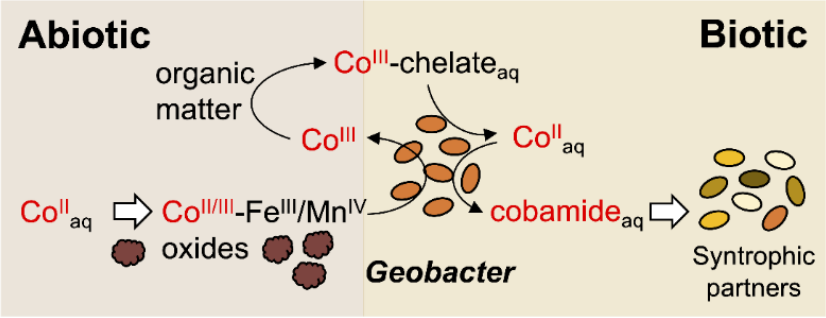

Figure 2.1 Known contribution of *Geobacter* species to the cycling of cobalt (Co). *Geobacter* bacteria reduce chelated and mineral forms of Co^{III} to Co^{II}, whose bioavailability is limited by its tendency to adsorb and/or co-precipitate with Fe^{III} and Mn^{IV} oxides. The reduction of Fe^{III} and Mn^{IV} oxides by *Geobacter* bacteria solubilizes Co^{II} for the synthesis of cobamides that support the growth of syntrophic partners.

We gained insights into the environmental controls of *Geobacter* activities in cobamide-driven microbiomes by investigating the adaptive responses of *G. sulfurreducens* to growth and reproduction in the presence of Co^{II}. Consistent with environmental exposure, we demonstrate high Co^{II} resistance in this laboratory strain and describe pathways for protein and DNA repair, cell envelope modifications, and biofilm formation that allow the cells to effectively cope with Co^{II} stress. Importantly, we show that metal acclimation activates respiratory chains that could participate in the reductive precipitation of the metal on the cell's surface to alleviate toxicity. These adaptive

responses allow *Geobacter* species to grow in Co^{II}-rich environments, sustaining the productivity of the native microbiomes and contributing to hitherto unknown reactions of the Co cycle.

RESULTS

Genomic determinants of CoII homeostasis in G. sulfurreducens

Metal ions bridge the outer membrane by simple diffusion through nonselective pores [18] but require specific transporters to traverse the inner membrane (Fig. 2.2). We identified in *G. sulfurreducens* complete NikMNQO and CbiMNQO importers, the most widespread prokaryotic systems for Ni^{II} and Co^{II} uptake [19]. Although both systems can import Ni^{II} and Co^{II}, specific amino acid signatures in the M subunits make CbiMNQO the high affinity importer of Co^{II} [19]. At high enough concentrations, however, Co^{II} could selectively outcompete Ni^{II} and enter the cytoplasm via the NikMNQO system. These transporters are annotated as ATP-binding Cassette (ABC) transporters, but they are part of the prokaryotic family of energy-coupling factor (ECF) transporters that also transport water-soluble vitamins and cofactors [20]. The metal ECF subclass has a distinct modular architecture (A, T and S components) to bind the substrate (S component) without assistance from extracytoplasmic solute-binding proteins [20]. In most Nik/CbiMNQO systems, the S component is a heterodimer of M and N subunits [19] but these subunits are fused in a single gene in *G. sulfurreducens* (*nikMN*, GSU1279; *cbiMN*, GSU3004). The end result is the same: the assembly of a MN subcomplex (S component) that binds the metal and transports it across the membrane in a reaction energized by the O subunit dimer (A, or ATPase, component) and rate-modulated via interactions with the transmembrane Q subunit (T component) [20].

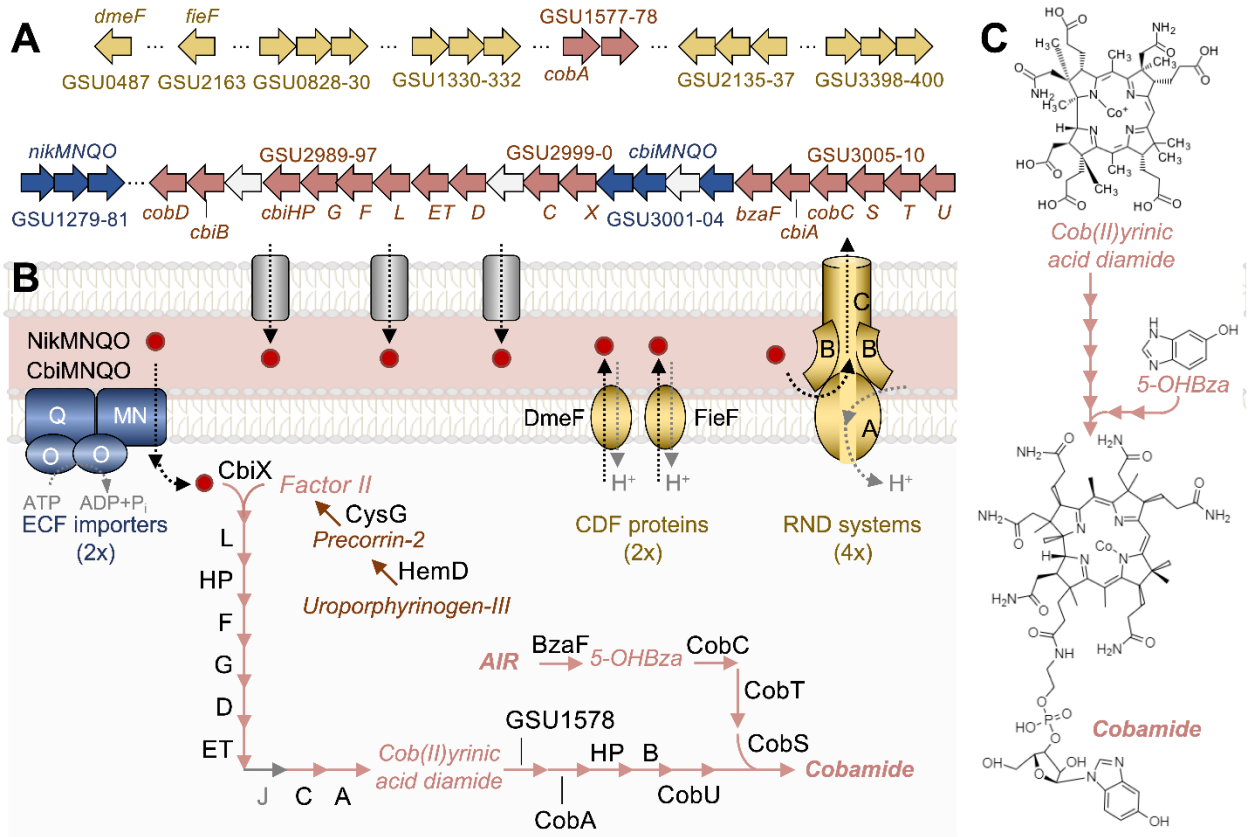

Figure 2.2 Genomic reconstruction of potential pathways for Co^{II} transport and assimilation in *G. sulfurreducens*. The genes (**A**) and model (**B**) show transmembrane ECF importers (in blue) as well as two CDF proteins for transmembrane export and four RND systems for exporting periplasmic metal across the outer membrane (gold color). Panel **B** also shows generic outer membrane porins for the simple diffusion of metal cations. The genome of *G. sulfurreducens* also encodes for Cbi (letter designation), Cob (full name) and other enzymes needed for the anaerobic synthesis of cobamide (pink arrows). The pathway starts with the incorporation by the cobaltochelatase CbiX of the metal into Factor II, which is synthesized from heme intermediates such as uroporphyrinogen-III. The genome encodes Cbi proteins that convert the Co^{II}-Factor II into cob(II)yrinic acid diamide, except for CbiJ (in gray) whose role in the pathway is yet to be experimentally validated. Cob (full name) and Cbi (only letters) proteins and other enzymes complete the synthesis of a cobamide with a 5-OHBza lower ligand (formula in **C**).

As shown in Fig. 2.2, the *cbiMNQO* genes are part of a large cluster (GSU2989-3010) encoding most of the enzymes needed for the anaerobic synthesis of a cobinamide intermediate (Cbi proteins) and its conversion into cobamide (Cob and Cbi proteins) [21]. We identified in a separate genomic location two additional cobamide biosynthetic

enzymes, GSU1578 and CobA (GSU1577). Also unlinked were two genes encoding enzymes for the methylation (HemD, GSU3286) and oxidation (CysG, GSU3282) of uroporphyrinogen III, the common precursor of cobamide and heme biosynthesis [21]. These two enzymes convert uroporphyrinogen III into Factor II, the preferred substrate for the anaerobic synthesis of cobamide [21]. The anaerobic cobaltochelatase CbiX (GSU3000) incorporates the metal into Factor II, while several Cbi proteins methylate, contract, amidate, and decarboxylate the molecule to generate a cobyrinic acid diamide intermediate (Fig. 2.2C). All of the proteins needed for these reactions were annotated or had a clear homolog in the genome of *G. sulfurreducens*, except for the precorrin-6X reductase CbiJ (highlighted in gray in Fig. 2.2B). This enzyme is often assigned to this reaction based on its homology with the aerobic enzyme CobK, but its biological role has never been confirmed [21]. The cob(II)yrinic acid diamide intermediate is then converted into adenosyl cobinamide in sequential reactions initiated by an adenosylcobamide-binding subunit of an (R)-methylmalonyl-CoA mutase (GSU1578). The step catalyzed by CobU (GSU3010) generates an adenosine-GDP-cobinamide substrate for attachment of the cobamide lower ligand. *G. sulfurreducens* produces a cobamide with a 5-hydroxybenzimidazole (5-OHBza) lower ligand (Fig. 2.2C) that is synthesized from 5-amino-imidazole ribonucleotide (AIR) by BzaF (GSU3005) [22]. The *bzaF* gene, which is unique to the *Geobacteraceae* and other members of the order *Desulfurococcales*, is a functional homologue of the *bzaA and bzaB* genes that catalyze the synthesis of 5-OHBza in other bacteria [22]. The attachment of the lower ligand to adenosine-GDP-cobinamide completes the synthesis of the cobamide (Fig. 2.2C).

At high enough concentrations, Co^{II} can also enter the inner membrane non-specifically via magnesium (Mg^{II}) uptake systems [23]. To compensate for the uncontrolled influx of the metal, cells express metal exporters [2]. We identified in the genome two genes (GSU0487 and GSU2613) encoding the cation diffusion facilitator (CDF) proteins, DmeF and FieF (Fig. 2.2). These proton-driven antiporters export a broad range of divalent cations (Co^{II}, Zn^{II}, Fe^{II}, Cd^{II} and Ni^{II}) across the inner membrane [24]. However, the preferred substrate for DmeF is Co^{II} [25] while FieF specializes in the export of excess Fe^{II} [26]. The intracellular accumulation of Co^{II} can disrupt the homeostatic balance with Fe^{II} and allow FieF to move more Co^{II} than Fe^{II} across the inner membrane. The genome also contains four tripartite metal efflux systems of the Resistance-Nodulation-Division (RND) superfamily [25] (Fig. 2.2). RND efflux pumps use the proton gradient to energize the export of cytoplasmic or periplasmic substrates [27]. Some of these exporters function as multidrug efflux pumps [28] while others specialize in proton-dependent transport of divalent metal cations [29,30]. As in other Gram-negative bacteria [28], the *Geobacter* metal RND systems contain a transmembrane pump, a periplasmic adaptor protein and an outer membrane porin. This trimeric configuration facilitates the export of periplasmic metals using the electrochemical gradient [28]. Collectively, inner and outer metal exporters ensure that Co^{II} does not accumulate to toxic levels inside the cytoplasm [2].

High Co^{II} tolerance in *G. sulfurreducens* suggests significant environmental exposure to the metal

As metal resistance evolves under selective pressure, we determined the growth efficiency of *G. sulfurreducens* in the presence of Co^{II} (Fig. 2.3). For these experiments, we inoculated cells at low densities (OD_{660}, ~0.03) in a medium optimized for growth of

G. sulfurreducens (DB medium) [31] with acetate and fumarate (DBAF medium) and supplemented with various concentrations of $CoCl_2$. We measured growth with up to 1 mM $CoCl_2$ (Fig. 2.3A), a concentration commonly used to enrich for metal-resistant bacteria from soils and industrial wastes contaminated with heavy metals [32]. Generation times increased (Fig. 2.3B) and planktonic biomass yields (maximum OD_{660} during entry in stationary phase) decreased (Fig. 2.3C) in a dose-dependent manner, as cells coped with higher levels of metal toxicity. For example, *G. sulfurreducens* cells doubled every 4.58(±0.05) hours in the untreated cultures, which we estimated to have approximately 27 μM of Co^{II} using an assay we developed for the colorimetric detection of $CoCl_2$ in the culture medium. Supplementation with an additional 100 or 250 μM $CoCl_2$ increased generation times to 5.41(±0.25) and 10.13(±0.54) hours, respectively (Fig. 2.3B). Generation times increased even more at higher $CoCl_2$ concentrations (500 and 1000 μM) and, on average, one out of three replicate cultures did not resume growth after a week (Fig. 2.3B). Furthermore, cultures that resumed growth did so after extended phases of acclimation (long *lag* phases before entering exponential phase) and reached lowest biomass yields (Fig. 2.3C).

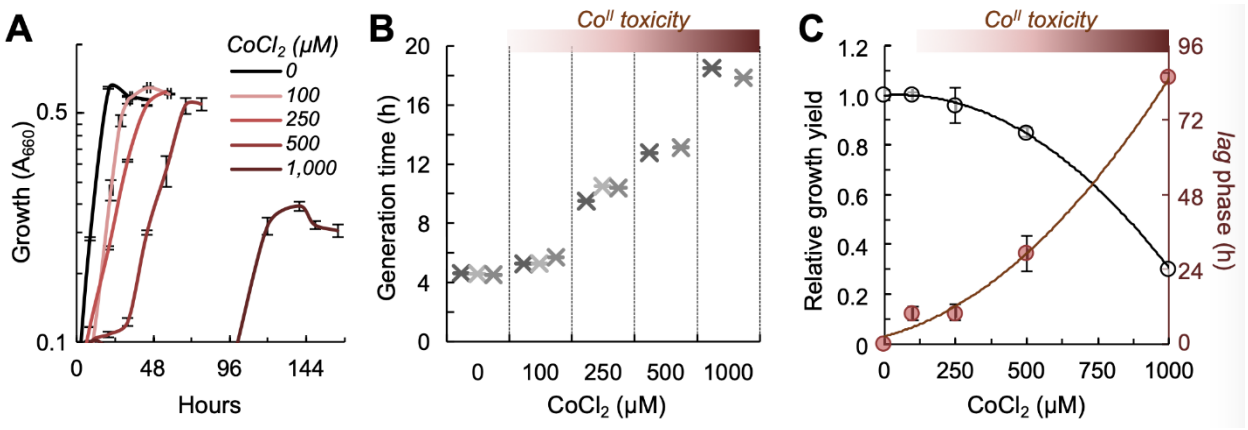

Figure 2.3 Effect of Co^{II} on *G. sulfurreducens* growth. (A) Cell growth (absorbance at 660 nm) in acetate-fumarate cultures with or without $CoCl_2$ supplementation (up to 1,000 μM). Data points for 0-250 μM $CoCl_2$ treatments show average and standard deviation of triplicate cultures. Treatments with 500 and 1,000 μM $CoCl_2$ show average and standard error of the only two replicates that resumed growth within a week. **(B-C)** Effect of Co^{II} toxicity on growth efficiency. Panel (**B**) shows generation (doubling) times for each of the replicates in the untreated (0 μM) and treated (100-1,000 μM) cultures shown in (**A**). Panel (**C**) shows the effect of the $CoCl_2$ treatment in reducing the culture's growth yields (OD_{660} in early stationary phase relative to the untreated 0 μM cultures) or in extending the *lag* phase (time before entry in exponential phase). The trendlines in **(C)** are the polynomial fits for the average data points of relative growth yields (R^2=0.999) and *lag* phases (R^2=0.994) from the cultures shown in (**A**).

Transcriptomic analysis reveals multiple mechanisms for Co^{II} detoxification

We gained insights into the mechanisms that allow *G. sulfurreducens* to cope with Co^{II} stress by comparing the transcript abundance of mid-log phase cells grown with or without 250 μM $CoCl_2$ supplementation (Fig 2.4). Co^{II} intoxication led to the differential expression of 47 genes. Of them, 32 were upregulated (Table 2.1) and 15 were downregulated (Table 2.2). This is approximately 0.9% (upregulated) and 0.4% (downregulated) of the genes annotated in the genome of *G. sulfurreducens*. Most of the upregulated genes encoded proteins with predicted roles in metal detoxification such as efflux pumps, protein and DNA repair enzymes, cell envelope modification pathways, and transcriptional regulation (Table 2.1). We also identified among the upregulated genes pathways for extracellular electron transfer that could provide a mechanism for energy transduction and Co^{II}

mineralization on the cell surface. By contrast, most of the downregulated genes coded for non-essential proteins with metal-binding domains or amino acids that Co^{II} is known to bind strongly (Table 2.2). Thus, their downregulation reduces the burden of Co^{II} retention in the cell's proteome.

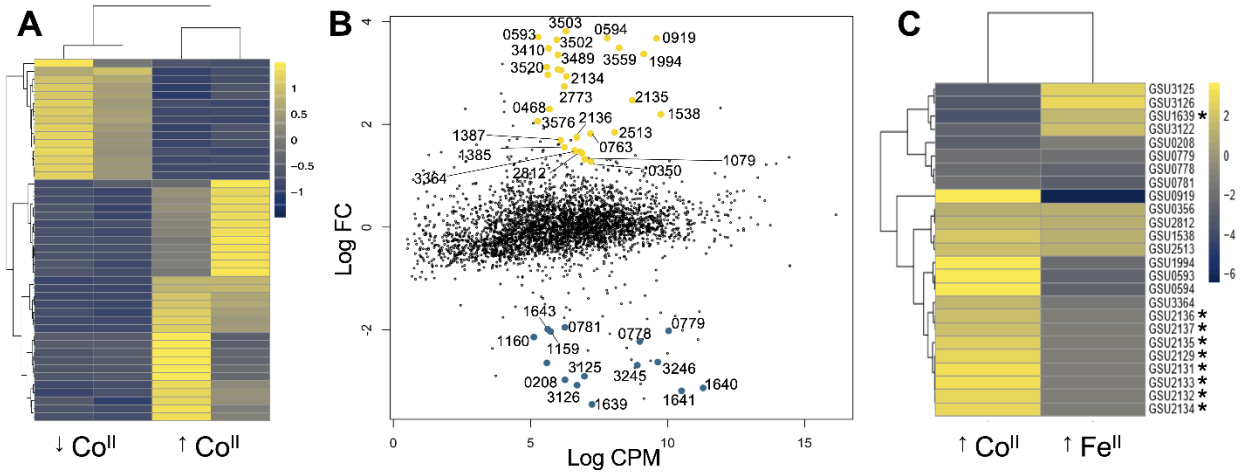

Figure 2.4 Transcriptional response of *G. sulfurreducens* to Co^{II}. (A) Heatmap of the transcriptional response in two replicates for the untreated ($\downarrow Co^{II}$) and treated ($\uparrow Co^{II}$) cultures. The datasets and statistical analyses of the expression data are provided in Supplementary file 1. **(B)** Dispersion plot of transcript abundance (log fold change [*log*FC] versus log counts per million [*log*CPM]) identifying the significantly upregulated (yellow) and downregulated (blue) genes. **(C)** Heatmap of genes differentially expressed with excess Co^{II} or Fe^{II}. The latter was calculated as the inverse ratio of the log_2 fold transcriptional changes reported for *G. sulfurreducens* cultures growing with sufficient versus excess Fe^{II} [33]. The asterisk shows genes under Fur control [33]. The calculations and data comparisons are provided in Supplementary file 2.

Periplasmic detoxification of Co^{II}.

The diffusion of Co^{II} through non-selective outer membrane porins [18] leads to its rapid accumulation in the periplasmic space and risks disruption of essential cellular functions such as protein secretion and respiration. Co^{II} toxicity in the periplasm is consistent with the upregulation of two periplasmic cytochromes (GSU1538 and GSU2513) with predicted roles in hydrogen peroxide (H_2O_2) detoxification (Fig. 2.5). This suggests that Co^{II} accumulated in the periplasm at levels high enough to catalyze Fenton-chemistry

reactions yielding reactive oxygen species (ROS) [5]. GSU1538 has the conserved domain of di-heme cytochrome *c* peroxidases (PF03150), a group of periplasmic enzymes that reduce H_2O_2 to prevent oxidative stress [34]. Bacterial cytochrome *c* peroxidases can receive electrons from small monoheme cytochromes [34]. The upregulation of GSU2513, a periplasmic monoheme cytochrome *c* protein, suggests a similar redox partnership with the GSU1538 peroxidase.

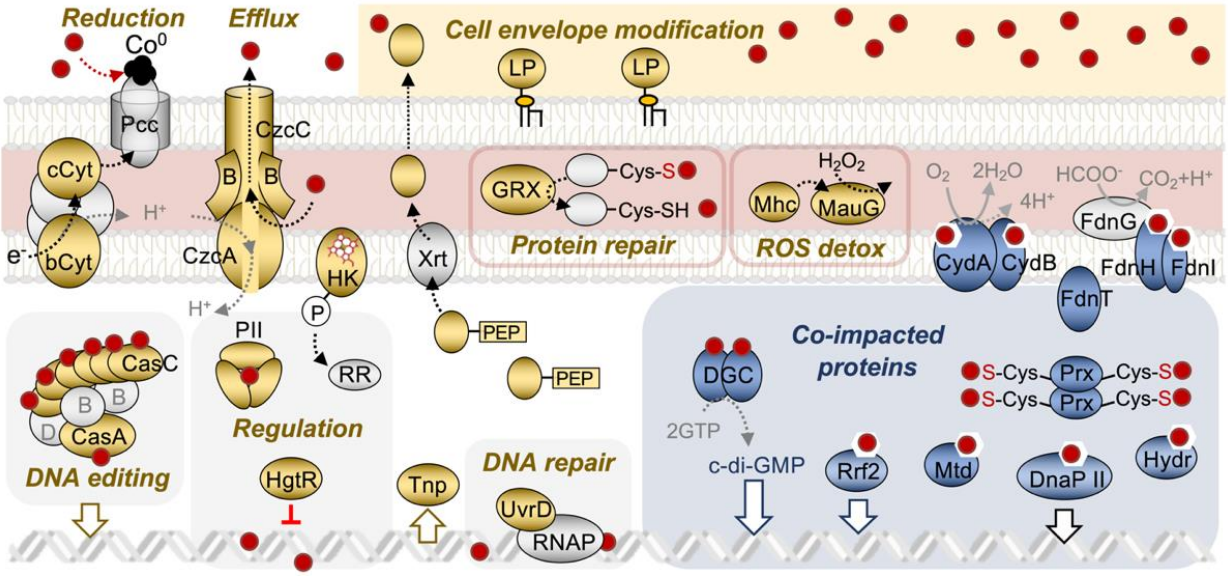

Figure 2.5 Transcriptional response of *G. sulfurreducens* during growth under Co^{II} stress. The figure illustrates pathways (upregulated, gold; downregulated, blue) differentially expressed under Co^{II} stress. Proteins in gray represent proteins predicted to participate in the detoxification pathways that did not undergo differential expression. Additional information for the proteins and encoding genes is available in Tables 2.1 and 2.2. Abbreviations: bCyt: Cytochrome *b;* CasABCD: CRISPR-Cas complex; b/cCyt: Cytochrome *b* or *c*; CydAB: Cytochrome *bc* oxidase complex; DGC: diguanylate cyclase; FdhT: formate dehydrogenase chaperone; FdnGHI: formate dehydrogenase; GRX, glutaredoxin; HgtR: hydrogen-dependent growth transcriptional regulator; HK: heme-binding histidine kinase; Hydr: Hydrolase; LP: lipoprotein; MauG: MauG-like diheme peroxidase; Mhc: monoheme cytochrome *c*; Mtd: mannitol dehydrogenase; PII: P-II family nitrogen regulator; Pcc: Porin-cytochrome complex; RNAP: RNA polymerase; UvrD: UV repair protein D (DNA helicase of the nucleotide excision repair pathway); Xrt: exosortase.

Co^{II}-stressed cells also upregulated GSU2812, a glutaredoxin-family protein (glutaredoxin motif, PF00462) containing a signal peptide (amino acids 1-27) for export to the periplasm. Glutaredoxins, like thioredoxins, are thioldisulfide oxidoreductases that

reduce or oxidize disulfide bonds depending on the redox potential of the cellular compartment (cytoplasm or periplasm) where they operate [35]. For example, *E. coli* secretes several thioredoxin proteins (e.g., DsbA, DsbC) to the periplasm to form disulfide bonds and fold proteins [36]. A periplasmic monothiol glutaredoxin (glutaredoxin 3, Grx3) complements the activities of DsbA and DsbC in reactions dependent on the glutathione biosynthetic pathway [35]. The high affinity of Co^{II} for thiol groups in cysteines leads to the rapid oxidation of the amino acid and the formation of non-native disulfide bonds, which glutaredoxins can resolve to prevent protein inactivation [37].

We also identified among the upregulated genes an operon containing the three subunits of one of the four RND systems (GSU2135-2137) identified in the genome of *G. sulfurreducens* (Fig. 2.2). This RND transporter has a membrane-bound metal pump (GSU2135) homologous to CzcA from *Cupriavidus metallidurans* strain CH34 and CusA from *E. coli* [27]. The pump binds the metal in the periplasm and undergoes conformational changes that move one proton into the cytoplasm and translocate the metal through a channel formed by the B and C subunits (Fig. 2.5). CusABC complexes often work coordinately with periplasmic metal chaperones (CusF) to transport monovalent cations (Cu^{I} and Ag^{I}). The lack of CusF chaperones in the *G. sulfurreducens* genome suggests that the Co^{II} RND transporter is a CzcABC system. Indeed, CzcABC transporters receive their name for their ability to mobilize the divalent cations cobalt, zinc and cadmium [27]. Furthermore, this metal efflux system plays roles in Co^{II} detoxification and resistance in other bacteria [38]. Thus, we designated the GSU2135-2137 genes as *czcABC* (Table 2.1).

Cytoplasmic detoxification of Co^{II}.

The first gene in the *czcABC* operon (GSU2134) codes for a protein with the conserved P_{II} domain (PF00543) of nitrogen regulatory proteins. These proteins form homotrimers to bind metabolites signaling the energy (ATP, ADP), carbon (2-oxogluratate) and nitrogen (glutamine and 2-oxoglutarate) levels inside the cell [39]. GSU2134 belongs to a phylogenetically distinct clade of proteobacterial P_{II} proteins (PII-NG) that evolved from canonical nitrogen regulators GlnB and GlnK [40]. Like most of the PII-NG proteins [40], GSU2134 clusters in the genome with the genes encoding a proton-cation CzcABC antiporter. Furthermore, PII-NG is a structural homolog of the metal-binding protein CutA1 of *E. coli* [41]. CutA1 binds the divalent copper cation (Cu^{II}) at a site structurally equivalent to the ATP binding site of PII-NG proteins [41] and uses metal binding to regulate genes involved in Cu^{II} tolerance [42]. The structural homology of PII-NG and metal sensors and its cytoplasmic location are consistent with a role in intracellular Co^{II} sensing and modulation of the regulatory cascade needed for cell acclimation to metal stress.

Indirect effects of Co^{II} stress on Fe^{II} homeostasis.

In *G. sulfurreducens,* the operon encoding the PII-NG regulator (GSU2134) and CzcABC proton/metal antiporter (GSU2135-2137) is also upregulated under Fe^{II} limitation via the master regulon of Fe^{II} homeostasis, Fur [33]. To test if Co^{II} intoxication could indirectly limit the availability of Fe^{II}, we used published transcriptomic data for *G. sulfurreducens* grown with sufficient versus excess Fe^{II} [33] to identify genes differentially expressed under Fe^{II} intoxication. More than half of the genes responding to Co^{II} stress (24 in total) were also differentially expressed during Fe^{II} intoxication (Fig. 2.4C). Most of the genes had opposite patterns of expression, supporting the idea that Co^{II} intoxication limits Fe^{II}

availability. For example, a cluster of Fur-regulated genes comprised of the PII-NG-*czcABC* operon (GSU2134-2137) and upstream genes (GSU2129, GSU2131-33) were upregulated by Co^{II} intoxication but downregulated in cells growing with excess Fe^{II}.

We also identified a protein (GSU1639) with the conserved Rrf2 domain (PF02082) of Fe^{II}-dependent transcriptional regulators [43,44] that was downregulated under Co^{II} stress but upregulated during Fe^{II} intoxication (Fig. 2.4C). The Rrf2 domain ligates Fe or Fe-S clusters via redox-sensitive cysteine residues to tune the protein's DNA specificity to Fe^{II} homeostasis [45]. For example, the Rrf2 domain of *E. coli* IscR has three cysteines and one glutamic acid that bind Fe-S clusters, changing its DNA recognition to regulate genes involved in Fe-S cluster to Fe^{II} availability [44]. GSU1639 shares 55% similarity (33% identity) with IscR and has the conserved cysteines and glutamic acid needed for Fe-S cluster coordination at the Rrf2 domain. Furthermore, it is under direct control of Fur, the master regulator of Fe^{II} homeostasis [33]. This suggests that GSU1639 binds Fe-S clusters to co-regulate the cluster's biosynthetic pathways to Fe^{II} homeostasis. Co^{II} infiltration in Fe-S clusters and/or its high affinity for the cysteines in the Rrf2 binding site could prevent the regulator from sensing the Fe-S cluster signal and impair the ability of the cells to sense Fe^{II} availability.

Co^{II} but not Fe^{II} intoxication upregulated the hydrogen-dependent growth transcriptional repressor HgtR (GSU3364), a master regulator of central metabolism (Fig. 2.4C). HgtR downregulates genes involved in energy generation and biosynthesis such as *gtlA* (citrate synthase in TCA cycle), *atpG* (ATP synthase F0 β' subunit), and *nuoA* (NADH dehydrogenase I, A subunit) to tune growth rates to the cell's nutritional status [46]. The overexpression of the repressor provides a mechanism to adjust growth to the energy

demands of cells coping with Co^{II} intoxication and low Fe^{II} availability. Fe^{II} limitation may have also triggered the induction of GSU0356, a heme-binding sensor histidine kinase that could regulate the cellular response to the accumulation of metal-free or Co^{II}-impacted heme groups (Table 2.1). The heme sensor lacks a signal peptide but contains three internal helices for insertion in the inner leaflet of the inner membrane, a subcellular localization optimal for cytoplasmic sensing. In addition to phosphoacceptor (HisKinA, PF00512) and ATPase (HATPase, PF02518) domains, GSU0356 has a domain of unknown function (DUF3365, PF11845) with a heme-binding site (CXXCH sequence). Heme-responsive histidine kinases typically bind the heme group reversibly [47]. This sensory capacity allows the proteins to prevent the toxic build-up of metal-free hemes [48]. The upregulation of the heme sensor during Co^{II} and Fe^{II} intoxication (Fig. 2.4C) suggests that both conditions may have resulted in heme toxicity.

Evidence for DNA damage.

Co^{II}-stressed cells upregulated components of one of the two Type I CRISPR loci (CRISPR2) in *G. sulfurreducens* (GSU1385 and GSU1387) (Table 2.1). The CRISPR2 locus (GSU1384-1393) contains 8 CRISPR-associated (Cas) proteins and an array with 143 spacers. The locus lacks a Cas4 protein but has Cse1 and Cse2 (named after the CRISPR system of *E. coli*) components, meeting the criterion for classification as a subtype I-E CRISPR [49]. Co^{II}-stressed cells upregulated Cse1 (GSU1385, also known as CasA), the large subunit of the antiviral defense Cas complex (Cascade) that facilitates RNA-guided recognition of complementary DNA [50]. Cse1 recognizes a short protospacer adjacent motif (PAM) in the crRNA and discriminates self from foreign DNA targets [51]. A Zn-finger motif in Cse1 binds Zn^{II} to control interactions with the target DNA [52]. This

structural motif is sensitive to infiltration by Co^{II}, a metal that changes the selectivity of the Cas complex for the target DNA and stimulates its nicking activity [53]. Co^{II} also upregulated Cse4 (GSU1387, also known as CasC or Cas7), a protein that polymerizes as a hexameric arch along the spacer region of the crRNA within the Cascade complex [54]. Cse4 has a ferredoxin-like fold in its RNA recognition motif [50] with a conserved metal-binding βαββαβ fold that could bind Co^{II} [55,56]. The final result is a Co^{II}-compromised Cascade complex with increased nicking activity that could lead to DNA damage. Co^{II} can also infiltrate the DNA helix and cause structural changes and breaks in the strands [57]. Consistent with the need to repair damaged DNA, cells upregulated a UvrD helicase (GSU0763) of the nucleotide excision repair pathway. UvrD can also bind RNA polymerase (RNAP) stalled on the DNA lesions and backtrack the enzyme to expose the damaged site to DNA repair proteins [58]. This mechanism allows the RNAP to resume transcription as soon as the repair has concluded.

Downregulation of non-essential metalloproteins.

Most of the downregulated genes encoded non-essential proteins with prosthetic groups, metal-binding motifs and amino acids sensitive to Co^{II} inactivation (Table 2.2). Almost all of the targets where cytoplasmic or periplasmic redox-active proteins with Fe^{II}-prosthetic groups (e.g., hemes and Fe-S clusters) or proteins with thiol-containing cysteines that Co^{II} readily binds and inactivates (Fig. 2.5). For example, metal-stressed cells downregulated the two subunits (CydAB) of the cytochrome *bd* complex (GSU1640-1641), a respiratory quinol:O_2 oxidoreductase widespread in prokaryotes that conserves energy from the transfer of electrons from the menaquinone pool to O_2 [59]. Thus, the CydAB complex is not needed under the strictly anaerobic conditions used in our study.

Similarly, cells downregulated two subunits (GSU0778-0779) of the trimeric formate dehydrogenase enzyme, FdnGHI, and the associated secretory protein FdnT (GSU0781), which are only needed when growing with formate as electron donor. Another example of a downregulated protein is Prx-2 (GSU3246), a cytoplasmic thioredoxin peroxidase of the 2-cysteine peroxiredoxin subfamily [60]. These thiol-based peroxidases scavenge the low levels of H_2O_2 produced intracellularly during normal growth and transduce the H_2O_2 signal to control cellular homeostasis [61]. When hyperoxidized, however, the enzymes aggregate and become chaperone holdases to protect proteins from denaturation [61]. The affinity of Co^{II} for the thiol groups of peroxiredoxins could impair these functions. Thus, cells downregulate its expression to minimize negative impacts of metal inactivation on the cellular stress response.

Reductive precipitation of Co^{II} as a detoxification mechanism

We identified among the most upregulated genes two cytochrome-encoding genes (GSU0593 and GSU0594) that could participate in the extracellular reduction of Co^{II}. GSU0593 and GSU0594 are the cytochrome *b* (CbcB) and cytochrome *c* (CbcA) subunits, respectively, of the Cbc5 menaquinol:ferricytochrome *c* oxidoreductase, a pentasubunit complex that expressed during the reduction of Fe^{III} oxide minerals [62]. The cytochromes (*b* and *c1*) and Fe-S proteins in this type of cytochrome *bc* complexes transfer electrons from the menaquinone pool via a proton motive Q-cycle pathway [63]. To complete the Q cycle, Cbc5 catalyzes two “redox turnovers” that consume two protons in the cytoplasm and release four protons in the periplasm. Thus, each Q cycle transfers two electrons and contributes two protons to the transmembrane proton gradient. The Cbc5 complex could electronically connect with extracellular electron acceptors through

Geobacter outer membrane porin-cytochrome *c* complexes (Pcc) [64]. Given the known role of Pcc complexes in the reductive precipitation of other divalent cations to their elemental, metallic form [65], we examined untreated and Co^{II}-treated cells by transmission electron microscopy (TEM) for the extracellular formation of metal nanoclusters (Fig. 2.6A). To prevent artifactual mineralization of heavy metal salts used to negatively stain cells for TEM [66], we examined unstained cells. This approach allowed us to visualize numerous electron dense nanoparticles on the surface of Co^{II}-stressed cells that were absent in untreated samples (Fig. 2.6A). The homogenous dispersal of the nanoclusters is consistent with the distribution of outer membrane cytochrome foci in *G. sulfurreducens* [64]. Further, X-ray energy dispersive spectroscopy (EDS) analyses confirmed the presence of Co on the outer surface of the treated cells but not in cell-free controls, consistent with the immobilization of the metal on the cell surface (Fig. 2.6B). Using a colorimetric assay based on the color response of Co^{II} when bound by 2-beta-mercaptoethanol (Fig. 2.6B), we estimated that Co^{II}-stressed cells had removed from the solution an average of 25 μM of the metal (Fig. 2.6C). These results suggest that the detoxification response of *G. sulfurreducens* also included pathways for Co^{II} mineralization, as reported for the uranyl cation [67].

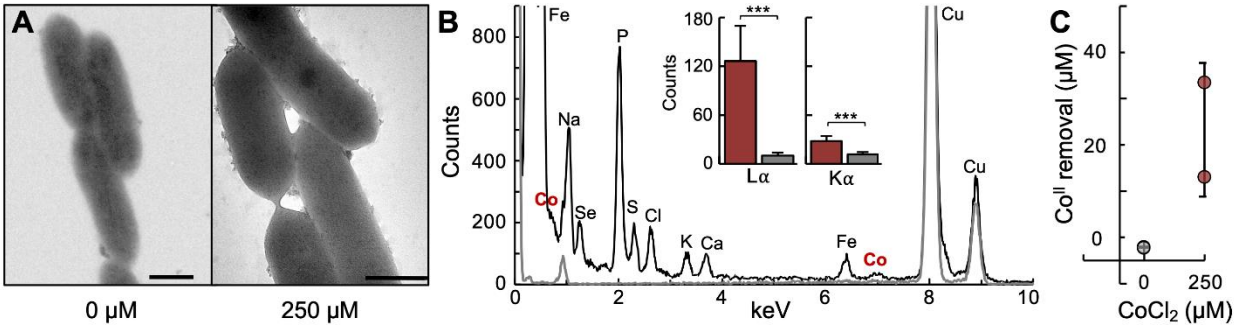

Figure 2.6 Co^{II} mineralization at the cell outer surface. (A) Transmission electron microscopy (TEM) images of unstained cells from untreated (0 µM $CoCl_2$) and treated (250 µM $CoCl_2$) cultures. Scale bar, 500 nm. **(B)** Representative X-ray energy dispersive (EDS) spectra of cells from 250 µM $CoCl_2$ cultures (black) and cell-free control areas examined by TEM identifying Co energy signatures from the cells. The inset shows the average energy intensity (counts) detected for the primary X-ray Co emission peaks (Lα, 0.776 keV; Kα, 6.924 keV) for four different cells (maroon) and control (gray) samples. Pairwise comparisons (*t*-test) between the cell and cell-free Lα and Kα average intensities produced *p* values below 0.0001 (***). **(C)** Co^{II} removal by cells in cultures with or without 250 µM $CoCl_2$ supplementation. The initial and final (early stationary phase) Co^{II} concentrations in culture supernatant fluids were calculated colorimetrically after complexation with 2-beta-mercaptoethanol and using a standard curve (linear fit from 0 to 500 µM $CoCl_2$; $R^2 = 0.9947$). The difference between the final and initial concentration of Co^{II} was the amount of metal removed by the cells.

Cell envelope modifications to prevent Co^{II} infiltration and form biofilms

The transcriptomics analyses identified lipoproteins (GSU2133 and 3576) and EPS-associated proteins (GSU1079 and GSU1994) that could have modulated the properties of the cell surface to prevent metal infiltration and promote its extracellular immobilization [68]. At least one of the lipoproteins was predicted to be targeted to the outer membrane, the other one could only be confirmed as non-cytoplasmic (Table 2.1). Lipid modification of exported hydrophilic proteins facilitates their anchoring to the inner leaflet of the outer membrane yet most, if not all, of the lipoproteins get translocated to the outer leaflet [69,70]. Surface-exposed lipoproteins control the permeability of the cell to soluble substrates and can also mediate cell adhesion [69]. Additional modifications to the cell envelope are expected from the upregulation of two proteins (GSU1079 and GSU1994) carrying the

PEP-CTERM motif (PF07589) of EPS-associated proteins [71]. The motif comprises a carboxy-terminal (CTERM) Pro-Glu-Pro (PEP) recognition peptide, a transmembrane helix and an arginine-rich cluster [71]. The protein sorting signal is recognized and cleaved by a dedicated exosortase (Xrt) in the inner membrane and the mature protein is then exported to the EPS matrix by yet unknown secretory pathways [71]. Except for the presence of the conserved sorting signal, PEP-CTERM proteins have little homology to other proteins. Most are, however, rich in serine and threonine, suggesting they are glycosylated during export [72]. The genome of *G. sulfurreducens* encodes 5 PEP-CTERM proteins, an EpsH family Xrt exosortase (GSU1979) and a two-component system (PrsK histidine kinase, GSU1941; PrsR response regulator, GSU1940) predicted to regulate export [71].

The widespread presence of PEP-CTERM proteins in Gram-negative bacteria that form biofilms suggests a role for these proteins in the development of surface-attached communities [71]. In support of this, the expression of EPS-associated proteins in Co^{II}-stressed cells of *G. sulfurreducens* preceded the formation of thick biofilms at the bottom of the tube once the cultures reached stationary-phase (Fig. 2.7A). We did not identify in the transcriptome any of the genes that encode proteins required for the synthesis of the biofilm EPS, Xap [73]. This is not unexpected, because *G. sulfurreducens* expresses the *xap* genes during exponential growth in acetate-fumarate cultures [73]. The Xap EPS anchors outer membrane cytochromes [73] and provides a mechanical and redox barrier to the permeation of soluble divalent metal cations in biofilms [68]. To test for a similar protective effect by the EPS produced by planktonic cells, we challenged mid-log phase cultures with up to 1 mM concentrations of $CoCl_2$ and monitored the effect of the metal

treatments in growth (OD_{660}). As shown in Fig. 2.7B, metal shock had little effect on growth efficiency in any of the cultures. Such high levels of metal resistance are consistent with the role of the EPS matrix in preventing metal permeation. Furthermore, planktonic cultures challenged with the metal did not form thick biofilms in stationary phase (Fig. 2.7A). Thus, biofilm formation appears to be an adaptive response to persistent metal toxicity.

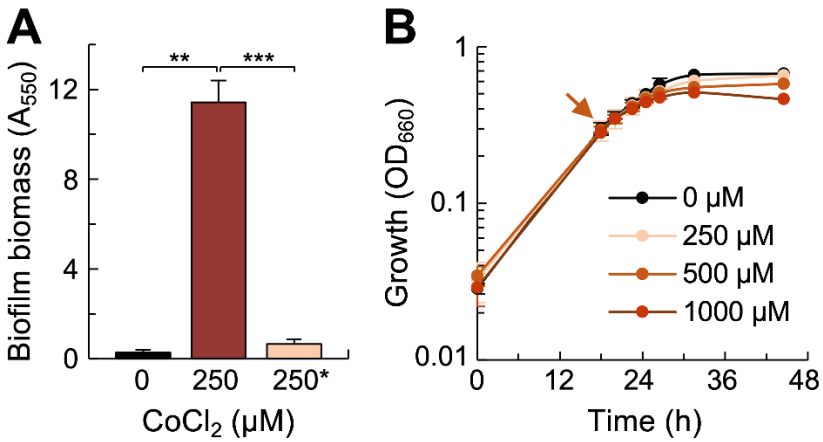

Figure 2.7 Adaptive responses of cells to Co^{II} stress. (A) Biofilm formation in stationary phase cultures growing with 250 μM $CoCl_2$ compared to the lack of biofilms in cultures growing without $CoCl_2$ supplementation (0 μM) or challenged with the $CoCl_2$ in mid-log phase (~0.3 OD_{660}) (250*). Statistically significant differences in pairwise comparisons (*t*-test) are highlighted with asterisks (p<0.0002 [**] or p<0.0001 [***]). **(B)** Planktonic growth of cultures challenged with increasing concentrations of $CoCl_2$ (arrow) in mid-log phase (~0.3 OD_{660}), including the ones used for the biofilm assays shown in panel (**A**) (250*).

DISCUSSION

The high Co^{II} tolerance and complex acclimation response of *G. sulfurreducens* is consistent with selection mechanisms during long-term environmental exposure to the metal. Fe^{III} and Mn^{IV} oxides form heterogenous mixes with natural organic matter and metal micronutrients [74] that provide optimal conditions for the growth of *Geobacter* species [13]. The high reactivity of the Fe^{III} and Mn^{IV} (hydr)oxides sequesters Co^{II} and other

metal cations in the mineral phases [11,12], concentrating them in the metal oxide-rich epigenetic zones [17]. The reductive dissolution of the metal-bearing minerals mobilizes the metal cations [74] and increases their concentration in the pore-water to toxic levels [40]. Cu^{II}, for example, can be mobilized to levels (~20 μM) above the minimum concentration (10 μM) that inhibits the growth of *G. sulfurreducens* in the laboratory [75]. Yet, this bacterium grew from low cell densities, albeit with trade-offs in growth efficiency, in the presence of up to 1 mM $CoCl_2$ (Fig. 2.3). Furthermore, it was relatively unaffected when exposed to the same metal concentrations during the exponential phase of growth (Fig. 2.7). We attributed this to the expression in exponentially-growing cells of the biofilm EPS [73], which can shield the cells from metal infiltration. Cell density can also affect cellular metabolism and the secretion of metabolites that change the chemical speciation, bioavailability, and toxicity of metals [76]. Furthermore, increases in cell numbers activate stress responses that acclimate the population and increase tolerance to a number of stressors [77]. By contrast, cells inoculated at low cell densities must first reprogram their physiology to acclimate to the presence of the stressor. Acclimation is evident in the extended periods of growth arrest (*lag* phase) that *G. sulfurreducens* cultures experienced when growing with sublethal concentrations of $CoCl_2$ (Fig. 2.3) and in the multiple cellular pathways that were activated to couple growth to Co^{II} detoxification (Fig. 2.4).

The transcriptomic studies provided insights into the extensive transcriptional reprogramming that allowed *G. sulfurreducens* to cope with Co^{II} stress (Fig. 2.5). Transcript levels for Co^{II} importers remained constant, consistent with the absence in *G. sulfurreducens* of transcriptional regulators (e.g., CzrA and CoaR) that other bacteria use to directly control Co^{II} uptake for metal homeostasis [56]. Instead, *G. sulfurreducens*

acclimation involved metal (PII-NG) and heme (GSU0356 histidine kinase) sensors and a transcriptional regulator of central metabolism (HgtR) (Fig. 2.5). Cells also upregulated a CzcABC pump for proton-driven export of metal traversing the outer membrane, a canonical mechanism used by other Gram-negative bacteria to increase metal resistance [38]. In addition, Co^{II} upregulated a periplasmic glutaredoxin, which repairs and rejoins cysteines oxidized by Co^{II} to refold proteins to their native and functional conformation [78]. The activation of a periplasmic MauG-like di-heme cytochrome *c* peroxidase (GSU1538) suggested that Co^{II} accumulated in the periplasm at levels sufficiently high to generate H_2O_2 [5]. Di-heme cytochrome *c* peroxidases detoxify H_2O_2 in the periplasm by reducing it to two H_2O molecules [34]. This reaction receives electrons from a dedicated electron donor such as the monoheme cytochrome GSU2513, which was also upregulated by Co^{II} (Table 2.1). Without the peroxidase-cytochrome pair, H_2O_2 would oxidize solvent-exposed [4Fe-4S]$^{2+}$ clusters in proteins, producing inactive [3Fe-4S]$^{3+}$ species that abolish the redox activity of the metalloprotein [79]. The detoxification of H_2O_2 is also important to prevent Fenton-like reactions that generate highly toxic $^{\bullet}OH$ radicals and exacerbate oxidative stress [80].

Despite mechanisms for periplasmic detoxification, Co^{II} may have infiltrated the cytoplasm and damaged essential macromolecules. The presence of cytoplasmic chelators such as glutathione facilitates reactions between Co^{II} and H_2O that generate ROS and oxidatively damage DNA [80]. Co^{II} can also bind components of the CRISPR Cascade complex that mediates antiviral defense, changing its specificity for target DNA and stimulating its RNA-independent DNA cleavage activity [53]. To cope with DNA damage, *G. sulfurreducens* activated the expression of UvrD, a helicase of the nucleotide

excision repair pathway [81] and transcription-coupled repair [58]. The latter is particularly important to maintain the transcriptional activity of the cell during metal intoxication. This is because UvrD associates with NusA to backtrack RNAP when stalled at a DNA lesion. The helicase then recruits the UvrAB repair complex to the damaged site [58]. This intervention allows the RNAP to resume transcription as soon the lesion is repaired [81].

The Irving-Williams series (Mn^{II} <Fe^{II} <Co^{II} <Ni^{II} <Cu^{II} >Zn^{II}) predicts greater stability for Co^{II} than Fe^{II} or Mn^{II} complexes independently of the ligand [82]. As a result, Co^{II} intoxication preferentially impacts Fe^{II} and Mn^{II} metalloproteins. To prevent the retention of the toxic metal in the metalloproteome, *G. sulfurreducens* downregulated non-essential proteins with Fe^{II} prosthetic groups (Fig. 2.5). Nearly all of the downregulated proteins contained Fe-S clusters or metallocenters coordinating Fe^{II} atoms (Table 2.2). The chemical similarities with Fe^{II} facilitate the infiltration of Co^{II} into Fe-S clusters but the greater electron density of Co^{II} alters the coordination of the metal with the enzyme and its activity [56,83]. Co^{II} is also able to compete with Fe^{II} for binding to the porphyrin ring of heme groups such as those in cytochromes [83]. This could be catastrophic in the periplasm, where heme-containing respiratory chains are particularly abundant. Co^{II}-hemes are weaker transporters of charges than the native Fe^{II}-hemes [84], impairing, or even abolishing, respiratory growth. To compensate for this, *G. sulfurreducens* downregulated non-essential heme-containing proteins such as the cytochrome *bd* oxidase subunits CydAB required for aerobic respiration (Fig. 2.5). Similarly, cells downregulated genes encoding the formate dehydrogenase complex (the Fe-S cluster protein FdnH and the cytochrome *b* FdnI) and the secretory accessory protein FdnT, as these proteins are only needed for formate-dependent growth. Cells also downregulated

an Rrf2 protein (GSU1639), which uses cysteine residues to bind Fe-S clusters and co-regulate Fe-S cluster biosynthesis and Fe^{II} homeostasis [44]. The high affinity of Co^{II} for cysteines may prevent Rrf2 protein from sensing Fe-S cluster availability in the cytoplasm. To prevent further deregulation of Fe^{II} homeostasis, cells downregulated the *rrf2* gene.

The principles of the Irving-Williams series [82] also explain the high affinity of Co^{II} for Fe^{II}-heme. Downregulating non-essential proteins with Fe^{II}-hemes can provide some partial relief (Table 2.2). However, Co^{II} can also infiltrate the Fe^{II}-hemes during their biosynthesis and prevent their incorporation into proteins. This leads to the accumulation of free Co^{II}-hemes in the cytoplasm and cytotoxicity [85]. The upregulation of a heme-containing histidine kinase (GSU0356) (Table 2.1) could provide a mechanism to sense the impact of Co^{II} on the heme pool and coordinate the heme detoxification response, as reported in other bacteria [86]. The advantage of this heme-sensing mechanism is that cells can simultaneously co-regulate heme biosynthesis to Co^{II} and Fe^{II} homeostasis [48]. We initially reasoned that Co^{II} infiltration in the free hemes could have increased the intracellular levels of Fe^{II} and exacerbate metal toxicity [85,86]. For example, free Fe^{II}, like Co^{II}, can generate ROS via Fenton chemistry and cause intracellular damage [87]. However, although Co^{II} and Fe^{II} intoxication had overlapping transcriptional responses, most of the shared gene targets were reversely regulated (Fig. 2.4C). Thus, cells faced conditions of Fe^{II} limitation during Co^{II} intoxication. The accumulation of Co^{II} in the periplasm could competitively exclude Fe^{II} from import across the inner membrane, reducing its intracellular availability. Furthermore, once removed from metalloproteins and prosthetic groups, Fe^{II} can be sequestered non-specifically by cytoplasmic chelators, effectively reducing its intracellular availability.

In addition to mechanisms for metal detoxification in the periplasm and cytoplasm, *G. sulfurreducens* induced pathways that could have promoted the extracellular immobilization of the metal. For examples, cells upregulated outer membrane lipoproteins that could have modulated the permeability of the outer membrane [18] and/or function as adhesins to promote cell-cell aggregation [69]. Additionally, Co^{II} triggered the expression of EPS-associated proteins (PEP-CTERM proteins) typically expressed by biofilm-forming bacteria [71]. The synthesis by planktonic cells of *G. sulfurreducens* of the biofilm EPS (Xap) precedes biofilm formation and allows the cell to anchor to the Xap matrix cytochromes needed for metal reduction [73]. This redox activity could allow the planktonic cells to reductively precipitate Co^{II} on the cell surface, generating the metal nanoclusters visualized by TEM (Fig. 2.6A). The mineral particles resolved by TEM formed on discreet foci on the cell surface, similarly to the distribution of outer membrane cytochromes of the Pcc complexes [88]. Furthermore, the Pcc outer membrane cytochromes can bind and reductively precipitate divalent metal cations to their elemental form (e.g., Hg^{II} to Hg^{0}) [65]. A similar reaction could allow the cytochromes to reductively precipitate Co^{II} to Co^{0} on the cell surface. The Pcc outer membrane cytochrome complexes contain periplasmic and extracellular *c*-type cytochromes within an outer membrane porin to electronically connect periplasmic carriers to extracellular electron acceptors [64]. The upregulation by Co^{II} of a respiratory cytochrome *bc* complex (Cbc5) could provide a mechanism for energy conservation from the reduction of Co^{II} at the Pcc foci (Fig. 2.5). The Cbc5 complex is anchored to the inner and outer membranes and could interact with the periplasmic cytochrome of the Pcc complex to complete the electron transfer pathway to Co^{II} (Fig. 2.5). We did not detect any of the Pcc genes in the Co^{II} transcriptome but confirmed the

upregulation of the Pcc outer membrane *c*-cytochrome OmcC (GSU2731) when the false discovery rate (FDR) threshold was increased from 0.05 to 0.08. This could indicate that some cells may be upregulating the PccC cytochrome. Experimental testing of this hypothesis is warranted.

The expression of lipoprotein adhesins and a redox-active EPS could also have allowed cells to aggregate and form biofilms (Fig. 2.7A), an adaptive response that confers on *G. sulfurreducens* increased resistance to soluble, toxic metals [68]. The downregulation of a cytoplasmic diguanylate cyclase (DGC) with a canonical GGDEF domain (GSU1643) (Table 2.2) in Co^{II}-stressed cells may have reduced the intracellular levels of c-di-GMP in order to regulate the planktonic-to-biofilm transition. Most DGC enzymes contain sensory domains that modulate the synthesis of the bacterial second messenger bis-(3′ ,5′)-cyclic dimeric guanosine monophosphate (c-di-GMP) to specific input signals, including metals. For example, Zn^{II} reversibly binds the subunits of the *E. coli* DgcZ dimer (formerly YdeH) to allosterically regulate the synthesis of c-di-GMP [89]. The *Geobacter* DGC enzyme does not have metal-binding domains but has instead the N-terminal phosphoreceiver (REC) domain of DGCs in the PelD superfamily (Table 2.2). The best studied PelD-like DGC is WspR, the response regulator of the Wsp chemosensory pathway, which regulates cell-cell aggregation and biofilm formation in *Pseudomonas aeruginosa* [90]. Phosphorylation of the receiver domain in the WspR dimer activates the synthesis of c-di-GMP and autoaggregative/biofilm phenotypes [91]. Mg^{II} cations bind near the receiver's active site of the WspR dimer and contribute to its activity [92]. The downregulation in Co^{II}-stressed cells of the DGC enzyme could reflect a feedback mechanism to the infiltration of Co^{II} in the protein [56]. Alternatively, Co^{II}-stressed cells may

have downregulated the WspR-like DGC to reduce GTP demand for c-di-GMP and increase the availability of the nucleotide triphosphate for EPS synthesis [93]. The EPS matrix can then promote cell-cell aggregation and biofilm formation as a protective mechanism against metal toxicity [68].

Biofilm formation in *G. sulfurreducens* embeds the cells in an electroactive biofilm matrix of cytochromes and conductive pili that effectively immobilizes metals outside of the cells [68]. The conductive pili are particularly important to overcome metal toxicity because they provide a large redox surface area for the extracellular immobilization and reductive precipitation of toxic metals [67,68]. The pilus surface is decorated with specialized motifs optimal for the coordination of divalent metal cations [94]. These metal traps have high affinity for Co^{II} and, at high enough potentials, can reductively precipitate it as Co^{0} nanoparticles [14]. Furthermore, the conductive pili are retractable appendages [95], a dynamic feature that allows cells to detach the minerals and recycle the structural peptides in the membrane for a new cycle of pilus polymerization and metal reduction [96]. We did not identify in the Co^{II} transcriptome any of the genes encoding proteins of the pilus biosynthetic apparatus (Table 2.1) nor did we observe pilus filaments by TEM (Fig. 2.6). This was not unexpected because we used growth temperatures (30^{o}C) that prevent pilus assembly in planktonic cells [67,97]. Under these conditions, cytochrome respiratory chains involving Pcc cytochromes provided the primary pathway for extracellular electron transfer in CoII-stressed cells. Thus, Pcc cytochromes could have promoted the mineralization of Co^{II} on discreet surface foci as a detoxification mechanism (Fig. 2.6).

The presence of metal nanoclusters on the surface of Co^{II}-treated cells suggests that hitherto unknown biological reactions could contribute to the geochemical cycling of

this important metal. We estimated that, on average, cells removed from the solvent 25 μM concentrations of Co^{II} (Fig. 2.6C). As a comparison, the intracellular Co^{II} quota is in the low to sub-μM range and typically below the limits of detection of mass spectrometry assays [3]. Co^{II} biomineralization may be more significant in biofilms, thanks to the concentration in the biofilm matrix of conductive pili [68,98] with high affinity motifs for Co^{II} binding and reduction to Co^0 [14]. These adaptive responses confer on *Geobacter* a competitive advantage for growth in metal-rich environments despite the mobilization of Co^{II} during the reductive dissolution of metal oxide mineral phases. The ability of *Geobacter* bacteria to reductively precipitate Co^{II} could also alleviate metal stress on syntrophic partners that depend on interspecies cobamide transfer to sustain their metabolism. Furthermore, the formation of Co^0 nanoparticles effectively metallizes the cell surface and could allow *Geobacter* cells to gain energy from the reduction of low potential electron acceptors and to transfer respiratory electrons with syntrophic partners. Hence, Co^{II} mineralization may help define the niche space of *Geobacter*-driven microbiomes and provide molecular markers to predict the impact of their activities in the fate of this and other essential elements.

MATERIALS AND METHODS

Genomic reconstruction of pathways for Co^{II} transport and assimilation

We performed a literature survey and used the KEGG database and BLAST searches to identify genes in the *G. sulfurreducens* genome with a predicted role in Co^{II} homeostasis and assimilation into cobamide synthesis. The subcellular localization of the protein products was predicted with PSORTb 3.0 [99].

Bacterial strains and culture conditions

G. sulfurreducens strain PCA was obtained from our laboratory culture collection and routinely maintained in anaerobic mineral medium DB with 20 mM acetate and 40 mM fumarate, as described elsewhere [31]. The cultures were incubated at 30°C while periodically monitoring growth as optical density at 660 nm (OD_{660}). Unless otherwise indicated, culture transfers to fresh medium were in mid-log phase (OD_{660}, 0.3-0.4) and diluting the cells to an initial OD_{660} of 0.03. When indicated, the media was supplemented with $CoCl_2$ from stock anaerobic solutions of 5 and 50 mM $CoCl_2$ prior to cell inoculation. For some experiments, $CoCl_2$ was added to mid-log phase cultures (~0.3 OD_{660}) incubated at 30°C. All growth experiments were performed in triplicate cultures. Cultures that did not initiate growth for 7 days were discarded (routinely one out of three replicates grown from low cell densities with 500 and 1,000 μM $CoCl_2$, as shown in Fig. 2.3). Growth curves (OD_{660}) for each of the replicate cultures were analyzed to calculate the length of the *lag* phase (time before start of exponential growth), generation (doubling) time in exponential phase, and biomass yields (OD_{660} reached once the cultures entered stationary phase). The latter was expressed as relative growth yield in the treated (with 100-1,000 μM $CoCl_2$) versus the untreated (0 μM $CoCl_2$) cultures.

RNA Extraction and sequencing (RNAseq)

Cells were grown to mid-log phase (~0.3 OD_{660}) in the presence or absence of sublethal concentrations of $CoCl_2$ (250 μM) before adding 1 ml of water saturated phenol (5% [v/v] Ambion® water saturated phenol, pH 6.6 in ethanol) to stop transcription. We harvested the cells by centrifugation (3,800 rpm, 8 min, 4°C) extracted their RNA with the QIAGEN RNeasy kit (QIAGEN) following manufacturer's recommendations. DNA digestion in the

RNA samples used the QIAGEN RNase-free DNase Set and was confirmed by Reverse Transcriptase (RT)-PCR (Verso 1-step kit, Ambion). After assessing RNA integrity in a BioAnalyzer 2100 (Agilent), we selected the samples with the best RNA quality (two biological replicates from each treatment, 0 or 250 μM) for RNA sequencing at Michigan State's Research Technology Support Facility (RTSF, Genomic core). The facility uses validated procedures for rRNA depletion, library preparation, and Illumina Hi-Seq 4000 sequencing. Briefly, rRNA depletion used an Illumina TruSeq Total RNA Library Preparation kit with QIAseq FastSelect – 5S/16S/23S rRNA depletion (QIAGEN). Libraries were quantified using Qubit and Advanced Analytical Fragment Analyzer High Sensitivity DNA NGS assays. The libraries were then pooled in equimolar amounts for multiplexed sequencing and the pool was quantified using the Kapa Biosystems Illumina Library Quantification qPCR kit. Sequencing was in one lane of the Illumina HiSeq 4000 flow cell in 1x50bp single read format and using SBS reagents. Base calling was with the Illumina Real Time Analysis (RTA) v2.7.7 software while demultiplexing and conversion to FastQ format was with Illumina Bcl2fastq v2.19.1 package.

We analyzed the RNAseq data from the Co^{II}-treated and untreated samples with the SPARTA pipeline [100], using FastQC and Trimmomatic tools for quality control and trimming and used Bowtie to align the sequences to the reference genome (GCA_000007985.2 *Geobacter sulfurreducens* PCA). Gene-level transcript level abundance was calculated with the HTSeq software while the *edgeR* tool provided the differential expression values. Data filtering used a false discovery rate FDR< 0.05, log CPM>5, and a $\log_2$ FC<-1 (downregulated genes) or > 1 (upregulated genes) [100]. We used the R software (www.r-project.org) with *pheatmap* function to draw clustered

heatmaps of differentially expressed genes. Individual searches in BioCyc 24.0 [101] predicted the operon organization of the genes and identified one gene in an RND efflux pump operon (GSU2137) that did not make the maximum FDR value yet met the log CPM and fold-change thresholds. We added this gene to Table 2.1. We also searched each of the differentially expressed genes in the UniProtKB [102] and KEGG databases to assign functional roles. The subcellular localization was predicted using the sequence analysis tools at UniProtKB (SignalP), PSORTb 3.0 [99] and CELLO v.2.5 [103]. Predictions about the domain organization of each protein and identification of metal-binding motifs used the Pfam 33.1 [104] tool available at the UniProtKB database. The RNAseq data (Supplementary file 1) has been deposited in the Gene Expression Omnibus (GEO) functional genomics data repository (https://www.ncbi.nlm.nih.gov/geo/) under accession number GSE157146. We also identified in the RNAseq data genes differentially regulated in *G. sulfurreducens* under Fe^{II} intoxication, which were calculated as the ratio between Fe excess and homeostatic transcript abundance reported elsewhere [33]. The transcriptomic data comparisons used to generate a heatmap of Co^{II} versus Fe^{II} intoxication (Fig. 2.4C) are provided as a Supplementary file 2.

Transmission Electron Microscopy (TEM) and X-ray Energy-Dispersive Spectroscopy (EDS)

Mid-log phase cells from untreated or treated (0 or 250 μM $CoCl_2$ supplementation, respectively) cultures were fixed with 2.5% glutaraldehyde before deposition for 5 min on Formvar-coated grids (150 square-mesh Ni, Electron Microscopy Sciences). After three washes with ddH_2O (30 sec each), we side-blotted the excess liquid and stored the samples at room temperature until ready for TEM examination. The cells were unstained

to prevent stain and mineral artifacts during examination with a JEOL 1400 Flash 120kV transmission electron microscope. For EDS elemental analyses, we deposited Co^{II}-stressed cells on a PELCO NetMesh™ copper grid coated with a lacey formvar/carbon support film and examined the samples with a JEM-2200FS ultra-high resolution TEM instrument equipped with an EDS detector. To minimize interference during EDS detection, we collected energy spectra from cells exposed in the holes of the support film and, as controls, from similar areas within the grid that had no cells. We used the two primary X-ray signatures of Co around 0.776 keV (Lα peak) and 6.924 keV (Kα peak) to compare the average intensity of the cell-associated Co^{II} to the cell-free controls. Because the detection limit of the EDS system is 0.001 keV, we averaged the counts detected at 0.76, 0.77, and 0.78 keV to calculate the intensity of the Lα peak and of 6.91, 6.92, and 6.93 keV for the Kα peak. The peak intensities from cells and cell-free samples on the grid were compared with the unpaired, unequal variance *t*-test function of the Excel software.

Colorimetric detection of Co^{II}

We developed a colorimetric assay for the detection of Co^{II} in culture supernatant fluids based on the color response of the metal after complexation with 2-β-mercaptoethanol (BME). The reducing agent, BME, replaces the water molecules in the cobalt hexaaqua complex $(Co[H_2O]_6)^{2+}$, turning the solution brown and permitting the spectrophotometric detection of Co^{II} at 475 nm. Prior to the assay, we grew *G. sulfurreducens* in DBAF medium at 30°C with or without 250 μM $CoCl_2$ supplementation, collected 200-μl samples periodically, and recovered the culture supernatant fluids after centrifugation at 20,000 rcf for 3 min. To initiate the complexation reaction, we added 10 μl of BME (from a 100 mM

aqueous stock) to 190 μl of supernatant sample. After mixing the solution by aspiration with a pipette, we incubated the reactions at 30ºC for 20 min to reach the maximum color response and measured the absorbance at 475 nm against $CoCl_2$ standards (0 to 500 μM $CoCl_2$) prepared in DBAF medium.

Biofilm assay

Biofilm formation in stationary phase cultures was measured with a crystal violet assay [105]. Briefly, we poured out the liquid culture once the cells reached stationary phase, gently rinsed the tubes with ddH_2O and added 1 ml of 0.1% crystal violet to stain for 15 min the biomass of biofilms formed at the bottom of the tube. After 15 min, we poured out the crystal violet solution, rinsed the tubes with ddH_2O and left them to dry overnight. We used 1 ml of 30% acetic acid to solubilize the biomass-associated crystal violet for 15 min and measured its absorbance at 550 nm to estimate the biofilm biomass.

ACKNOWLEDGEMENTS

This work was supported by Grant EAR1629439 from the National Science Foundation and Hatch project 1011745 from the USDA National Institute of Food and Agriculture to GR.

TABLES

Table 2.1 Upregulated genes in cobalt transcriptome

Function (no. of genes)	Locus	Gene	Gene product	log(2) FC	Metal-binding motif (Pfam)	Subcellular localization
Transmembrane transport (3)	GSU2135	*czcA*	CusA/CzcA heavy metal efflux RND transporter	2.47		Inner membrane
	GSU2136	*czcB*	Efflux RND transporter, periplasmic adaptor subunit	1.75		Periplasm
	GSU2137	*czcC*	Outer membrane pore/TolC family protein	1.69		Outer membrane
Electron transfer (4)	GSU0593	*cbcB*	Cytochrome *b*, putative	3.70	Prokaryotic cytochrome *b561* (PF01292)	Inner membrane
	GSU0594	*cbcA*	Cytochrome *c*, heptaheme	3.68	Doubled CXXCH motif (PF09699)	Periplasm (membrane-bound)
	GSU1538		Cytochrome *c* peroxidase	2.19	Di-haem cytochrome *c* peroxidase (PF03150)	Periplasm
	GSU2513		Cytochrome *c*, monoheme	1.85	Cytochrome *c* oxidase, *cbb3*-type (PF13442)	Periplasm
Type-I CRISPR-Cas system (2)	GSU1385	*cse1*	CRISPR processing complex protein CasA	1.56	CRISPR_Cse1 (PF09481)	Cytoplasm
	GSU1387	*cse4*	CRISPR processing complex protein CasC	1.69		Cytoplasm
Cell redox homeostasis (1)	GSU2812		glutaredoxin family protein	1.44		Periplasm
Cell envelope (4)	GSU1079		PEP motif-containing protein, putative exosortase substrate	1.32		Extracellular
	GSU1994		PEP motif-containing protein, putative exosortase substrate	3.37		Extracellular
	GSU2133		Lipoprotein	3.07		Non-cytoplasmic
	GSU3576		Lipoprotein, putative	2.06		Outer membrane
Signal transduction (3)	GSU0356		Sensor histidine kinase, heme-binding	1.27	Heme-binding (PF11845)	Inner membrane
	GSU2134		P-II family nitrogen regulator	2.93		Cytoplasm
	GSU3364	*hgtR*	Hydrogen-dependent growth transcriptional repressor	1.49		Cytoplasm
DNA repair (1)	GSU0763		Helicase, putative	1.82		Cytoplasm
Transposon functions (1)	GSU2772		Transposase of ISGsu3, IS5 family	1.46		
Unknown function (13)	GSU0468		Hypothetical protein	2.30		Inner membrane
	GSU0919		Hypothetical protein	3.67		Unknown
	GSU0959		Hypothetical protein	1.61		Cytoplasm
	GSU2129		Hypothetical protein	3.49		Non-cytoplasmic
	GSU2131		Hypothetical protein	3.05		Non-cytoplasmic
	GSU2132		Hypothetical protein	2.99		Unknown
	GSU2773		Hypothetical protein/ATP-dependent Clp protease proteolytic subunit	2.74		Unknown
	GSU3410		Hypothetical protein	3.48		Inner membrane
	GSU3489		Hypothetical protein	3.35		Inner membrane
	GSU3502		Hypothetical protein	3.64		Inner membrane
	GSU3503		Hypothetical protein	3.81		Cytoplasm
	GSU3520		Hypothetical protein	3.11		Inner membrane
	GSU3559		Hypothetical protein	3.49		Non-cytoplasmic

Table 2.2 Downregulated genes in Co^{II} transcriptome

Function (no. of genes)	Locus	Gene	Gene product	log(2) FC	Metal-binding motif (Pfam)	Subcellular localization
Folding, secretion, and degradation (1)	GSU0781	*fdnT*	Twin-arginine translocation pathway protein, TatA/TatE family	-1.95		Inner membrane
Carbohydrate metabolism (3)	GSU0778	*fdnH*	Periplasmically oriented, membrane-bound formate dehydrogenase, iron-sulfur cluster-binding subunit	-2.23	Two [4Fe-4S]-binding (PF13247, PF12800)	Inner membrane
	GSU0779	*fdnI*	Periplasmically oriented, membrane-bound formate dehydrogenase, b-type cytochrome subunit, putative	-2.02	NrfD, polysulphide reductase (PF03916)	Inner membrane
	GSU3125	*mtd*	mannitol dehydrogenase	-2.90	Zn^{II}-binding dehydrogenase (PF00107)	Cytoplasm
Energy metabolism (2)	GSU1640	*cydA*	cytochrome bd menaquinol oxidase, subunit I	-3.13	Cytochrome bd terminal oxidase subunit I (PF01654)	Inner membrane
	GSU1641	*cydB*	cytochrome bd menaquinol oxidase, subunit II	-3.19	cytochrome bd terminal oxidase subunit II (PF02322)	Inner membrane
Cell redox homeostasis (2)	GSU3126		oxidoreductase, aldo/keto reductase family	-3.08		Cytoplasm
	GSU3246	*prx-2*	peroxiredoxin, typical 2-Cys subfamily	-2.63		Cytoplasm
Hydrolases (2)	GSU1159		Intracellular protease, PfpI family, putative/type 1 glutamine amidotransferase	-2.03		Cytoplasm
	GSU3122		Metal-dependent hydrolase, beta-lactamase superfamily	-2.14		Cytoplasm
Signal transduction (2)	GSU1639	*rrf2*	Winged helix-turn-helix transcriptional regulator, Rrf2 family	-3.45	Fe^{II}dependent transcriptional regulator (PF02082)	Cytoplasm
	GSU1643		Response receiver-modulated diguanylate cyclase	-1.99		Cytoplasm
DNA binding, replication, repair (1)	GSU3245		DNA polymerase II, putative	-2.69		Cytoplasm
Unknown function (2)	GSU0208		Hypothetical Protein/DUF4350 domain-containing protein	-2.97		Inner membrane
	GSU1160		Hypothetical protein	-2.14		Non-cytoplasmic

REFERENCES

1 Buccella, D., Lim, M. H. & Morrow, J. R. Metals in biology: From metallomics to trafficking. *Inorg Chem* **58**, 13505-13508 (2019). https://doi.org/10.1021/acs.inorgchem.9b02965

2 Chandrangsu, P., Rensing, C. & Helmann, J. D. Metal homeostasis and resistance in bacteria. *Nat Rev Microbiol* **15**, 338-350 (2017). https://doi.org/doi:10.1038/nrmicro.2017.15

3 Outten, C. E. & O'Halloran, T. V. Femtomolar sensitivity of metalloregulatory proteins controlling zinc homeostasis. *Science* **292**, 2488-2492 (2001). https://doi.org/10.1126/science.1060331

4 Valko, M., Morris, H. & Cronin, M. T. Metals, toxicity and oxidative stress. *Curr Med Chem* **12**, 1161-1208 (2005). https://doi.org/10.2174/0929867053764635

5 Barras, F. & Fontecave, M. Cobalt stress in *Escherichia coli* and *Salmonella enterica*: molecular bases for toxicity and resistance. *Metallomics* **3**, 1130-1134 (2011). https://doi.org/10.1039/c1mt00099c

6 Shelton, A. N. *et al.* Uneven distribution of cobamide biosynthesis and dependence in bacteria predicted by comparative genomics. *ISME J* **13**, 789-804 (2019). https://doi.org/10.1038/s41396-018-0304-9

7 Zhang, Y. & Gladyshev, V. N. General trends in trace element utilization revealed by comparative genomic analyses of Co, Cu, Mo, Ni, and Se. *J Biol Chem* **285**, 3393-3405 (2010). https://doi.org/10.1074/jbc.M109.071746

8 Seth, E. C. & Taga, M. E. Nutrient cross-feeding in the microbial world. *Front Microbiol* **5**, 350 (2014). https://doi.org/10.3389/fmicb.2014.00350

9 Crowther, D. L., Dillard, J. G. & Murray, J. W. The mechanisms of Co(II) oxidation on synthetic birnessite. *Geochim Cosmochim Acta* **47**, 1399-1403 (1983). https://doi.org/10.1016/0016-7037(83)90298-3

10 Kay, J. T., Conklin, M. H., Fuller, C. C. & O'Day, P. A. Processes of nickel and cobalt uptake by a manganese oxide forming sediment in Pinal Creek, Globe Mining District, Arizona. *Environ Sci Technol* **35**, 4719-4725 (2001). https://doi.org/10.1021/es010514d

11 Krupka, K. M. & Serne, R. J. (ed Pacific Northwest National Laboratory) (Washington, 2002).

12 Backes, C. A., McLaren, R. G., Rate, A. W. & Swift, R. S. Kinetics of cadmium and cobalt desorption from iron and manganese oxides. *Soil Sci Soc Am J* **59**, 778-785 (1995). https://doi.org/10.2136/sssaj1995.03615995005900030021x

13 Reguera, G. & Kashefi, K. The electrifying physiology of Geobacter bacteria, 30 years on. *Adv Microb Physiol* **74**, 1-96 (2019). https://doi.org/10.1016/bs.ampbs.2019.02.007

14 Cosert, K. M. & Reguera, G. Voltammetric study of conductive planar assemblies of Geobacter nanowire pilins unmasks their ability to bind and mineralize divalent cobalt. *J Ind Microbiol Biotechnol* **46**, 1239-1249 (2019). https://doi.org/10.1007/s10295-019-02167-5

15 Hau, H. H., Gilbert, A., Coursolle, D. & Gralnick, J. A. Mechanism and consequences of anaerobic respiration of cobalt by *Shewanella oneidensis* strain MR-1. *Appl Environ Microbiol* **74**, 6880-6886 (2008). https://doi.org/10.1128/AEM.00840-08

16 Yan, J., Ritalahti, K. M., Wagner, D. D. & Löffler, F. E. Unexpected specificity of interspecies cobamide transfer from *Geobacter* spp. to organohalide-respiring *Dehalococcoides mccartyi* strains. *Appl Environ Microbiol* **78**, 6630-6636 (2012). https://doi.org/10.1128/aem.01535-12

17 Burkhardt, E.-M., Meißner, S., Merten, D., Büchel, G. & Küsel, K. Heavy metal retention and microbial activities in geochemical barriers formed in glacial sediments subjacent to a former uranium mining leaching heap. *Geochemistry* **69**, 21-34 (2009). https://doi.org/10.1016/j.chemer.2008.12.003

18 Nikaido, H. Molecular basis of bacterial outer membrane permeability revisited. *Microbiol Mol Biol Rev* **67**, 593-656 (2003). https://doi.org/10.1128/mmbr.67.4.593-656.2003

19 Rodionov, D. A., Hebbeln, P., Gelfand, M. S. & Eitinger, T. Comparative and functional genomic analysis of prokaryotic nickel and cobalt uptake transporters: evidence for a novel group of ATP-binding cassette transporters. *J Bacteriol* **188**, 317-327 (2006). https://doi.org/10.1128/JB.188.1.317-327.2006

20 Cracan, V. & Banerjee, R. Cobalt and corrinoid transport and biochemistry. *Met Ions Life Sci* **12**, 333-374 (2013). https://doi.org/10.1007/978-94-007-5561-1_10

21 Moore, S. J. & Warren, M. J. The anaerobic biosynthesis of vitamin B12. *Biochem Soc Trans* **40 3**, 581-586 (2012).

22 Hazra, A. B. *et al.* Anaerobic biosynthesis of the lower ligand of vitamin B12. *Proc Natl Acad Sci USA* **112**, 10792-10797 (2015). https://doi.org/10.1073/pnas.1509132112

23 Nies, D. H. Microbial heavy-metal resistance. *Appl Microbiol Biotechnol* **51**, 730-750 (1999). https://doi.org/10.1007/s002530051457

24 Kolaj-Robin, O., Russell, D., Hayes, K. A., Pembroke, J. T. & Soulimane, T. Cation Diffusion Facilitator family: Structure and function. *FEBS Lett* **589**, 1283-1295 (2015). https://doi.org/10.1016/j.febslet.2015.04.007

25 Munkelt, D., Grass, G. & Nies, D. H. The chromosomally encoded cation diffusion facilitator proteins DmeF and FieF from *Wautersia metallidurans* CH34 are transporters of broad metal specificity. *J Bacteriol* **186**, 8036 (2004). https://doi.org/10.1128/JB.186.23.8036-8043.2004

26 Grass, G. *et al.* FieF (YiiP) from *Escherichia coli* mediates decreased cellular accumulation of iron and relieves iron stress. *Arch Microbiol* **183**, 9-18 (2005). https://doi.org/10.1007/s00203-004-0739-4

27 Kim, E. H., Nies, D. H., McEvoy, M. M. & Rensing, C. Switch or funnel: how RND-type transport systems control periplasmic metal homeostasis. *J Bacteriol* **193**, 2381-2387 (2011). https://doi.org/10.1128/JB.01323-10

28 Nikaido, H. & Takatsuka, Y. Mechanisms of RND multidrug efflux pumps. *Biochim Biophys Acta* **1794**, 769-781 (2009). https://doi.org/10.1016/j.bbapap.2008.10.004

29 Pak, J. E. *et al.* Structures of intermediate transport states of ZneA, a Zn(II)/proton antiporter. *Proc Natl Acad Sci USA* **110**, 18484-18489 (2013). https://doi.org/10.1073/pnas.1318705110

30 Bagai, I., Rensing, C., Blackburn, N. J. & McEvoy, M. M. Direct metal transfer between periplasmic proteins identifies a bacterial copper chaperone. *Biochemistry* **47**, 11408-11414 (2008). https://doi.org/10.1021/bi801638m

31 Speers, A. M. & Reguera, G. Electron donors supporting growth and electroactivity of *Geobacter sulfurreducens* anode biofilms. *Appl Environ Microbiol* **78**, 437-444 (2012). https://doi.org/10.1128/aem.06782-11

32 Schmidt, T. & Schlegel, H. G. Nickel and cobalt resistance of various bacteria isolated from soil and highly polluted domestic and industrial wastes. *FEMS Microbiol Lett* **62**, 315-328 (1989). https://doi.org/10.1016/0378-1097(89)90014-1

33 Embree, M. *et al.* The iron stimulon and Fur regulon of *Geobacter sulfurreducens* and their role in energy metabolism. *Appl Environ Microbiol* **80**, 2918-2927 (2014). https://doi.org/10.1128/aem.03916-13

34 Pettigrew, G. W., Echalier, A. & Pauleta, S. R. Structure and mechanism in the bacterial dihaem cytochrome *c* peroxidases. *J Inorg Biochem* **100**, 551-567 (2006). https://doi.org/10.1016/j.jinorgbio.2005.12.008

35 Eser, M., Masip, L., Kadokura, H., Georgiou, G. & Beckwith, J. Disulfide bond formation by exported glutaredoxin indicates glutathione's presence in the *E. coli* periplasm. *Proc Natl Acad Sci USA* **106**, 1572-1577 (2009). https://doi.org/10.1073/pnas.0812596106

36 Hatahet, F., Boyd, D. & Beckwith, J. Disulfide bond formation in prokaryotes: history, diversity and design. *Biochim Biophys Acta* **1844**, 1402-1414 (2014). https://doi.org/10.1016/j.bbapap.2014.02.014

37 Hiniker, A., Collet, J. F. & Bardwell, J. C. Copper stress causes an in vivo requirement for the *Escherichia coli* disulfide isomerase DsbC. *J Biol Chem* **280**, 33785-33791 (2005). https://doi.org/10.1074/jbc.M505742200

38 Ma, X., Yan, Y., Wang, W., Guo, J. & Wang, Y. Metatranscriptomic analysis of adaptive response of anammox bacteria *Candidatus* 'Kuenenia stuttgartiensis' to Zn(II) exposure. *Chemosphere* **246**, 125682 (2020). https://doi.org/10.1016/j.chemosphere.2019.125682

39 Huergo, L. F., Chandra, G. & Merrick, M. P_{II} signal transduction proteins: nitrogen regulation and beyond. *FEMS Microbiol Rev* **37**, 251-283 (2013). https://doi.org/10.1111/j.1574-6976.2012.00351.x

40 Sant'Anna, F. H. *et al.* The P_{II} superfamily revised: a novel group and evolutionary insights. *J Mol Evol* **68**, 322-336 (2009). https://doi.org/10.1007/s00239-009-9209-6

41 Arnesano, F. *et al.* The evolutionarily conserved trimeric structure of CutA1 proteins suggests a role in signal transduction. *J Biol Chem* **278**, 45999-46006 (2003). https://doi.org/10.1074/jbc.M304398200

42 Fong, S. T., Camakaris, J. & Lee, B. T. Molecular genetics of a chromosomal locus involved in copper tolerance in *Escherichia coli* K-12. *Mol Microbiol* **15**, 1127-1137 (1995). https://doi.org/10.1111/j.1365-2958.1995.tb02286.x

43 Keon, R. G., Fu, R. & Voordouw, G. Deletion of two downstream genes alters expression of the *hmc* operon of *Desulfovibrio vulgaris* subsp. *vulgaris* Hildenborough. *Arch Microbiol* **167**, 376-383 (1997). https://doi.org/10.1007/s002030050458

44 Schwartz, C. J. *et al.* IscR, an Fe-S cluster-containing transcription factor, represses expression of *Escherichia coli* genes encoding Fe-S cluster assembly proteins. *Proc Natl Acad Sci USA* **98**, 14895-14900 (2001). https://doi.org/10.1073/pnas.251550898

45 Rajagopalan, S. *et al.* Studies of IscR reveal a unique mechanism for metal-dependent regulation of DNA binding specificity. *Nat Struct Mol Biol* **20**, 740-747 (2013). https://doi.org/10.1038/nsmb.2568

46 Ueki, T. & Lovley, D. R. Genome-wide gene regulation of biosynthesis and energy generation by a novel transcriptional repressor in *Geobacter* species. *Nucleic Acids Res* **38**, 810-821 (2010). https://doi.org/10.1093/nar/gkp1085

47 Girvan, H. M. & Munro, A. W. Heme sensor proteins. *J Biol Chem* **288**, 13194-13203 (2013). https://doi.org/10.1074/jbc.R112.422642

48 Dailey, H. A. *et al.* Prokaryotic heme biosynthesis: Multiple pathways to a common essential product. *Microbiol Mol Biol Rev* **81**, e00048-00016 (2017). https://doi.org/10.1128/MMBR.00048-16

49 Makarova, K. S. & Koonin, E. V. Annotation and classification of CRISPR-Cas systems. *Methods Mol. Biol.* **1311**, 47-75 (2015). https://doi.org/10.1007/978-1-4939-2687-9_4

50 Makarova, K. S. & Koonin, E. V. Annotation and classification of CRISPR-Cas systems. *Methods Mol Biol* **1311**, 47-75 (2015). https://doi.org/10.1007/978-1-4939-2687-9_4

51 Westra, E. R. *et al.* Type I-E CRISPR-Cas systems discriminate target from non-target DNA through base pairing-lindependent PAM recognition. *PLOS Genetics* **9**, e1003742 (2013). https://doi.org/10.1371/journal.pgen.1003742

52 Gorelsky, S. I. *et al.* Spectroscopic and DFT investigation of [M{HB(3,5-iPr2pz)3}(SC6F5)] (M = Mn, Fe, Co, Ni, Cu, and Zn) model complexes: Periodic trends in metal−thiolate bonding. *Inorg Chem* **44**, 4947-4960 (2005). https://doi.org/10.1021/ic050371m

53 Sundaresan, R., Parameshwaran, H. P., Yogesha, S. D., Keilbarth, M. W. & Rajan, R. RNA-independent DNA cleavage activities of Cas9 and Cas12a. *Cell Rep* **21**, 3728-3739 (2017). https://doi.org/10.1016/j.celrep.2017.11.100

54 Zheng, Y. *et al.* Endogenous Type I CRISPR-Cas: From foreign DNA defense to prokaryotic engineering. *Front Bioeng Biotechnol* **8**, 62 (2020). https://doi.org/10.3389/fbioe.2020.00062

55 Smith, A. T., Barupala, D., Stemmler, T. L. & Rosenzweig, A. C. A new metal binding domain involved in cadmium, cobalt and zinc transport. *Nat Chem Biol* **11**, 678-684 (2015). https://doi.org/10.1038/nchembio.1863

56 Waldron, K. J. & Robinson, N. J. How do bacterial cells ensure that metalloproteins get the correct metal? *Nat Rev Microbiol* **7**, 25-35 (2009). https://doi.org/10.1038/nrmicro2057

57 Kanellis, V. G. & Dos Remedios, C. G. A review of heavy metal cation binding to deoxyribonucleic acids for the creation of chemical sensors. *Biophys Rev* **10**, 1401-1414 (2018). https://doi.org/10.1007/s12551-018-0455-y

58 Epshtein, V. *et al.* UvrD facilitates DNA repair by pulling RNA polymerase backwards. *Nature* **505**, 372-377 (2014). https://doi.org/10.1038/nature12928

59 Borisov, V. B., Gennis, R. B., Hemp, J. & Verkhovsky, M. I. The cytochrome *bd* respiratory oxygen reductases. *Biochim Biophys Acta* **1807**, 1398-1413 (2011). https://doi.org/10.1016/j.bbabio.2011.06.016

60 Poole, L. B. & Nelson, K. J. Distribution and features of the six classes of peroxiredoxins. *Mol Cells* **39**, 53-59 (2016). https://doi.org/10.14348/molcells.2016.2330

61 Toledano, M. B. & Huang, B. Microbial 2-Cys peroxiredoxins: Insights into their complex physiological roles. *Mol Cells* **39**, 31-39 (2016). https://doi.org/10.14348/molcells.2016.2326

62 Aklujkar, M. *et al.* Proteins involved in electron transfer to Fe(III) and Mn(IV) oxides by *Geobacter sulfurreducens* and *Geobacter uraniireducens*. *Microbiology* **159**, 515-535 (2013). https://doi.org/10.1099/mic.0.064089-0

63 Trumpower, B. L. Cytochrome *bc1* complexes of microorganisms. *Microbiol Rev* **54**, 101-129 (1990).

64 Shi, L. *et al.* Extracellular electron transfer mechanisms between microorganisms and minerals. *Nat Rev Microbiol* **14**, 651-662 (2016). https://doi.org/10.1038/nrmicro.2016.93

65 Hu, H. *et al.* Mercury reduction and cell-surface adsorption by *Geobacter sulfurreducens* PCA. *Environ Sci Technol* **47**, 10922-10930 (2013). https://doi.org/10.1021/es400527m

66 Brenner, S. & Horne, R. W. A negative staining method for high resolution electron microscopy of viruses. *Biochim Biophys Acta* **34**, 103-110 (1959). https://doi.org/10.1016/0006-3002(59)90237-9

67 Cologgi, D. L., Lampa-Pastirk, S., Speers, A. M., Kelly, S. D. & Reguera, G. Extracellular reduction of uranium via Geobacter conductive pili as a protective cellular mechanism. *Proc Natl Acad Sci U S A* **108**, 15248-15252 (2011). https://doi.org/10.1073/pnas.1108616108

68 Cologgi, D. L., Speers, A. M., Bullard, B. A., Kelly, S. D. & Reguera, G. Enhanced uranium immobilization and reduction by *Geobacter sulfurreducens* biofilms. *Appl Environ Microbiol* **80**, 6638-6646 (2014). https://doi.org/10.1128/AEM.02289-14

69 Konovalova, A. & Silhavy, T. J. Outer membrane lipoprotein biogenesis: Lol is not the end. *Philos Trans R Soc Lond B Biol Sci* **370** (2015). https://doi.org/10.1098/rstb.2015.0030

70 Schulze, R. J. & Zuckert, W. R. *Borrelia burgdorferi* lipoproteins are secreted to the outer surface by default. *Mol Microbiol* **59**, 1473-1484 (2006). https://doi.org/10.1111/j.1365-2958.2006.05039.x

71 Haft, D. H., Paulsen, I. T., Ward, N. & Selengut, J. D. Exopolysaccharide-associated protein sorting in environmental organisms: the PEP-CTERM/EpsH system. Application of a novel phylogenetic profiling heuristic. *BMC Biol* **4**, 29 (2006). https://doi.org/10.1186/1741-7007-4-29

72 Haft, D. H., Payne, S. H. & Selengut, J. D. Archaeosortases and exosortases are widely distributed systems linking membrane transit with posttranslational modification. *J Bacteriol* **194**, 36-48 (2012). https://doi.org/10.1128/JB.06026-11

73 Rollefson, J. B., Stephen, C. S., Tien, M. & Bond, D. R. Identification of an extracellular polysaccharide network essential for cytochrome anchoring and biofilm formation in *Geobacter sulfurreducens*. *J Bacteriol* **193**, 1023-1033 (2011). https://doi.org/10.1128/JB.01092-10

74 Huang, J. & Zhang, H. Redox reactions of iron and manganese oxides in complex systems. *Front Environ Sci Eng* **14**, 76 (2020). https://doi.org/10.1007/s11783-020-1255-8

75 Kimber, R. L. *et al.* Biomineralization of Cu_2S nanoparticles by *Geobacter sulfurreducens*. *Appl Environ Microbiol*, AEM.00967-00920 (2020). https://doi.org/10.1128/aem.00967-20

76 Franklin, N. M., Stauber, J. L., Apte, S. C. & Lim, R. P. Effect of initial cell density on the bioavailability and toxicity of copper in microalgal bioassays. *Environ Toxicol Chem* **21**, 742-751 (2002). https://doi.org/10.1897/1551-5028(2002)021<0742:eoicdo>2.0.co;2

77 Li, Y. H., Hanna, M. N., Svensater, G., Ellen, R. P. & Cvitkovitch, D. G. Cell density modulates acid adaptation in *Streptococcus mutans*: implications for survival in biofilms. *J Bacteriol* **183**, 6875-6884 (2001). https://doi.org/10.1128/JB.183.23.6875-6884.2001

78 Ezraty, B., Gennaris, A., Barras, F. & Collet, J. F. Oxidative stress, protein damage and repair in bacteria. *Nat Rev Microbiol* **15**, 385-396 (2017). https://doi.org/10.1038/nrmicro.2017.26

79 Imlay, J. A. Cellular defenses against superoxide and hydrogen peroxide. *Annu Rev Biochem* **77**, 755-776 (2008). https://doi.org/10.1146/annurev.biochem.77.061606.161055

80 Leonard, S. *et al.* Cobalt-mediated generation of reactive oxygen species and its possible mechanism. *J Inorg Biochem* **70**, 239-244 (1998). https://doi.org/10.1016/S0162-0134(98)10022-3

81 Kamarthapu, V. & Nudler, E. Rethinking transcription coupled DNA repair. *Curr Opin Microbiol* **24**, 15-20 (2015). https://doi.org/10.1016/j.mib.2014.12.005

82 Hill, H. A. O. & Sadler, P. J. Bringing inorganic chemistry to life with inspiration from R. J. P. Williams. *J Biol Inorg Chem* **21**, 5-12 (2016). https://doi.org/10.1007/s00775-016-1333-3

83 Thorgersen, M. P. & Downs, D. M. Cobalt targets multiple metabolic processes in *Salmonella enterica*. *J Bacteriol* **189**, 7774-7781 (2007). https://doi.org/10.1128/jb.00962-07

84 Majtan, T., Frerman, F. E. & Kraus, J. P. Effect of cobalt on *Escherichia coli* metabolism and metalloporphyrin formation. *Biometals* **24**, 335-347 (2011). https://doi.org/10.1007/s10534-010-9400-7

85 Lin, H. & Everse, J. The cytotoxic activity of hematoheme: evidence for two different mechanisms. *Anal Biochem* **161**, 323-331 (1987). https://doi.org/10.1016/0003-2697(87)90458-1

86 Anzaldi, L. L. & Skaar, E. P. Overcoming the heme paradox: heme toxicity and tolerance in bacterial pathogens. *Infect Immun* **78**, 4977-4989 (2010). https://doi.org/10.1128/iai.00613-10

87 Everse, J. & Hsia, N. The toxicities of native and modified hemoglobins. *Free Radic Biol Med* **22**, 1075-1099 (1997). https://doi.org/10.1016/S0891-5849(96)00499-6

88 Qian, X., Reguera, G., Mester, T. & Lovley, D. R. Evidence that OmcB and OmpB of *Geobacter sulfurreducens* are outer membrane surface proteins. *FEMS Microbiol Lett* **277**, 21-27 (2007). https://doi.org/10.1111/j.1574-6968.2007.00915.x

89 Zähringer, F., Lacanna, E., Jenal, U., Schirmer, T. & Boehm, A. Structure and signaling mechanism of a zinc-sensory diguanylate cyclase. *Structure* **21**, 1149-1157 (2013). https://doi.org/10.1016/j.str.2013.04.026

90 D'Argenio, D. A., Calfee, M. W., Rainey, P. B. & Pesci, E. C. Autolysis and autoaggregation in *Pseudomonas aeruginosa* colony morphology mutants. *J Bacteriol* **184**, 6481-6489 (2002). https://doi.org/10.1128/jb.184.23.6481-6489.2002

91 Hickman, J. W., Tifrea, D. F. & Harwood, C. S. A chemosensory system that regulates biofilm formation through modulation of cyclic diguanylate levels. *Proc Natl Acad Sci USA* **102**, 14422-14427 (2005). https://doi.org/10.1073/pnas.0507170102

92 De, N. *et al.* Phosphorylation-independent regulation of the diguanylate cyclase WspR. *PLoS Biol* **6**, e67 (2008). https://doi.org/10.1371/journal.pbio.0060067

93 Rehm, B. H. Bacterial polymers: biosynthesis, modifications and applications. *Nat Rev Microbiol* **8**, 578-592 (2010). https://doi.org/10.1038/nrmicro2354

94 Feliciano, G. T., Steidl, R. J. & Reguera, G. Structural and functional insights into the conductive pili of Geobacter sulfurreducens revealed in molecular dynamics simulations. *Phys Chem Chem Phys* **17**, 22217-22226 (2015). https://doi.org/10.1039/c5cp03432a

95 Speers, A. M., Schindler, B. D., Hwang, J., Genc, A. & Reguera, G. Genetic identification of a PilT motor in *Geobacter sulfurreducens* reveals a role for pilus retraction in extracellular electron transfer. *Front Microbiol* **7**, 1578 (2016). https://doi.org/10.3389/fmicb.2016.01578

96 Reguera, G. Harnessing the power of microbial nanowires. *Microb Biotechnol* **11**, 979–994 (2018). https://doi.org/10.1111/1751-7915.13280

97 Reguera, G. *et al.* Extracellular electron transfer via microbial nanowires. *Nature* **435**, 1098-1101 (2005). https://doi.org/10.1038/nature03661

98 Steidl, R., Lampa-Pastirk, S. & Reguera, G. Mechanistic stratification in electroactive biofilms of *Geobacter sulfurreducens* mediated by pilus nanowires. *Nat Commun* **7**, 12217 (2016). https://doi.org/10.1038/ncomms12217

99 Yu, N. Y. *et al.* PSORTb 3.0: improved protein subcellular localization prediction with refined localization subcategories and predictive capabilities for all prokaryotes. *Bioinformatics* **26**, 1608-1615 (2010). https://doi.org/10.1093/bioinformatics/btq249

100 Johnson, T. A. *et al.* Clusters of antibiotic resistance genes enriched together stay together in swine agriculture. *mBio* **7**, e02214-02215 (2016). https://doi.org/10.1128/mBio.02214-15

101 Karp, P. D. *et al.* The BioCyc collection of microbial genomes and metabolic pathways. *Brief Bioinform* **20**, 1085-1093 (2019). https://doi.org/10.1093/bib/bbx085

102 UniProt, C. UniProt: a worldwide hub of protein knowledge. *Nucleic Acids Res* **47**, D506-D515 (2019). https://doi.org/10.1093/nar/gky1049

103 Yu, C. S., Lin, C. J. & Hwang, J. K. Predicting subcellular localization of proteins for Gram-negative bacteria by support vector machines based on n-peptide compositions. *Protein Sci* **13**, 1402-1406 (2004). https://doi.org/10.1110/ps.03479604

104 El-Gebali, S. *et al.* The Pfam protein families database in 2019. *Nucleic Acids Res* **47**, D427-D432 (2019). https://doi.org/10.1093/nar/gky995

105 Merritt, J. H., Kadouri, D. E. & O'Toole, G. A. Growing and analyzing static biofilms. *Curr Protoc Microbiol* **Chapter 1**, Unit 1B 1 (2005). https://doi.org/10.1002/9780471729259.mc01b01s00

Chapter 3: Contribution of the low-voltage CbcBA cytochrome respiratory chain to Co^{II} detoxification by *Geobacter sulfurreducens*

ABSTRACT

Exposure of *Geobacter sulfurreducens* to toxic concentrations of Co^{II} induces a complex detoxification response that leads to the mineralization of some metal on the outer surface. The upregulation in metal-stressed cells of two cytochromes (CbcBA) required for the reduction of electron acceptors with half potentials as low as the Co^{II}/Co^{0} pair suggested their involvement in the reductive precipitation of the metal. Transcript abundance and protein expression profiles in Co^{II}-stressed cells confirmed the higher expression of not only CbcBA but also several periplasmic and outer membrane cytochromes involved in extracellular electron transfer. Consistent with increased sensitivity to Co^{II}, a mutant carrying a deletion of the *cbcBA* genes (Δ*cbcBA*) agglutinated more than the wild type (WT) cells and a genetically complemented strain when challenged with non-lethal concentrations of $CoCl_2$ in mid-exponential phase. However, given sufficient time to acclimate to non-lethal concentrations of the metal, the mutant cells overcame Co^{II} intoxication and grew similarly to the WT cultures. . Furthermore, Co^{II} penetrated more rapidly in the mutant cells, exacerbating intoxication and slowing down the growth recovery of the cells. Additionally, the CbcBA deficiency exacerbated the release of outer membrane vesicles under Co^{II} stress, a compensatory effect associated with the detoxification of toxic metals bound to the outer membrane lipopolysaccharide and increased membrane permeability. These findings demonstrate that the CbcBA cytochromes are needed for optimal detoxification of Co^{II} and highlight the important role of complementary pathways in Co^{II} detoxification.

INTRODUCTION

Metal respiration supports the growth of many microorganisms in redox environments where O_2, oxidized N-species and other electron acceptors have been depleted [1,2]. This metabolic process produces large scale transformations to the local environment and is pivotal in the biogeochemical cycling of elements essential for life [2,3]. The reductive dissolution of the abundant insoluble iron (Fe^{III}) oxides by dissimilatory metal reducing (DMR) bacteria, such as those in the genus *Geobacter*, cycles metals essential to ecosystem function [1]. Indeed, these bacteria solubilize Fe and Mn from the abundant metal oxide minerals as species (Fe^{II} and Mn^{II}) that cells can assimilate for the synthesis of heme and metalloenzymes [1,4]. Studies with the model DMR bacterium *Geobacter sulfurreducens* have identified several pathways for extracellular electron transport to metal oxides. Respiratory electrons from the quinone pool reduce membrane-bound quinol oxidases (ImcH, CbcL and CbcBA), which then transfer the electrons to the abundant periplasmic cytochromes (Ppc) of *Geobacter* species [5]. Several porin cytochrome complexes (Pcc) across the outer membrane then transfer electrons from the Ppc to the extracellular electron acceptors [6]. To expand the redox-active surface of the cell, *Geobacter* species also assemble electrically conductive pili monolaterally [7]. The pili electronically connect the periplasmic cytochromes to soluble and insoluble metal acceptors and to other cells in biofilms [1,8,9].

The dissolution of Fe^{III} and Mn^{IV} oxides by DMR bacteria also releases metals that coprecipitate with and/or adsorb to the mineral phases [10]. Micronutrients such as cobalt (Co^{III} or Co^{II} species) are solubilized from the minerals and made bioavailable in this manner [11]. Through their role in the Co cycle, DMR bacteria supply a metal that is

essential for the synthesis of the catalytic center of the cobamide-class of vitamins [12,13]. *Geobacter* species are in fact among the few known bacteria with genomes encoding complete pathways for cobamide synthesis, which they secrete to support the activities of syntrophic partners [13,14]. To continue to secrete cobamides while respiring Fe^{III} oxides, *Geobacter* cells must overcome the toxic effects of Co on cellular metabolism, the formation of free radicals, and its infiltration into the active sites of metalloenzymes [15,16]. As I described in Chapter 2, a complex detoxification response that includes the expression of RND efflux pumps, protein repair pathways, hydrogen peroxide detoxification, and membrane remodeling allows *Geobacter* cells to grow in the presence of otherwise toxic concentrations of Co^{II} [12]. Metal-stressed cells of *G. sulfurreducens* also upregulate the genes encoding the inner membrane cytochrome complex CbcBA [12]. The two *cbc* genes are part of a cluster of cytochromes and redox proteins proposed to assemble as a large protein complex (Cbc5) anchored in the inner membrane and spanning the periplasmic space [17]. The predicted organization of the Cbc5 complex in the cell envelope could facilitate the transfer of electrons from the menaquinone pool in the inner membrane to outer membrane Pcc, which serve as electron donors to various extracellular electron acceptors [6,18,19]. Hence, the Cbc complex could provide a pathway for the extracellular reduction of Co^{II}, explaining the accumulation of Co nanoparticles on the outer surface of *G. sulfurreducens* cells grown under Co^{II} stress [12]. In support of this, the *cbcBA* genes are required for the reduction of extracellular electron acceptors with potentials (-0.21 to -0.28 V vs Standard Hydrogen Electrode or SHE) [5] as low as the standard redox potential (E^0) of the half reaction $Co^{2+} + 2e^- \rightarrow Co^0$ (E^0 = –0.277 V vs SHE).

The upregulation of the low-voltage CbcBA pathway in metal-stressed cells and the deposition of Co-containing nanoparticles on their surface[12] led us to hypothesize that cells may express CbcBA to detoxify Co^{II} by reductively mineralizing it to Co^{0} nanoparticles outside of the cell [12]. To test this hypothesis, I reconstructed the CbcBA cytochrome pathway for the extracellular transfer of electrons to Co^{II} from the transcriptomic data (RNAseq) of Co^{II}-stressed cells of *G. sulfurreducens* [12] and investigated the Co^{II} detoxification response of a Δ*cbcBA* strain and a genetically complemented strain. The results support the involvement of the low-voltage CbcBA reductive pathway in the Co detoxification response of *G. sulfurreducens*. However, the extent of its contribution may be masked by compensatory effects of complementary pathways involved in Co^{II} detoxification. These findings further define the mechanisms that allow *G. sulffureducens* to thrive in Co-contaminated environments and the role that cytochrome respiratory chains play in metal detoxification.

RESULTS

Transcriptional upregulation of cytochrome respiratory chains under Co^{II} stress

Previous transcriptomic analysis (RNAseq) of mid-exponential phase cultures (DBAF medium) of *G. sulfurreducens* identified *cbcBA* among the most differentially upregulated genes by non-lethal concentrations of Co^{II} (provided as 250 µM $CoCl_2$) [12]. The two *cbc* genes encode two cytochromes of a large periplasmic protein complex (Cbc5) anchored in the inner membrane [17] that could transfer electrons from the menaquinone pool in the inner membrane to outer membrane Pcc, and from them to Co^{II} (Fig. 3.1A). Consistent with this model, transcripts for cytochromes (OmcB and OmcC) exposed on the outer membrane by the Pcc conduits were among the most abundant in Co^{II}-stressed cells (Fig.

3.1B). Together, the Cbc5 and Pcc complexes could enable the reductive precipitation of Co^{II} as a cellular detoxification mechanism [12].

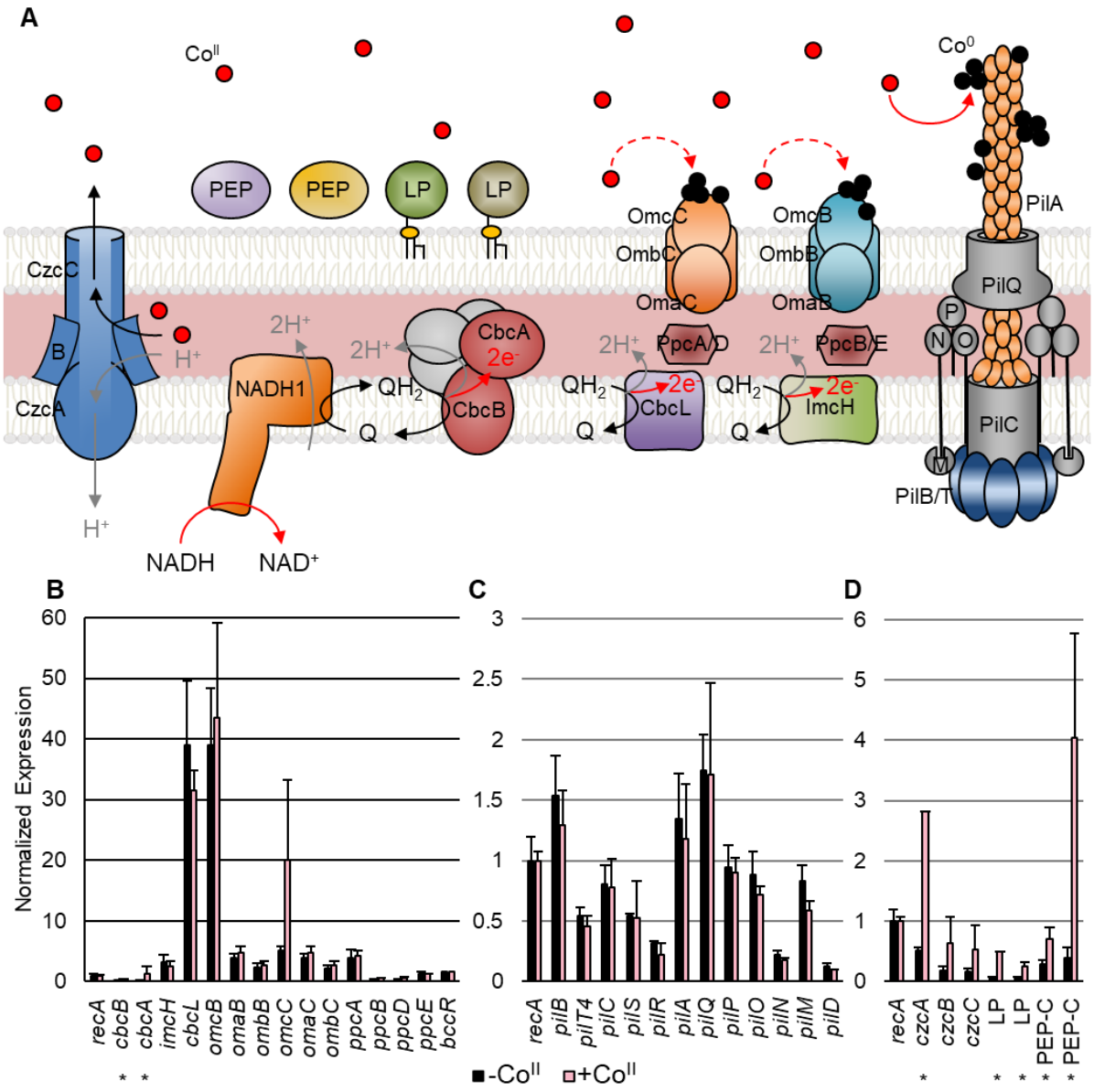

Figure 3.1 Cell envelope pathways for Co^{II} Detoxification. (A) Illustration of cell envelope proteins predicted to detoxify Co^{II} via metal export, modulation of membrane composition, and reductive mineralization on the cell surface. **(B-D)** Transcript levels (normalized to the *recA* gene; $n = 2$) of genes encoding cell envelope *c*-type cytochromes (**B**), components of the Type IV pilus apparatus (**C**), and efflux pumps and outer membrane proteins differentially upregulated under Co^{II} stress (**D**). Shown are expression levels in the transcriptomes sequenced from mid-exponential phase DBAF cultures incubated at 30°C without Co^{II} supplementation (-Co^{II}, in black) or with

Figure 3.1 (cont'd)
250 µM $CoCl_2$ (+Co^{II}, in pink). Statistical differences (FDR < 0.05) are marked with an asterisk. Abbreviations: CbcAB: *b*- and *c*- type cytochrome complex; CbcL: low-potential cytochrome with a b- and c- type domain; CzcABC: Co^{II}, Zn^{II}, Cd^{II} RND-efflux pump; ImcH: high-potential inner membrane cytochrome; LP: membrane-bound lipoprotein; NADH1: NADH dehydrogenase; OmaB/C: periplasmic-facing cytochrome of the PccB or PccC conduits; OmbB/C: porins of the PccB or PccC conduits; OmcB/C: extracellular outer membrane cytochromes of the PccB or PccC conduits; PEP-C: C-terminal Pro-Glu-Pro recognition peptide (PEP-CTERM); PilABCMNOPQT: structural proteins of the Type IV pilus apparatus; PpcA/B/D/E: periplasmic cytochromes. Data previously published [20].

The transcriptomic data also suggests that the expression of a cytochrome pathway for extracellular electron transfer to Co^{II} is redox-controlled. The expression of *cbcBA* in cultures grown with low potential electron acceptors such as crystalline forms of Fe^{III} oxides and electrodes poised at a sufficiently low reduction potential is controlled by the transcriptional regulator BccR [5]. The *bccR* gene was also expressed during Co^{II} treatment (Fig. 3.1B), albeit at much lower levels than the *cbcBA* genes. By contrast, quinol oxidases required for the reduction of electron acceptors with medium (CbcL, –0.15 to –0.2 V vs SHE) or high (ImcH, above –0.15 V vs SHE) half potentials, had a lower relative transcript abundance in Co^{II}-stressed cells (Fig. 3.1B). This is consistent with the redox-controlled regulation of quinol oxidases by BccR [5]. Like CbcBA, the relative transcript abundance for periplasmic cytochromes (PpcA, B, D and E), which receive electrons from the quinol oxidases [21], was high in Co^{II}-treated cultures (Fig. 3.1B). However, the genes the PpcA-E cytochromes were not differentially expressed under Co^{II} stress compared to untreated cultures. This result is in agreement with previous studies reporting high but constitutive levels of expression of these cytochromes independent of the electron acceptor [22]. Transcript levels were also high for the exposed cytochromes (OmcB and OmcC) of the Pcc conduits that transport electrons across the outer membrane (Fig. 3.1A). *G. sulfurreducens* upregulates these cytochromes during growth

with extracellular metals such as Fe^{III} [18,23] and in stationary-phase via the sigma factor RpoS [24]. As shown in Fig. 3.1B, transcript levels for *omcC* were particularly high though highly variable in the Co^{II}-treated cultures (20 ± 13 relative to *recA*, compared to 5.2 ± 0.7 in the untreated controls). The high expression of genes encoding CbcBA, periplasmic cytochromes and outer membrane Pcc conduits support the notion that *G. sulfurreducens* upregulates a cytochrome pathway for the transport of respiratory electrons from the menaquinone pool in the inner membrane to the extracellular Co^{II}.

G. sulfurreducens can also assemble conductive pili of the Type IVa class to reduce extracellular electron acceptors such as Fe^{III} oxide minerals [7] and the soluble uranyl cation [25]. The anionic metal traps that decorate the pilus surface [8] can also bind and reductively precipitate Co^{II} as Co^0 nanoparticles [26,27]. Any contribution by pili to the reductive detoxification of Co^{II} in the metal-stressed cultures is unlikely because the incubation temperature (30^{o}C) used for these studies prevented pilus assembly [7,25]. Further supporting this, none of the structural genes of the *Geobacter* pilus apparatus were differentially upregulated by Co^{II} (Fig. 3.1C). Rather, Co^{II} stress significantly upregulated pathways for metal export (Czc metal pump) and surface chemistry modification (lipoproteins and exopolysaccharide (EPS)-associated PEP-CTERM proteins) (Fig. 3.1D). While lipoproteins and EPS-associated proteins may modulate the permeability of the outer membrane in ways that could prevent the permeation of the metal, the CzcCBA pump extrudes any Co^{II} traversing the outer membrane [28,29]. The transcriptional upregulation of the genes encoding CzcCBA in *G. sulfurreducens* [12] emphasizes the essential role that RND-efflux pumps play in metal detoxification in bacteria [30]. CzcA, one of the three proteins of the CzcCBA pump, confers substrate

specificity and functions as a proton-cation antiporter to translocate the metal across the cell envelope [31]. CzcA transcripts were also among the most significantly upregulated genes in the Co^{II} transcriptome (Fig. 3.1D). CzcB, on the other hand, is not essential for metal translocation but can enhance substrate binding by CzcA by forming a complete pump-channel complex [31]. In support of this, relative transcript abundances of *czcB* were only slightly elevated in Co^{II}-treated cultures and did not reach statistical significance (0.63 ± 0.44 relative to *recA* compared to 0.19 ± 0.06 in untreated controls, $p = 0.4$).

Role of CbcBA in Co^{II} detoxification during exponential growth

Co^{II} detoxification is critical during the exponential phase of growth, when cells must invest most of their energy gains into growth-supporting processes and cell division. We thus hypothesized that the CbcBA deficiency would exacerbate growth defects in cells challenged with Co^{II}. To test this, I grew the wild-type (WT) and a CbcBA-deficient (Δ*cbcBA*) mutant strain in freshwater medium (FW) with acetate and fumarate (FWAF) and challenged the cells with non-lethal concentrations of Co^{II} (200 µM $CoCl_2$) during the exponential phase of growth. For these experiments, cell growth (absorbance at 660 nm, A_{660}) was monitored before and after $CoCl_2$ addition and in reference to untreated controls (Fig. 3.2A). A genetically complemented strain, Δ*cbcBA::cbcBA,* was also included as a control. WT cells initially grew like the untreated cultures after the metal challenge but agglutinated and settled as a biofilm at the bottom of the tube (0.169 ± 0.060 A_{660}), a phenotype associated with metal intoxication [12]. Agglutination is a protective mechanism against metal stress [32,33] that *G. sulfurreducens* triggers through changes in the cell surface chemistry [12], such as those resulting from the production of the redox-active Xap exopolysaccharide of *G. sulfurreducens* [34]. The agglutination response was exacerbated

in the Δ*cbcBA* mutant cultures (0.302 ± 0.029 A_{660}, p = 0.005 vs the WT cells) (Fig. 3.2B). Complementation of the *cbcBA* deletion in the Δ*cbcBA::cbcBA* strain partially rescued the agglutination phenotype of the mutant (0.236 ± 0.035 A_{660}, p = 0.06 vs the WT cells). By contrast, the untreated culture controls had no measurable agglutination (Fig. 3.2A). The agglutination phenotypes revealed in these experiments are thus consistent with the need of cells to express CbcBA to overcome Co^{II} intoxication.

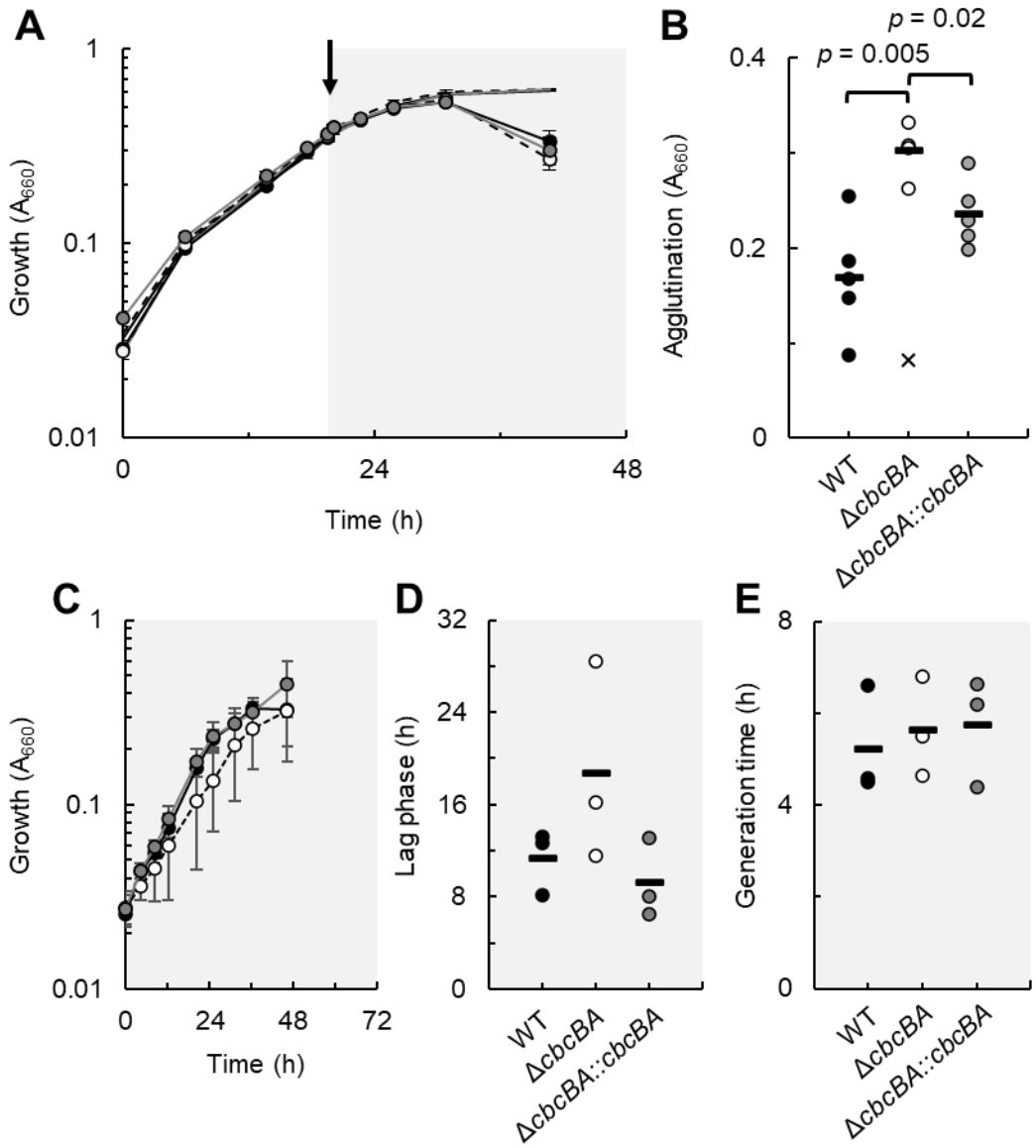

Figure 3.2 Role of CbcBA in Co^{II} detoxification by exponentially-growing cells. (A) Growth (A_{660}) of WT (black), Δ*cbcBA* mutant (white), and the genetically complemented Δ*cbcBA::cbcBA* (gray) strains in FWAF medium with (circles) or without (lines) Co^{II} addition (200 µM $CoCl_2$, arrow) in mid-exponential phase (A_{660} = 0.3-0.4). **(B)** Agglutination (A_{660}) of Co^{II} treated cultures, measured as the A_{660} difference between the undisturbed and gently resuspended cultures at the end of the incubation period. Symbols show agglutination for each replicate culture and the horizontal lines, the average (n = 5). Significant differences were calculated using a student's T-test and are shown as *p* values. Any outliers identified using Grubb's test are indicated as an 'X' and were excluded from statistical analyses. **(C)** Growth (A_{660}) of viable cells recovered from the exponential Co^{II} treatment in panel (**A**). **(D)** Length of the lag phase (estimated as the amount of time before cultures exceeded A_{660} = 0.05) and **(E)** the generation times of the recovering cultures.

Further supporting a higher level of Co^{II} intoxication in the CbcBA-deficient cells, the Δ*cbcBA* mutant cultures challenged with the $CoCl_2$ (Fig. 3.2A) did not readily resume growth once transferred to fresh medium without the metal (Fig. 3.2C). Metal toxicity requires repair of cellular damage and can delay, if not impair, the ability of metal-stressed cells to resume growth in standard culture media [25]. This phenotype manifests as an extended lag phase prior to growth initiation that is proportional to the initial degree of metal intoxication of the cells [25]. Consistent with this, the Δ*cbcBA* cultures had extended lag phases compared to the WT and Δ*cbcBA::cbcBA* cultures (Fig. 3.2D). Variability in the length of the lag phase was however high for the mutant cultures (18.7 ± 8.7 h), which reduced the statistical significance of the data compared to the WT (11.3 ± 2.9 h, $p = 0.2$) and genetically complemented (9.2 ± 3.4 h, $p = 0.2$) strain (Fig. 3.2D). Phenotypic variability is not uncommon in metal-stressed cultures, where cells stochastically respond to toxicity via multiple pathways to extrude the metal, repair damage, and coordinate protective responses that minimize metal permeation [12]. Hence, the higher variability observed during the growth recovery of metal-stressed Δ*cbcBA* cells (Fig. 3.2A) is also consistent with a higher degree of intoxication resulting from the past exposure to the Co^{II} (Fig. 3.2C). However, once exponential growth was initiated, the mutant cells grew at rates (generation or doubling times, Fig. 3.2E) similar to the WT and the genetically complemented cells. This is because Co^{II} stress also triggers in *G. sulfurreducens* several pathways for the repair of metal damage [12]. Furthermore, the true contribution of the cytochrome pathway to metal detoxification may be masked by the many additional pathways (metal stress, repair, cell surface chemistry changes, etc.) that cells can activate to overcome Co^{II} stress.

The CbcBA respiratory chain is dispensable for growth after acclimation to Co^{II} stress

The metal challenge to mid-exponential grown cells and post-recovery experiments described above (Fig. 3.2) supported a role for CbcBA in metal detoxification and highlighted the important role that agglutination plays in rapidly protecting cells from Co^{II} intoxication. Acclimation to metal stress is however possible when starting *G. sulfurreducens* cultures at low cell densities in the presence of sub-lethal concentrations (200 µM) of $CoCl_2$ [12]. After a variable lag phase to activate pathways for metal detoxification, cells initiate exponential growth [12]. To test if the activation of other detoxification pathways could compensate for the CbcBA deficiency, we investigated the effect of Co^{II} in the acclimation of the WT and the Δ*cbcBA* mutant cells to metal stress. For this experiment, untreated cultures were transferred in mid-exponential phase to FWAF at low cell densities (starting A_{660} ~0.05) before adding Co^{II} (200 µM $CoCl_2$) and growth was monitored spectrophotometrically in reference to the untreated controls. As previously reported [12], the WT strain underwent a phase of acclimation characterized by an extended lag phase (54.3 ± 6.0 h with Co^{II} compared to 5.60 ± 0.02 h without the metal, $p = 0.005$) (Fig. 3.3A). Additionally, Co^{II} stress slowed down exponential growth in the WT cultures (8.9 ± 6.3 h with Co^{II} vs 4.03 ± 0.13 h without the metal, $p = 0.3$) (Fig. 3.3A, inset) as energy is diverted towards metal extrusion, repair and other detoxification pathways. Cultures of the Δ*cbcBA* strain supplemented with $CoCl_2$ also had an extended lag phase (57.8 ± 9.8 h compared to 5.37 ± 0.71 h without Co^{II}, $p = 0.01$) and grew more slowly than the untreated cultures after acclimation (Fig. 3.3A). However, generation times after acclimation were similar in the WT and mutant strains (Fig. 3.2A, inset) as

were growth yields (0.37 ± 0.10 WT vs 0.35 ± 0.13 Δ*cbcBA*; p = 0.8). Additionally, the Co^{II}-stressed WT and mutant cultures agglutinated once they reached stationary phase (0.19 ± 0.10 A_{660} and 0.14 ± 0.10 A_{660} in the WT and Δ*cbcBA* cultures, respectively; p = 0.5). Hence, given sufficient time to acclimate, cells can overcome Co^{II} intoxication in a CbcBA-independent manner.

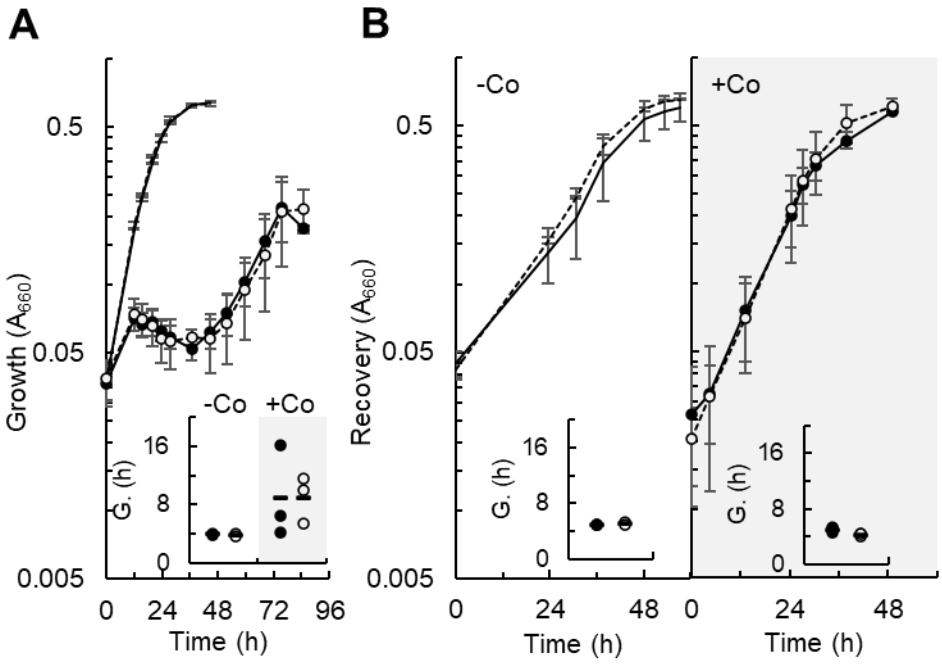

Figure 3.3 Growth from low cell densities with non-lethal Co^{II} concentrations. (A) Growth (A_{660}) of the WT (black) and Δ*cbcBA* (white) in FWAF cultures in the absence (lines) or presence (solid symbols) of 200 µM $CoCl_2$. Data show the average and standard errors for duplicate (untreated) and triplicate (treated) cultures for each strain. Inset shows the individual data points (circle) and average (line) generation times (G) in the untreated (-Co) and treated (+Co) cultures for both strains. **(B)** Growth (A_{660}) recovery in metal-free FWAF medium of cultures from (**A**). The average generation time (G) in the post-recovery cultures is shown in the inset.

As in previous assays (Fig. 3.2), we also measured the degree of metal intoxication in the Co^{II}-stressed cells by recovering them in metal-free medium (Fig. 3.3B). Both strains resumed growth after a similar lag phase (12.6 ± 1.4 h WT vs 13.4 ± 3.0 h Δ*cbcBA*, p = 0.7). Generation times were also comparable in both strains (5.02 ± 0.39 h and 4.25

± 0.17 h in the WT and mutant strains, respectively; $p = 0.06$). These results support our earlier conclusion that cells do not absolutely require the CbcBA pathway to acclimate to and grow in the presence of Co^{II}.

Contribution of CbcBA to Co^{II} immobilization

We also investigated a role for CbcBA in preventing the permeation of Co^{II} inside the cells in assays developed to study the enzymatic immobilization and reduction of metals by resting (non-growing) cells of *G. sulfurreducens* [25]. Resting cell suspensions of the WT and Δ*cbcBA* strains were prepared in a reaction buffer that preserved cell viability for at least 6 h [25]. Appendix 1 describes the optimization of this buffer and the importance of identifying buffer formulations that provide sufficient osmoprotection to cells maintained in the resting state for several hours. Unable to actively extrude the metal, resting cells are more vulnerable to Co^{II} permeation and more readily intoxicated, which slows down their recovery once grown in fresh medium without the metal [25]. Recovery of cells from assays performed at 30°C as previously described [25] were highly variable among the triplicates for each strain, preventing comparisons. However, lowering the temperature of the resting cell assay to 25°C reduced some of the variability among the replicates and unmasked the linearity of Co^{II} removal during the first 1 h of incubation ($R^2 = 0.99$ and 0.94 for the WT and Δ*cbcBA*, respectively) (Fig. 3.4A). From the linearity of the reaction, we calculated WT rates of Co^{II} removal of 29 µM/h and much higher (49 µM/h) for the Δ*cbcBA* mutant, consistent with increased permeability of Co^{II} in the mutant cells. Despite the more rapid kinetics of removal by the resting mutant cells during the first hour of exposure to Co^{II}, yields of metal removed after 6 h (41.4 ± 5.7 µM) were not significantly different than in the WT (30 ± 19 µM Co^{II},, $p = 0.4$) (Fig. 3.4A). This is consistent with

previous growth studies that found that WT and Δ*cbcBA* cultures removed comparable amounts of Co^{II} (24.6 ± 0.57 µM and 27.6 ± 2.8 µM Co^{II}, respectively) when allowed to acclimate to the metal.

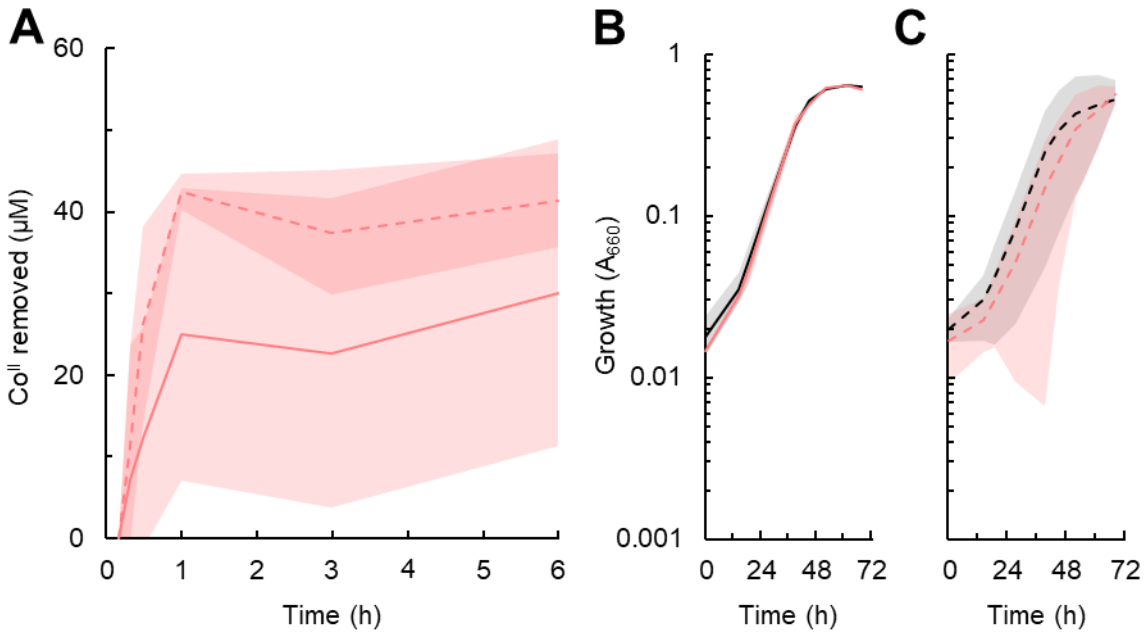

Figure 3.4 Role of CbcBA in Co^{II} removal by resting cells (A) and growth recovery in metal-free medium (B-C). (A) Amount (µM) of Co^{II} removed by resting cells of the WT (solid line) and Δ*cbcBA* (dashed line) cells over 6 hours. The resting cells were suspended in an osmotically balanced buffer with 200 µM $CoCl_2$ at 25ºC. Shown are the average removal by triplicate WT (solid line) and duplicate Δ*cbcBA* (dashed line) resting cell suspensions and the standard error (shaded areas). **(B-C)** Growth (A_{660}) recovery in metal-free FWAF medium of WT **(B)** and Δ*cbcBA* **(C)** resting cells exposed (pink) or not exposed (black) to Co^{II}. Lines are the average of triplicate cultures, except for the Co^{II}-treated WT cultures, which were tested in duplicates. Shaded areas represent the standard deviation.

The deletion of cytochromes required for the extracellular immobilization of metals in *G. sulfurreducens* often increases metal removal rates, because more metal penetrates inside the cell envelope [35]. As a result, mutant cells are more intoxicated and recovered from the resting state in metal-free growth medium more slowly [25]. Consistent with this, the Δ*cbcBA* cells recovered, on average, more slowly than the WT cells once transferred

to metal-free growth medium (Fig. 3.4B-C). The WT resting cells, for example, recovered from the Co^{II} treatment after a lag phase (23.1 ± 2.1 h) nearly identical to that of untreated controls (23.0 ± 1.4 h, $p = 0.96$) (Fig. 3.4B). By contrast, the resting mutant cells recovered required a longer lag phase (35 ± 10 h) to initiate growth (Fig. 3.4C). Variability was also higher in the mutant cultures, as expected of cells with a much higher level of intoxication. Notably, untreated controls of the mutant also needed variable but extended lag phases (32 ± 15 h) to recover from the resting state (Fig. 3.4C). Thus, not only is CbcBA needed to reduce Co^{II} intoxication, but for growth activation after the resting state.

Vesiculation as a mechanism for Co^{II} detoxification in the absence of the CbcBA pathway

Atomic Force Microscopy (AFM) images of WT, Δ*cbcBA*, and Δ*cbcBA::cbcBA* cells deposited on the surface of highly oriented pyrolytic graphite (HOPG) revealed increased (albeit variable) vesiculation in the mutant and phenotypic rescuing of WT vesiculation in the complemented strain (Fig. 3.5). Hypervesiculation is typically associated with changes in the fluidity and permeability of the outer membrane [36,37], which matches well with the increased permeability of the Δ*cbcBA* cells to Co^{II} (Fig. 3.4A) and the increased sensitivity of the mutant cells during osmotic shifts from the resting state (Fig. 3.4C).

Hypervesiculation in *G. sulfurreducens* has also been proposed to promote the detoxification of LPS-bound metals [28]. *Geobacter* cells synthesize a rough (no O-antigen) LPS that sequesters toxic divalent cations such as the uranyl cation to prevent them from traversing the outer membrane [28]. Once saturated, the cell sheds the metal-containing LPS via outer membrane vesicles (OMVs), preparing the outer membrane for further metal binding [28]. Consistent with this, Co^{II}-stressed WT cells were hypervesiculated (14.3

± 2.6 OMVs/μm^2) compared to untreated controls (3.8 ± 1.4 OMVs/μm^2, $p < 0.001$) (Fig. 3.5B). Vesiculation was also greater in the Δ*cbcBA* and ∆*cbcBA::cbcBA* cells grown with Co^{II} (18.2 ± 5.6 OMVs/μm^2 in Δ*cbcBA* compared to 4.9 ± 2.9 OMVs/μm^2 in untreated controls, $p = 0.003$; 9.4 ± 1.8 OMVs/μm^2 in ∆*cbcBA::cbcBA* compared to 2.4 ± 1.2 OMVs/μm^2 in untreated controls, $p = 0.001$) (Fig. 3.5B). Complementation of the ∆*cbcBA* mutation in the ∆*cbcBA::cbcBA* cells rescued the hypervesiculation phenotype during Co^{II} treatment ($p = 0.02$) to levels lower than WT cells ($p = 0.01$). The hypervesiculated phenotype of the CbcBA-deficient cells provides a pathway for Co^{II} detoxification via the rapid release of OMVs with metal-sequestered LPS. Such a compensatory mechanism may have masked the true contribution of the CbcBA cytochrome pathway to Co^{II} detoxification in some of the metal tolerance assays used in this study and may have contributed, at least partially, to the high phenotypic variability of Co^{II}-stressed mutant cells.

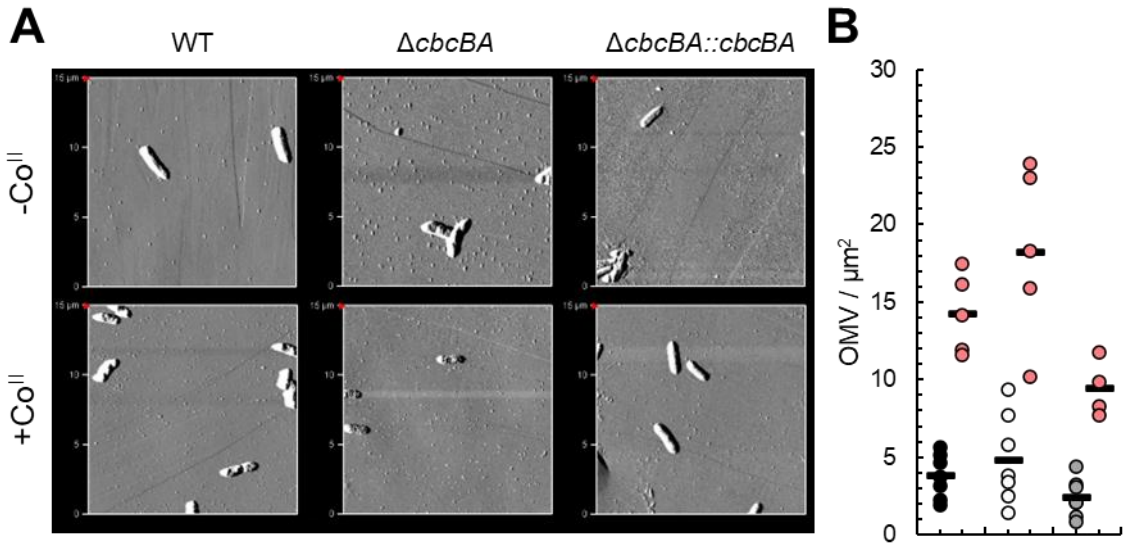

Figure 3.5 Effect of Co^{II} treatment on vesiculation. (A) Representative topographic AFM images of WT, *ΔcbcBA* and *ΔcbcBA::cbcBA* cells from FWAF cultures grown to late-exponential phase (A_{660} = 0.4-0.5) with or without 200 µM $CoCl_2$. **(B)** Quantification of the OMVs produced by treated (pink) or untreated cultures normalized to A_{660} 0.5. Individual micrographs (circles) and averages (lines) are presented.

Cytochrome abundance is affected by Co^{II} treatment

Metal exposure [12,17] and mutations in genes encoding cell envelope proteins [25,38,39] can significantly impact the type and levels of cytochromes expressed by *G. sulfurreducens*. To test for similar effects by Co^{II} and the Δ*cbcBA* mutation, we used an enhanced chemiluminescence (ECL) based heme stain to visualize the cytochrome profile of whole-cell and supernatant samples of the WT, Δ*cbcBA*, and Δ*cbcBA::cbcBA* strains in untreated versus Co^{II}-treated cultures (Fig. 3.6). Untreated controls revealed five dominant bands corresponding to heme-containing proteins with molecular mass of roughly 10, 22, 30, 50, and 75 kDa. These estimated masses matched well with the molecular weights reported for some of the most abundant *c*-cytochromes of *G. sulfurreducens*, mainly the periplasmic PpcA-E *c*-cytochromes [21] and the outer membrane *c*-cytochromes OmcE (~30 kDa) [40], OmcS (~50 kDa) [40], and OmcB (~76 kDa)

[6] and the secreted form of OmcZ (~30 kDa) [41]. These bands may be attributed to either extracellular or intercellular cytochromes as the growth medium was not separated from the cell pellets in this bulk measurement of heme-containing proteins. Deletion of *cbcBA* did not affect cytochrome expression (Fig. 3.6). However, the genetically complemented strain had a marked decrease in the expression levels of the four largest heme-containing bands, particularly the 22 and 75 kDa bands. Hence, although the Δ*cbcBA::cbcBA* strain expresses the *cbcBA* gene from its native promoter, its relocation to a different genome location (downstream of *glmS* (GSU0270) encoding a glutamine fructose-6-phosphate aminotransferase) [5] may have pleitropically affected the expression of other cytochromes. This difference helps explain why some of the phenotypic defects of the Δ*cbcBA* mutant were only partially rescued (Fig. 3.2) in the genetically complemented strain.

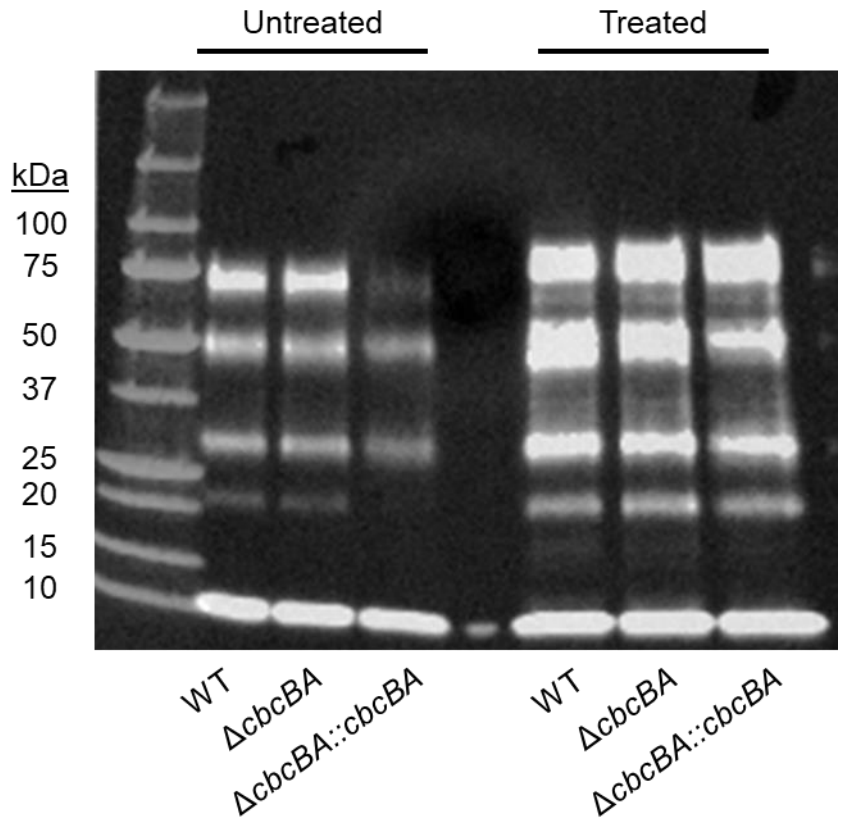

Figure 3.6 Heme-containing proteins in whole cells from untreated and Co^{II}-treated cultures. WT, Δ*cbcBA, and* Δ*cbcBA::cbcBA* cells were grown to stationary phase with (treated) or without (untreated) 200 μM $CoCl_2$ and harvested by centrifugation before resuspension in Laemmli buffer without β-mercaptoethanol and boiling. Samples were loaded into a polyacrylamide gel and separated by electrophoresis at 300 V. The gels were blotted to a membrane before staining the heme-containing proteins by detecting their peroxidase activity with an ECL stain. Whole cell samples were normalized to A_{660} 0.3 and ran alongside a 250 kDa protein ladder.

Despite differences noted in the expression of heme-containing proteins in the complemented strain, all of the strains produced brighter bands when grown with $CoCl_2$ (Fig. 3.6). The most notable increases in expression were for the bands (22, 30, 50, and 75 kDa) predicted to correspond to outer membrane *c*-cytochromes such as OmcE (~30 kDa) [40], OmcS (~50 kDa) [40], and OmcB (~76 kDa) [6] and the secreted form of OmcZ (~30 kDa) [41]. This result aligns well with previous reports of increased cytochrome expression in metal-exposed cells [12,22]. Most of the heme-stained bands were also present and had

comparable intensities in the complemented strain, consistent with distinct regulatory pathways for the activation of *c*-cytochromes during the Co^{II} detoxification response. Importantly, the higher expression under Co^{II}-stress of heme-containing proteins supports the notion that cell envelope respiratory chains are needed to detoxify the metal. This is again consistent with the predicted role of the CbcBA cytochrome pathway in extracellular electron transfer and reductive mineralization to Co^{II}.

DISCUSSION

Our previous transcriptomic studies of metal-stressed cells of *G. sulfurreducens* [12] revealed three main mechanisms for Co^{II} detoxification, all localized to the cell envelope: 1) extracellular mineralization of Co^{II} (cytochrome path); 2) periplasmic metal export (RND-pump); and 3) outer surface remodeling (lipoproteins and exopolysaccharide-associated proteins) (Fig. 3.1). While export and surface remodeling are conserved pathways for metal detoxification in other bacteria [42], the surface immobilization of Co^{II} as nanoparticles is a novel adaptive response specific to *Geobacter*. The differential upregulation of the CbcBA-encoding genes with Co^{II} [12] and the known role for these cytochromes in electron transfer to extracellular electron acceptors with reduction potentials (between –0.28 and –0.21 V) as low as the Co^{II}/Co^{0} pair [5] suggested a similar reductive pathway for the extracellular mineralization of the metal at the thermodynamic edge. Enabling this reaction requires a respiratory chain for the transfer of electrons from the menaquinone pool to extracellular cytochromes in the outer membrane. However, CbcBA is predicted to be part of a periplasmic complex anchored to the inner membrane [5,12] and, thus, lacks the exposure needed for the reductive precipitation of Co^{II} on the outer surface. The transcriptomic data (Fig. 3.1) confirmed the high expression of

periplasmic (Ppc) and outer membrane (Pcc conduits) *c*-cytochromes that promote extracellular electron transfer in *G. sulfurreducens* [6,17,21,43]. These redox carriers provide a likely pathway for the reductive mineralization of Co^{II} at the cell surface. Consistent with this, the sparse distribution of Co nanoparticles on the surface of metal-stressed cells [12] matches well with the localization of Pcc cytochromes on the outer membrane [19].

Unmasking the contribution of the CbcBA cytochromes to Co^{II} resistance via mineralization proved challenging given the many redundant pathways that exist for extracellular electron transfer [21] and Co^{II} detoxification [12] in *G. sulfurreducens*. Additionally, we observed a higher phenotypic variability in Co^{II}-stressed Δ*cbcBA* than any other culture due to higher susceptibility of the mutant cells to intoxication, which could have masked the true contribution of CbcBA to Co^{II} detoxification. Despite these challenges, we reproducibly measured higher levels of cell-cell agglutination in the CbcBA-deficient mutant after challenging exponentially growing cells to sub-lethal concentrations of $CoCl_2$ (Fig. 3.2), a mechanism often employed to mitigate metal intoxication [33]. Exponentially grown cells of *G. sulfurreducens* synthesize an EPS (Xap) that anchors cytochromes involved in extracellular electron transfer and promotes cell-cell agglutination [34,44]. The agglutinated cells form biofilms at the bottom of the culture vessel, an adaptive response that enhances metal tolerance [32] and increases catalytic rates and metabolic activity [45,46]. Average growth yields were also lower in the Δ*cbcBA* mutant after the mid-exponential metal challenge, as expected of a mutant that diverts more energy to detoxification and repair of metal-induced damage [12]. While the agglutination phenotype of the Δ*cbcBA* strain was effective at minimizing intoxication (Fig. 3.2C) the heightened variability in the length of the lag phase suggests that this

mechanism only partially shielded mutant cells (Fig. 3.2D). Although the genetic complementation of the Δ*cbcBA* had pleiotropic effects in the expression of heme-containing proteins (Fig. 3.6), these defects did not impair the ability of the cells to agglutinate once exposed to Co^{II} (Fig. 3.2). This is consistent with a generic response to metal detoxification that does not require the redox activity of the extracellular matrix.

It was, however, possible for the CbcBA-deficient mutant to acclimate to metal stress and grow in the presence of sub-lethal concentration of $CoCl_2$ from low cell densities (Fig. 3.3). After a phase of acclimation (~ 50 h lag phase), both the WT and mutant strains grew at similar rates and to comparable growth yields (Fig. 3.3). Acclimation to Co^{II} stress leads to the activation of a complex detoxification response involving macromolecular repair, metal export and surface chemistry modifications [12]. These complementary pathways could have compensated for the CbcBA deficiency. The high redundancy of cell envelope cytochromes in *G. sulfurreducens* [21], including other Cbc complexes [5,17], could have also provided alternative pathways for extracellular electron transfer to the Xap cytochromes and compensate, at least in part, for the genetic disruption of CbcBA. Indeed, growth with Co^{II} increases the expression on heme-containing proteins with molecular masses matching well those of outer membrane cytochromes (Fig. 3.6). This is consistent with a significant contribution of extracellular electron transfer chains to Co^{II} detoxification.

Taken together, the results support a model whereby the extracellular immobilization of Co^{II} via reductive pathways provides an additional, but dispensable, layer of protection from metal toxicity. The low-voltage reductive pathway involving the CbcBA quinol oxidase is central to this process and, for this reason, cells transcriptionally

upregulated the encoding genes to grow under metal stress (Fig. 3.1). The upregulation of the *cbcBA* genes and the accumulation of Co nanoparticles on the cell surface of metal-stressed cells suggested that the two processes are linked [12]. In support of this, resting mutant cells removed Co^{II} faster than the WT cells and showed greater signs of intoxication and reduced viability once recovering in metal-free medium (Fig. 3.4). This, and the faster Co^{II} removal by the mutant strain, suggests a greater degree of metal permeation in cells unable to express CbcBA. Outer membrane permeability changes can also explain the delayed growth recovery of the mutant cells from the resting state even in the absence of metal pressure (Fig. 3.4C) and their hypervesiculation (Fig. 3.5).

The data also suggests that the CbcBA cytochrome pathway is integrated into the unique adaptive responses used by *G. sulfurreducens* for metal respiration. The rough LPS of *G. sulfurreducens* sequesters metal cations to prevent them from traversing the outer membrane [28]. The cells shed the metal saturated LPS in OMVs to replenish the LPS in the outer membrane and maintain its metal sequestration capacity. Like other bacterial OMVs [37,47], *Geobacter* vesicles carry periplasmic and membrane-bound proteins including *c*-type cytochromes [48]. The high abundance of cytochromes in the cell envelope of *G. sulfurreducens* also makes their OMVs redox-active and able to catalyze the extracellular reduction of metals [48]. The increased vesiculation of WT cells grown under Co^{II} stress (Fig. 3.5) suggests that this pathway is also important for Co^{II} detoxification. Metal stress also exacerbated the hypervesiculation phenotype of the Δ*cbcBA* strain (Fig. 3.5). This result supports the idea that the respiratory chains and outer membrane remodeling pathways are tightly integrated in *G. sulfurreducens*. As such, vesiculation can be upregulated to compensate for the loss of the cytochrome

pathway and ensures that Co^{II} permeation is minimized. This compensatory effect may have masked the true contribution of the CbcBA cytochrome pathway to Co^{II} detoxification and contribute to the phenotypic variability observed in the metal toxicity assays. If so, the CbcBA contribution to metal detoxification in *G. sulfurreducens* may be more significant than predicted from the laboratory experiments and may be most relevant for the survival of these bacteria in metal-rich environments.

MATERIALS AND METHODS

Transcriptomic analysis

We used previously published RNAseq data [12] to estimate the transcript abundance of cytochromes, structural components of electrically conductive pili, and several Co^{II} detoxification pathways measured in treated (250 µM $CoCl_2$) and untreated cultures of *G. sulfurreduences.* The transcript abundance was then normalized to the expression levels of the housekeeping gene, *recA*, under each culture treatment. The average and standard deviation of the replicates was calculated using Excel and statistical significance was identified using *edgeR* with cutoffs of a false discovery rate FDR < 0.05, log CPM = 5, and a $\log_2$ FC > 1 [49].

Bacterial strains and culture conditions

Cultures of *G. sulfurreducens* strain PCA were obtained from our laboratory culture collection. The Δ*cbcBA* and Δ*cbcBA::cbcBA* strains [5] were generously donated by Dr. Daniel Bond (University of Minnesota). All strains were grown anaerobically (80:20 v/v CO_2:N_2 atmosphere) in fresh water (FW) medium (a minimal medium used for metal reduction studies [25]) supplemented with 15 mM acetate as electron donor and 40 mM fumarate as electron acceptor and incubated at 30°C. Growth in the cultures was

monitored spectrophotometrically as absorbance at 600 nm (A_{600}). Cultures were routinely grown to an optical density of 0.5-0.6 (late-exponential phase) before being transferred to fresh medium to an initial A_{600} of 0.05.

Co^{II} challenge to exponentially growing cells

The growth of strains in FWAF medium was monitored at 660 nm (A_{660}) until reaching mid-exponential phase (A_{660} 0.3-0.4). Cell growth was monitored at 660 nm (A_{660}) instead of 600 nm to ensure lack of colorimetric interference from the $CoCl_2$ in the medium. Cells were then treated with 200 µM $CoCl_2$ as previously described [12] or an equivalent volume of sterile, anaerobic ddH_2O (untreated). Growth was monitored until cells reached stationary phase (A_{660} 0.6-0.7). Agglutination of the stationary phase cultures was estimated as the difference in A_{660} between disturbed and undisturbed cultures. Culture supernatant fluids were harvested by centrifugation immediately after the Co^{II} addition and before measuring agglutination to assay the change in Co^{II} concentrations [12]. The Excel® software was used to test for similar variances using an F-test and significant differences using a student's t-test. In addition, GraphPad was used to perform a Grubb's test to identify outliers using $\alpha = 0.05$ as a cutoff.

Co^{II} acclimation assays

Strains were grown in FWAF medium in the presence (metal-treated) or absence (untreated controls) of 200 µM $CoCl_2$, as previously described [12]. The cultures were inoculated with cells previously grown in metal-free FWAF medium (A_{600} ~0.5-0.6) at a starting A_{600} of 0.05. All incubations were at 30^{o}C. Growth phenotypes (length of lag phase, generation time) were estimated with the Growthcurver R script (https://github.com/sprouffske/growthcurver). Briefly, growth curve data was matched to

the best sigmoidal curve fit to calculate the maximum generation time achieved, the maximum cell density (carrying capacity or growth yields), and initial population density of the culture. The length of the lag phase was calculated as the time it took cultures to rise above an absorbance of 0.05 using the standard equation for logarithmic growth.

Vesiculation measurements

OMV production was measured in culture samples deposited on the surface of a highly oriented pyrolytic graphite (HOPG) stage and imaged with an atomic force microscope (AFM), as previously described [28]. Briefly, samples were taken from mid-exponential cultures using a 1,000 µL pipette tip (slightly sliced with a razor blade to increase the size of the opening and minimize mechanical shearing of the cells). The culture droplets (~20 µl) were left to adsorb to the HOPG stage for 20 min before wicking away excess culture with absorbent paper. The adsorbed samples were then washed for 30 sec with ddH_2O three times and dried in a sealed container under the gentle flow of a N_2 gas stream. The stages were loaded into an Asylum Research Cypher S system equipped with an AC240TS tip (Asylum Research) and the samples (cells and OMVs) were imaged in tapping mode at a scan rate of 0.3 Hz in 15x15 µm scans. OMVs in the scanned fields were counted using the freehand tool in the ImageJ software (https://imagej.nih.gov/ij/index.html) and normalized to the A_{660} of the sample and μm^2 of scanned field.

Co^{II} permeability assays with resting cells

Resting cells were prepared as previously described [25], with some modifications. Unless otherwise indicated, all procedures were performed inside an anaerobic chamber (COY Labs). Mid-exponential cultures (A_{600} ~0,4) were dispensed into 50 mL conical tubes and

pelleted by centrifugation to remove growth media (10 min, 3,000 *g*). The cell pellets were then resuspended with a Pasteur pipette in a high salt (30 mM NaCl) wash buffer optimized to preserve the viability of *G. sulfurreducens* cells [25,35], pelleted again, and resuspended in the wash buffer. The washed cells were resuspended into 30 ml of reaction buffer to an A_{600} of 0.1 before adding 20 mM acetate as an electron donor and 200 µM of $CoCl_2$ as an electron acceptor and incubating at 30°C or 25°C. Samples were taken at different intervals to spectrophotometrically measure the concentration of Co^{II} with a colorimetric assay, as described elsewhere [12]. The Co^{II} concentrations were used to calculate the amount of Co^{II} removed by the resting cells. Co^{II} removal rates were calculated from the linear portion of metal removal by the resting cells (typically between 1 and 2 h). A 1-ml sample was taken at the end of the assay to inoculate 9 ml of fresh FWAF media and monitor the recovery of the resting cells as a function of their viability [25].

Denaturing Polyacrylamide Gel Electrophoresis (PAGE), blotting and heme stain

Changes in cytochrome expression were visualized using an enhanced chemiluminescence (ECL) method developed for the rapid staining of *c*-type cytochromes on filters [50]. Briefly, cells were grown in FWAF with or without 200 µM $CoCl_2$ until reaching stationary phase and their exact A_{600} was measured. Culture samples were then deposited into 15 mL falcon tubes and stored in a -20°C freezer. Upon thawing, the samples were normalized to an A_{660} 0.3 based on the growth yield measured at stationary phase. Normalized samples were mixed with equal volumes of 2X Laemmli buffer lacking reducing agents to preserve heme peroxidase activity. The samples were then incubated at 95°C for 10 minutes, cooled to room temperature and loaded into a 12% Mini-Protean

TGX precast gel (Bio-Rad). Proteins in the samples were then separated electrophoretically at 300 V for roughly 30 min in a Mini-Protean Tetra Vertical Electrophoresis Cell. The proteins in the gel were then transferred to a nitrocellulose membrane using a Turbo Transfer System and stained with a 1:1 mixture of the ECL peroxide and ECL luminol/enhancer solutions from the Clarity Western ECL Substrate Kit (Bio-Rad) for 5 minutes. Antibodies containing horseradish peroxidase are not required for protein detection with this stain because the peroxidase activity of the hemes promotes the breakdown of H_2O_2 in the ECL solution and the visualization of heme-containing proteins from the fluorescence of the ECL molecule. Membranes were then rinsed with sterile ddH_2O and photographed with a Bio-Rad Gel Doc XR+ set to chemiluminescent mode (detection of the heme-stained bands) and white light (detection of the ladder).

REFERENCES

1 Reguera, G. & Kashefi, K. The electrifying physiology of Geobacter bacteria, 30 years on. *Adv Microb Physiol* **74**, 1-96 (2019). https://doi.org/10.1016/bs.ampbs.2019.02.007

2 Nealson, K. H., Belz, A. & McKee, B. Breathing metals as a way of life: geobiology in action. *Antonie Van Leeuwenhoek* **81**, 215-222 (2002). https://doi.org/10.1023/a:1020518818647

3 Hansel, C. M. Manganese in marine microbiology. *Adv Microb Physiol* **70**, 37-83 (2017). https://doi.org/10.1016/bs.ampbs.2017.01.005

4 Lovley, D. R., Holmes, D. E. & Nevin, K. P. Dissimilatory Fe(III) and Mn(IV) reduction. *Adv Microb Physiol* **49**, 219-286 (2004). https://doi.org/10.1016/S0065-2911(04)49005-5

5 Joshi, K., Chan, C. H. & Bond, D. R. Geobacter sulfurreducens inner membrane cytochrome CbcBA controls electron transfer and growth yield near the energetic limit of respiration. *Mol Microbiol* **116**, 1124-1139 (2021). https://doi.org/10.1111/mmi.14801

6 Liu, Y. *et al.* A trans-outer membrane porin-cytochrome protein complex for extracellular electron transfer by Geobacter sulfurreducens PCA. *Environ Microbiol Rep* **6**, 776-785 (2014). https://doi.org/10.1111/1758-2229.12204

7 Reguera, G. *et al.* Extracellular electron transfer via microbial nanowires. *Nature* **435**, 1098-1101 (2005). https://doi.org/10.1038/nature03661

8 Feliciano, G. T., Steidl, R. J. & Reguera, G. Structural and functional insights into the conductive pili of Geobacter sulfurreducens revealed in molecular dynamics simulations. *Phys Chem Chem Phys* **17**, 22217-22226 (2015). https://doi.org/10.1039/c5cp03432a

9 Speers, A. M., Schindler, B. D., Hwang, J., Genc, A. & Reguera, G. Genetic identification of a PilT motor in *Geobacter sulfurreducens* reveals a role for pilus retraction in extracellular electron transfer. *Front Microbiol* **7**, 1578 (2016). https://doi.org/10.3389/fmicb.2016.01578

10 Backes, C. A., McLaren, R. G., Rate, A. W. & Swift, R. S. Kinetics of cadmium and cobalt desorption from iron and manganese oxides. *Soil Sci Soc Am J* **59**, 778-785 (1995). https://doi.org/10.2136/sssaj1995.03615995005900030021x

11 Krupka, K. M. & Serne, R. J. (ed Pacific Northwest National Laboratory) (Washington, 2002).

12 Dulay, H., Tabares, M., Kashefi, K. & Reguera, G. Cobalt resistance via detoxification and mineralization in the iron-reducing bacterium *Geobacter*

sulfurreducens. *Front Microbiol* **11**, 600463 (2020). https://doi.org/10.3389/fmicb.2020.600463

13 Shelton, A. N. *et al.* Uneven distribution of cobamide biosynthesis and dependence in bacteria predicted by comparative genomics. *ISME J* **13**, 789-804 (2019). https://doi.org/10.1038/s41396-018-0304-9

14 Yan, J., Ritalahti, K. M., Wagner, D. D. & Löffler, F. E. Unexpected specificity of interspecies cobamide transfer from *Geobacter* spp. to organohalide-respiring *Dehalococcoides mccartyi* strains. *Appl Environ Microbiol* **78**, 6630-6636 (2012). https://doi.org/10.1128/aem.01535-12

15 Barras, F. & Fontecave, M. Cobalt stress in *Escherichia coli* and *Salmonella enterica*: molecular bases for toxicity and resistance. *Metallomics* **3**, 1130-1134 (2011). https://doi.org/10.1039/c1mt00099c

16 Valko, M., Morris, H. & Cronin, M. T. Metals, toxicity and oxidative stress. *Curr Med Chem* **12**, 1161-1208 (2005). https://doi.org/10.2174/0929867053764635

17 Aklujkar, M. *et al.* Proteins involved in electron transfer to Fe(III) and Mn(IV) oxides by *Geobacter sulfurreducens* and *Geobacter uraniireducens*. *Microbiology* **159**, 515-535 (2013). https://doi.org/10.1099/mic.0.064089-0

18 Leang, C., Coppi, M. V. & Lovley, D. R. OmcB, a c-type polyheme cytochrome, involved in Fe(III) reduction in Geobacter sulfurreducens. *J Bacteriol* **185**, 2096-2103 (2003). https://doi.org/10.1128/JB.185.7.2096-2103.2003

19 Qian, X., Reguera, G., Mester, T. & Lovley, D. R. Evidence that OmcB and OmpB of *Geobacter sulfurreducens* are outer membrane surface proteins. *FEMS Microbiol Lett* **277**, 21-27 (2007). https://doi.org/10.1111/j.1574-6968.2007.00915.x

20 Dulay, H., Tabares, M., Kashefi, K. & Reguera, G. Cobalt Resistance via Detoxification and Mineralization in the Iron-Reducing Bacterium. *Front Microbiol* **11**, 600463 (2020). https://doi.org/10.3389/fmicb.2020.600463

21 Reguera, G. Microbial nanowires and electroactive biofilms. *FEMS Microbiol Ecol* **94** (2018). https://doi.org/10.1093/femsec/fiy086

22 Ding, Y. H. *et al.* The proteome of dissimilatory metal-reducing microorganism Geobacter sulfurreducens under various growth conditions. *Biochim Biophys Acta* **1764**, 1198-1206 (2006). https://doi.org/10.1016/j.bbapap.2006.04.017

23 Chin, K. J., Esteve-Núñez, A., Leang, C. & Lovley, D. R. Direct correlation between rates of anaerobic respiration and levels of mRNA for key respiratory genes in Geobacter sulfurreducens. *Appl Environ Microbiol* **70** (2004). https://doi.org/10.1128/AEM.70.9.5183-5189.2004

24 Leang, C. & Lovley, D. R. Regulation of two highly similar genes, omcB and omcC, in a 10 kb chromosomal duplication in Geobacter sulfurreducens. *Microbiology (Reading, England)* **151** (2005). https://doi.org/10.1099/mic.0.27870-0

25 Cologgi, D. L., Lampa-Pastirk, S., Speers, A. M., Kelly, S. D. & Reguera, G. Extracellular reduction of uranium via Geobacter conductive pili as a protective cellular mechanism. *Proc Natl Acad Sci U S A* **108**, 15248-15252 (2011). https://doi.org/10.1073/pnas.1108616108

26 Cosert, K. M., Steidl, R. J., Castro-Forero, A., Worden, R. M. & Reguera, G. Electronic characterization of Geobacter sulfurreducens pilins in self-assembled monolayers unmasks tunnelling and hopping conduction pathways. *Phys Chem Chem Phys* **19**, 11163-11172 (2017). https://doi.org/10.1039/c7cp00885f

27 Cosert, K. M. & Reguera, G. Voltammetric study of conductive planar assemblies of Geobacter nanowire pilins unmasks their ability to bind and mineralize divalent cobalt. *J Ind Microbiol Biotechnol* **46**, 1239-1249 (2019). https://doi.org/10.1007/s10295-019-02167-5

28 Clark, M. M., Paxhia, M. D., Young, J. M., Manzella, M. P. & Reguera, G. Adaptive synthesis of a rough lipopolysaccharide in *Geobacter sulfurreducens* for metal reduction and detoxification. *Appl Environ Microbiol* **87**, e0096421 (2021). https://doi.org/10.1128/AEM.00964-21

29 Konovalova, A. & Silhavy, T. J. Outer membrane lipoprotein biogenesis: Lol is not the end. *Philos Trans R Soc Lond B Biol Sci* **370**, 20150030 (2015). https://doi.org/10.1098/rstb.2015.0030

30 Ma, X., Yan, Y., Wang, W., Guo, J. & Wang, Y. Metatranscriptomic analysis of adaptive response of anammox bacteria *Candidatus* 'Kuenenia stuttgartiensis' to Zn(II) exposure. *Chemosphere* **246**, 125682 (2020). https://doi.org/10.1016/j.chemosphere.2019.125682

31 Nies, D. H. Efflux-mediated heavy metal resistance in prokaryotes. *FEMS Microbiol Rev* **27** (2003). https://doi.org/10.1016/S0168-6445(03)00048-2

32 Harrison, J. J., Ceri, H. & Turner, R. J. Multimetal resistance and tolerance in microbial biofilms. *Nat Rev Microbiol* **5**, 928-938 (2007). https://doi.org/doi:10.1038/nrmicro1774

33 Teitzel, G. M. & Parsek, M. R. Heavy metal resistance of biofilm and planktonic Pseudomonas aeruginosa. *Appl Environ Microbiol* **69**, 2313-2320 (2003).

34 Rollefson, J. B., Stephen, C. S., Tien, M. & Bond, D. R. Identification of an extracellular polysaccharide network essential for cytochrome anchoring and biofilm formation in *Geobacter sulfurreducens*. *J Bacteriol* **193**, 1023-1033 (2011). https://doi.org/10.1128/JB.01092-10

35 Shelobolina, E. S. *et al.* Importance of c-Type cytochromes for U(VI) reduction by Geobacter sulfurreducens. *BMC Microbiol* **7** (2007). https://doi.org/10.1186/1471-2180-7-16

36 McBroom, A. J. & Kuehn, M. J. Release of outer membrane vesicles by Gram-negative bacteria is a novel envelope stress response. *Mol Microbiol* **63**, 545-558 (2007). https://doi.org/10.1111/j.1365-2958.2006.05522.x

37 Schwechheimer, C. & Kuehn, M. J. Outer-membrane vesicles from Gram-negative bacteria: biogenesis and functions. *Nat Rev Microbiol* **13**, 605-619 (2015). https://doi.org/doi:10.1038/nrmicro3525

38 Steidl, R. J., Lampa-Pastirk, S. & Reguera, G. Mechanistic stratification in electroactive biofilms of Geobacter sulfurreducens mediated by pilus nanowires. *Nat Commun* **7**, 1-11 (2016). https://doi.org/doi:10.1038/ncomms12217

39 Kim, B. C. *et al.* Insights into genes involved in electricity generation in Geobacter sulfurreducens via whole genome microarray analysis of the OmcF-deficient mutant. *Bioelectrochemistry* **73**, 70-75 (2008). https://doi.org/10.1016/j.bioelechem.2008.04.023

40 Mehta, T., Coppi, M. V., Childers, S. E. & Lovley, D. R. Outer membrane c-type cytochromes required for Fe(III) and Mn(IV) oxide reduction in Geobacter sulfurreducens. *Appl Environ Microbiol* **71**, 8634-8641 (2005). https://doi.org/10.1128/AEM.71.12.8634-8641.2005

41 Wang, F. *et al.* Structure of *Geobacter* OmcZ filaments suggests extracellular cytochrome polymers evolved independently multiple times. *Elife* **11** (2022). https://doi.org/10.7554/eLife.81551

42 Chandrangsu, P., Rensing, C. & Helmann, J. D. Metal homeostasis and resistance in bacteria. *Nat Rev Microbiol* **15**, 338-350 (2017). https://doi.org/doi:10.1038/nrmicro.2017.15

43 Embree, M. *et al.* The iron stimulon and Fur regulon of *Geobacter sulfurreducens* and their role in energy metabolism. *Appl Environ Microbiol* **80**, 2918-2927 (2014). https://doi.org/10.1128/aem.03916-13

44 Cologgi, D. L., Speers, A. M., Bullard, B. A., Kelly, S. D. & Reguera, G. Enhanced uranium immobilization and reduction by *Geobacter sulfurreducens* biofilms. *Appl Environ Microbiol* **80**, 6638-6646 (2014). https://doi.org/10.1128/AEM.02289-14

45 Mah, T. F. & O'Toole, G. A. Mechanisms of biofilm resistance to antimicrobial agents. *Trends Microbiol* **9** (2001). https://doi.org/10.1016/s0966-842x(00)01913-2

46 Hall-Stoodley, L., Costerton, J. & Stoodley, P. Bacterial biofilms: from the natural environment to infectious diseases. *Nat Rev Microbiol* **2** (2004). https://doi.org/10.1038/nrmicro821

47 Kulp, A. & Kuehn, M. J. Biological functions and biogenesis of secreted bacterial outer membrane vesicles. *Annu Rev Microbiol* **64**, 163-184 (2010). https://doi.org/10.1146/annurev.micro.091208.073413

48 Liu, X. *et al.* Bacterial vesicles mediate extracellular electron transfer. *Environ Sci Technol Lett* **7**, 27-34 (2019). https://doi.org/10.1021/acs.estlett.9b00707

49 Johnson, T. A. *et al.* Clusters of antibiotic resistance genes enriched together stay together in swine agriculture. *mBio* **7**, e02214-02215 (2016). https://doi.org/10.1128/mBio.02214-15

50 Vargas, C., McEwan, A. G. & Downie, J. A. Detection of c-type cytochromes using enhanced chemiluminescence. *Anal Biochem* **209**, 323-326 (1993). https://doi.org/10.1006/abio.1993.1127

Chapter 4: Expression of electrically conductive pili as a mechanism for Co^{II} tolerance

This chapter presents data (growth experiments at 30^{o}C versus 25^{o}C and WT versus Δ*pilB* and Δ*pilT3/4* strains) generated as part of a collaborative effort with Marcela Tabares.

ABSTRACT

The use of electrically conductive pili for extracellular respiration and mineralization of metals is a hallmark of the physiology of *Geobacter* bacteria. *In vitro* studies with the model representative, *Geobacter sulfurreducens*, suggested that the pili can also bind Co^{II} and, at sufficiently low potentials, they can reductively precipitate it to Co^{0}. To test this hypothesis, we compared the effect of $CoCl_2$ on the growth of *G. sulfurreducens* at temperatures that induce (25ºC) or prevent (30ºC) pili assembly. Temperature-induced piliation rescued the intoxication effects of the metal on cell growth (reduced lag phase, generation times, growth yields). Mutants unable to assemble pili (Δ*pilB*) were also more sensitive to Co^{II} toxicity than the wild-type (WT) strain but the hyperpiliation of a pilus retraction-defective mutant (Δ*pilT3/4*) rescued the growth defects and accelerated the recovery of Co^{II}-stressed cells compared to WT cells. Transmission electron micrographs revealed extensive accumulation of metal nanoparticles along the Δ*pilT3/4* pili, in contrast to the modest and localized deposition of metal on the surface of the non-piliated cells. These results demonstrate that pili expression confers a growth advantage on *G. sulfurreducens* during and after metal stress. The rapid mineralization of the metal along the pili provides an effective mechanism for its extracellular detoxification that also mitigates Co^{II} permeation of the membrane.

INTRODUCTION

Bacteria in the genus *Geobacter* have long been studied as model organisms of metal respiration, particularly for the dissimilatory reduction of Fe^{III} and Mn^{IV} oxides that solubilizes the metals as Fe^{II} and Mn^{II} [1-3]. By coupling the catabolism of fermentation byproducts to the storage of electrons in periplasmic cytochromes, *Geobacter* cells build

a large cell envelope capacitance that allows for the rapid discharge of electrons upon contact with metal acceptors [4-6]. Outer membrane *c*-cytochromes provide a path for the discharge of periplasmic electrons onto extracellular electron acceptors [4,7]. To increase the redox-active surface of the cell during the reduction of metal oxide minerals, *Geobacter* bacteria assemble electrically conductive protein filaments (pili) of the Type IVa pilus class [8]. The expression of *Geobacter* pili is required for the cells to grow with Fe^{III} oxide minerals [8] and facilitates access to the solid metal phases through the narrow pores of soils [9]. Antagonistic cycles of pilus assembly and disassembly via ATPases of the Type IV pilus biosynthetic apparatus (PilB and PilT, respectively) ensure that reduced mineral byproducts are shed off and clean fibers are produced for new electron discharges [10,11]. Additionally, the dynamic pili promote electron transfer across biofilms [10,12] and are the primary mechanism for the reductive mineralization of the soluble uranyl cation (UO_2^{2+}), a reaction that simultaneously generates energy for growth and detoxifies the toxic U^{VI} species [12,13].

Like other Type IV pili, the *Geobacter* pilus fibers are assemblies of a peptide subunit (the PilA pilin) [13]. The *Geobacter* pilins lack the conserved globular domain of other bacterial pilins, which makes them shorter and predominantly helical in structure [8,14]. They also contain several aromatic residues that cluster close to each other in the pilin assembly to transport charges along the pilus fiber [8,14]. The formation of salt bridges between neighboring subunits during polymerization aligns the aromatic residues such that charge hopping is facilitated along the pilus and directed towards electron acceptors bound to the fiber's surface [14,15]. Indeed, alanine replacements of these aromatic residues do not prevent pilus assembly but drastically reduce their conductivity and the ability of

the cells to form electroactive biofilms [10]. The assembly of pilin subunits in the fibers exposes the peptide's C-terminal region on the pilus surface and forms motifs for metal binding and reduction [15,16]. Such metal traps can also be recreated in planar configurations of pilin assemblies onto electrodes [15] and their metal affinity probed electrochemically [16]. Such electrochemical studies revealed a high affinity of the pilin metal traps for the divalent cobalt cation, Co^{II}, which was reductively mineralized to Co^{0} nanoparticles [16]. This finding suggested that *Geobacter* may use the pili to reductively precipitate Co^{II} outside the cell, effectively preventing the permeation of the toxic cation inside the cell envelope.

Given the tendency of Fe^{III} and Mn^{VI} oxides to co-precipitate and adsorb Co^{II} [17-19], the mineralization of Co^{II} by *Geobacter* pili could provide an effective mechanism to detoxify the substantial amounts of toxic metal released during the reductive dissolution of the minerals [20]. Co^{II} detoxification by the pili would also impact the microbial communities that depend on *Geobacter* bacteria for the synthesis and secretion of Co-containing vitamins (cobamides) [21-23]. Indeed, the extracellular mineralization of Co^{II} by the pili would alleviate metal toxicity, at least locally, to *Geobacter* cells as well as their cobamide-dependent syntrophic partners. This way, *Geobacter* cells can assimilate the metal into the cobamide biosynthetic pathways [24] and secrete them to support the growth of syntrophic partners [21,25]. In this chapter, I explored the contribution of the pili to Co^{II} tolerance in *G. sulfurreducens*. For these studies, I used temperature switches that trigger or prevent pilin assembly (growth at 25°C and 30°C, respectively) [8,26] and tested the response to Co^{II} stress of mutants carrying deletions in the ATPases that power pilin assembly (PilB) or disassembly (PilT) [10,11]. The findings support the role for the electrically

conductive pili of *Geobacter* in overcoming Co^{II} toxicity via extracellular mineralization and expand the known reactions used by *Geobacter* bacteria to cycle this important metal.

RESULTS

Temperature-induced piliation partially rescues Co^{II} intoxication

Pilin assembly by *G. sulfurreducens* can be triggered in the absence of Fe^{III} oxides by dropping the temperature from 30ºC (standard laboratory conditions) to 25ºC, a temperature that presumably lowers growth rates to levels similar to those of cells during the respiration of Fe^{III} oxides [8,13]. We took advantage of this temperature effect in piliation to assess the contribution of pili expression to Co^{II} tolerance in cultures of *G. sulfurreducens* grown in DBAF medium in the presence or absence of non-lethal concentrations of Co^{II} (provided as 250 µM $CoCl_2$). As we previously reported [24], non-piliated cells (30ºC cultures) grown with the metal required a phase of acclimation and doubled slower than in untreated cultures (Fig. 4.1A). This response was stochastic as one of the replicate cultures grew similar to untreated cells. However, the non-piliated cultures acclimated quickly (Fig. 4.1A), albeit slower (1.73 ± 0.64-fold longer lag phase than untreated controls, $p = 0.2$). Once acclimated to metal stress, the non-piliated cells doubled at highly variable rates, another sign of stochasticity in culture tolerance (4.8 ± 3.3-fold slower than the untreated controls, $p = 0.2$) (Fig. 4.1C). This is consistent with metal-stressed cells diverting more energy from growth-sustaining processes towards metal detoxification. Another symptom of metal stress was the higher variability among replicates of the metal-treated cultures compared to the untreated controls (Fig. 4.1A),

which results from the stochastic activation of multiple detoxification pathways by the non-piliated cells under Co^{II} pressure [24].

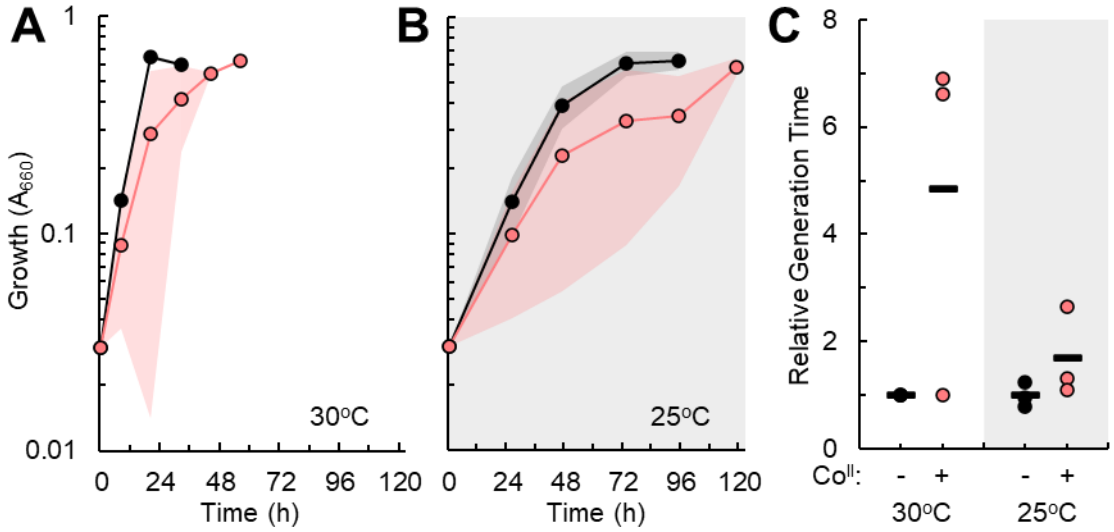

Figure 4.1 Growth response of *G. sulfurreducens* to $CoCl_2$ treatment at pili-inhibiting and -inducing temperatures. (A-B) Growth (A_{660}) of piliated (**A**) or non-piliated (**B**) cells in DBAF medium at 30°C (white) and 25°C (gray), respectively, in the absence (black circles) or presence (pink circles) of 250 µM $CoCl_2$. Shown are average (line) and standard deviation (shaded area) of triplicate cultures for each condition. **(C)** Average (line) and individual (circle) generation times of Co-treated cultures relative to the untreated controls from **A-B**.

Variability was even higher in the piliated cultures (25°C) (Fig. 4.1B). This result is not surprising, considering that cells must acclimate to both lower temperatures and metal stress. Consistent with this dual cause, some replicates had lag phases within the ranges of untreated controls while others required extended incubation (~48 h) before cells started to grow exponentially (Fig. 4.1B). The presence of at least one replicate with severely delayed growth at 25°C in the presence of Co^{II} was in fact a routine occurrence. Despite this variability, once the piliated cells resumed growth they doubled in the presence of Co^{II} at rates similar to the untreated controls (1.69 ± 0.84-fold slower, $p = 0.2$) (Fig. 4.1C). The partial rescue of the Co^{II}-triggered growth rate defects when growing

under pili-inducing conditions supports a role for pili in mitigating Co^{II} intoxication in exponentially growing cells.

Genetic disruption of pilus assembly and retraction reduces Co^{II} tolerance

The confounding effects of cold and metal stress adaptation in the temperature-controlled experiments (Fig. 4.1) masked a potential role for piliation in the acclimation to metal stress. To bypass this limitation, we used a genetic approach to investigate the effect of piliation on the acclimation of cells to Co^{II} stress. For these experiments, we grew the wild type (WT) strain at 30ºC (non-piliated conditions) in the presence of $CoCl_2$ concentrations (500 µM) that require a long phase of acclimation [24] and compared the phenotype to mutants carrying deletions in the genes encoding the ATPases that power pilus assembly (PilB) [10] and retraction (PilT3/4) [11] (Fig. 4.2). Fig. 4.2A shows typical results for the WT and mutant cultures, where two out of three replicates acclimated after an extended lag phase (Fig. 4.2A). (One replicate culture, which did not resume growth after 6 days of incubation, was discarded.) The average lag phase for the acclimated WT cultures was 37.5 ± 1.3 h but longer (and more variable) in the Δ*pilB* mutants (91.4 ± 55.4 h) (Fig. 4.2B). These phenotypes (extended and variable lag phase) are hallmarks of Co^{II} acclimation in *G. sulfurreducens* [24] and are consistent with the need for cells to induce pili assembly in order to acclimate to Co^{II} stress and resume growth in the presence of the metal. Two out of three Δ*pilT3/4* cultures also resumed growth after a long phase of acclimation (70.2 ± 1.0 h) (Fig. 4.2B). The extended acclimation phase of the Δ*pilT3/4* may be interpreted as supporting a role for pilus retraction in Co^{II} detoxification. Pilus depolymerization in *G. sulfurreducens* is mediated by the main PilT ATPase, PilT4, and assisted by PilT3 [11]. Together, PilT4 and PilT3 coordinate pili retraction to shed off

reduced mineral particles that remain attached to the fibers during the respiration of Fe^{III} oxides [11]. A similar model could describe the role of PilB in pilus protrusion to reductively precipitate Co^{II} at the pilus surface and the need for PilT3/4 to retract the pili to detach the Co^0 nanoparticles and enable a new cycle of pilus protrusion and Co^{II} mineralization.

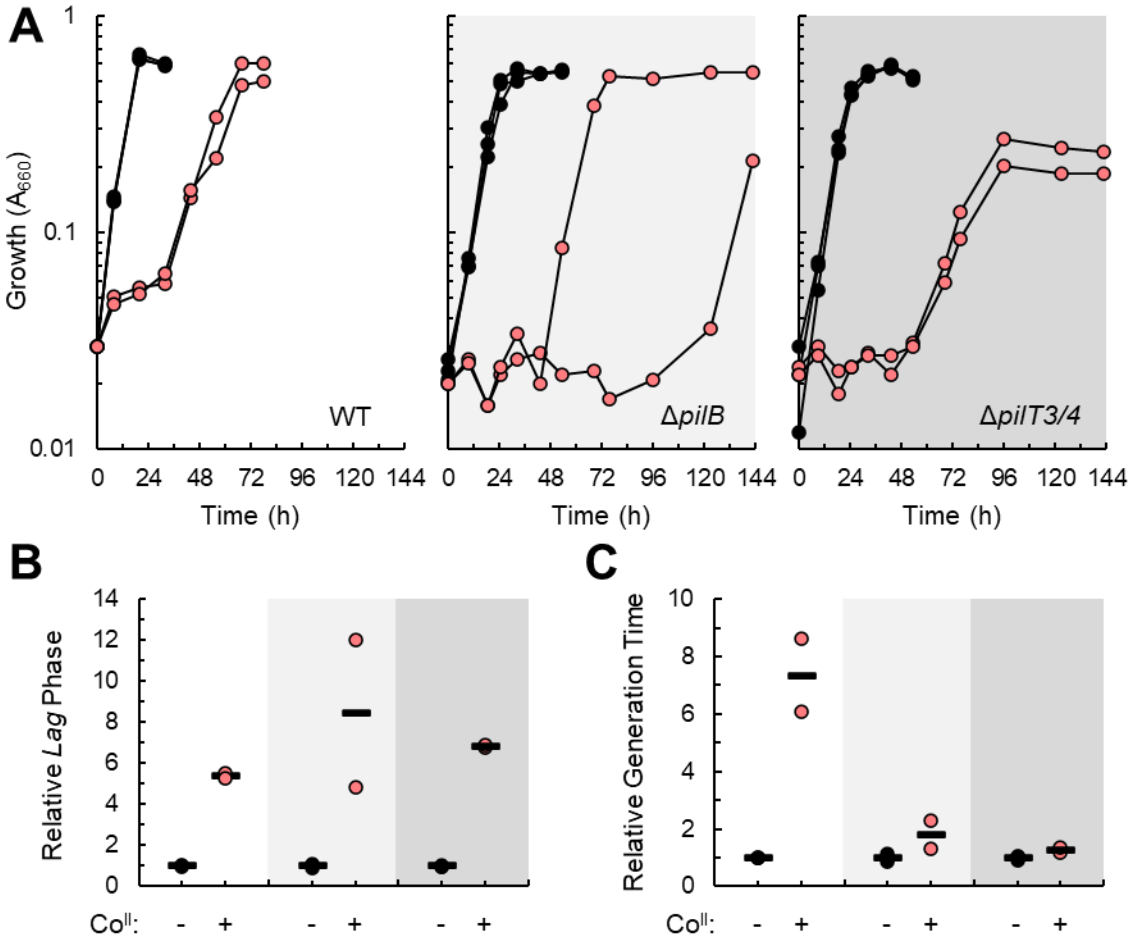

Figure 4.2 Contribution of pili assembly and retraction to Co^{II} tolerance. (A) Growth (A_{660}) of WT, pilus assembly mutant (*ΔpilB*) and pilus retraction mutant (*ΔpilT3/4*) in DBAF at 30°C in the absence (black symbols) or presence (pink symbols) of 500 µM $CoCl_2$. **(B-C)** Average (lines) and individual (circles) lag phase duration (**B**) and generation times (**C**; relative to untreated cultures) of the cultures shown in **A**.

While important for rapid acclimation to metal stress, the pili detoxification pathway was dispensable once acclimated cells resumed exponential growth (Fig. 4.2A). Indeed, the doubling times for the acclimated cultures of the Δ*pilB* and Δ*pilT3/4* strains were

similar to the untreated cultures (Fig. 4.2C). Transmission electron microscopy (TEM) images of unstained metal-stressed cells from the exponentially growing cultures revealed phenotypes consistent with different responses to Co^{II} intoxication by the WT and mutant cells (Fig. 4.3). WT cells were surrounded by a thick, electron-dense substance consistent with the reported production of Xap exopolysaccharide (EPS) during the exponential phase of growth [24]. Application of additional stains, such as uranium, were unnecessary given the ability of the Co^{II} salts to react with the amino groups of basic amino acids to form insoluble complexes that enhance the contrast of biological samples for TEM visualization [27]. This staining suggests that Co^{II} penetrated through the EPS barrier and into the cells. The EPS layer of WT cells was absent in the mutant strains (Fig. 4.3). Furthermore, the pili-deficient Δ*pilB* mutant cells accumulated Co nanoparticles sparsely on the cell surface, a phenotype associated with the reductive mineralization of the metal by outer membrane *c*-type cytochromes [24]. By contrast, the hyperpiliated *pilT3/4* strain [11] had substantial extracellular mineralization along the pili on one side of the cell (Fig. 4.3). Hence, although pili are not absolutely required for growth under Co^{II} stress (Fig. 4.2), they provide an efficient strategy for the detoxification of the metal. The experimental evidence also suggests that EPS and pili pathways may be co-regulated such that EPS production prevents pili assembly (WT cells in Fig. 4.3). The production of a thick EPS layer provides a physical and chemical barrier to the permeation of metals [28] and also promotes cell-cell aggregation and biofilm formation [29], thereby protecting the cells from metal intoxication. Pili production can also provide an effective mechanism for Co^{II} detoxification (Δ*pilT3/4* in Fig. 4.3) albeit on one side of the cell only. To protect the non-piliated side, cells coat the outer membrane with a rough (no O-

antigen) lipopolysaccharide (LPS), which sequesters metal cations, and vesiculate extensively to release the metal-saturated LPS [30].

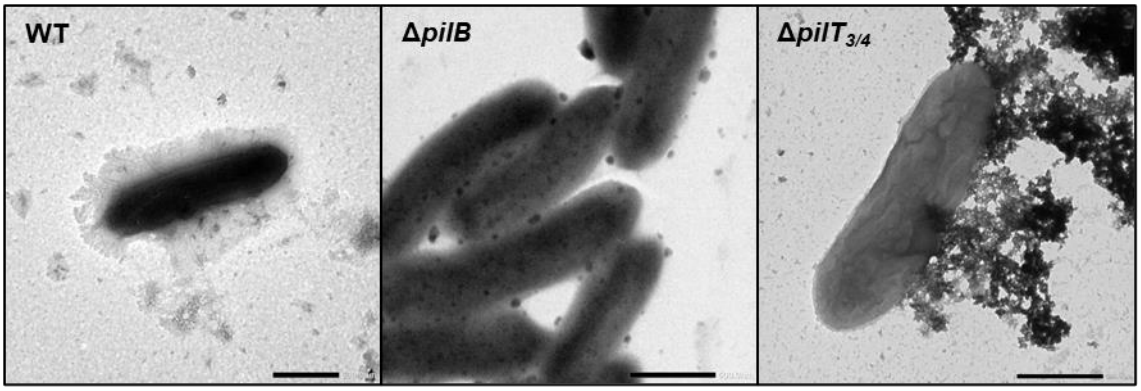

Figure 4.3 Transmission electron microscopy (TEM) images of Co^{II}-treated cells. Representative TEM micrographs of WT, Δ*pilB*, and Δ*pilT3/4* cells grown to mid-exponential phase (A_{660} ~0.3-0.4) in DBAF with 500 µM $CoCl_2$. Samples are unstained and fixed onto formvar-coated grids with 2.5% glutaraldehyde prior to imaging. Scale bars are 500 nm.

Expression of pili reduces Co^{II} toxicity in resting cells

Metal removal by resting (non-growing) cells and their consequent growth recovery in metal-free medium provide a suitable assay to assess the contribution of cellular appendages to mineralization and detoxification [13,31] without the interference of growth-supporting pathways [32]. Hence, we exposed resting cells of the WT and hyperpiliated Δ*pilT4* strains to 200 µM $CoCl_2$ for 2 h and tested the extent of intoxication by recovering the resting cells in growth medium (FWAF) without the metal (Fig. 4.4A). As previously reported in Chapter 3, the WT cells recovered from the Co^{II} challenge after a longer lag phase than untreated cell controls (Fig. 4.4B). However, once exponential growth started, the WT cells doubled at rates comparable to the untreated controls (Fig. 4.4C). The hyperpiliated Δ*pilT4* strain recovered from the Co^{II} challenge as rapidly as the untreated controls and without substantial variability among the replicates (Fig. 4.4A and B).

Furthermore, it grew at the same growth rates as untreated cultures (Fig. 4.4C). Hence, the mutant cells have a growth advantage after Co^{II} exposure. The constitutive production of the pili by the mutant cells bypassed the need that WT cells have in inducing their biosynthesis, while their retraction defect increases piliation and their ability to detoxify Co^{II} via its extracellular precipitation (Fig. 4.3). As a result, resting Δ*pilT4* cells readily resumed growth after Co^{II} exposure while the non-piliated WT cells required acclimation to induce the metal detoxification pathways (Fig. 4.4).

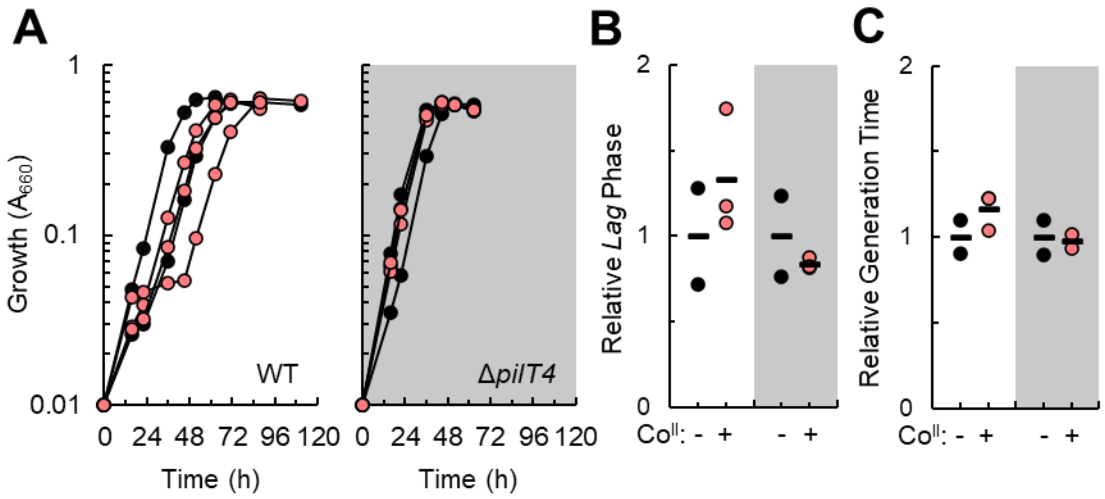

Figure 4.4 Effect of piliation on viability after Co^{II} exposure in a resting state. (A) Growth (A_{660}) of WT (non-piliated) and Δ*pilT4* (hyperpiliated) cells in metal-free FWAF medium after a 2-h resting cell assays in the presence (pink) or absence (black) of 200 μM $CoCl_2$. **(B-C)** Average (line) and individual (symbols) length of the *lag* phase (**B**) and generation times (**C**), relative to the average of the untreated controls of the cultures shown in panel **A**.

DISCUSSION

The electrochemical demonstration that the pilin's metal traps can bind Co^{II} with high affinity and reductively precipitate it as Co^0 nanoparticles [16] suggested a biological role for the *Geobacter* pili in the mineralization of this essential metal. In support of this hypothesis, temperature-induced piliation in *G. sulfurreducens* [8,13] partially rescued the

growth defects (longer lag phases and generation times) of cultures supplemented with non-lethal concentrations of Co^{II} (Fig. 4.1). The growth rescue by piliation is similar to that reported for the uranyl cation, a toxic radionuclide that the pili reductively precipitate outside of the cell to prevent its permeation and non-specific reduction inside the cell envelope [13]. The fact that pili are also required to reductively dissolve the Fe^{III}- and Mn^{IV}-oxides [8,9], which trap significant amounts of Co^{II} in the environment [17-20], suggests a dual role for the conductive appendages in supporting growth with the metal oxides and tolerance of the solubilized Co^{II} cation. The sudden exposure of the cells to Co^{II} exerts selective pressure to rapidly acclimate to metal toxicity (*adapt or die*). Genetic studies with a mutant unable to assemble the pilins (Δ*pilB*) [10] suggested an important role for the pili in acclimation to metal stress as well. In support of this function, the pili-deficient mutant cells required extended lag phases to acclimate to potentially lethal concentrations of Co^{II} (500 µM $CoCl_2$) (Fig. 4.2). A mutant (Δ*pilT3/4*) carrying deletions in the primary and secondary ATPases (PilT4 and PilT3, respectively) that energize pili depolymerization [11] required a longer phase of acclimation, albeit shorter than the Δ*pilB* (Fig. 4.2). Pili retraction sheds off pilus-bound minerals and recycles the pilin subunits for new rounds of polymerization [11]. Antagonistic cycles of pilus protrusion and retraction may thus be needed for *G. sulfurreducens* to acclimate to Co^{II} stress and resume growth in the presence of the metal. However, other explanations are possible. The Δ*pilT3/4* mutation also leads to the constitutive production of pili and, by preventing their retraction, the mutant cells become hyperpiliated [11]. Hence, the delayed acclimation of this mutant to Co^{II} stress compared to the WT cells may have been the result of these additional phenotypes. For example, the hyperpiliation phenotype, rather than the pilus retraction

defect, of a Δ*pilT* mutant of *Pseudomonas aeruginosa* interferes with secretory functions [33]. Similar pleiotropic effects of the retraction mutant could have delayed the activation of pili-independent pathways for Co^{II} detoxification.

Piliation may also provide a first layer of defense to the cells, reducing intoxication so sufficient energy may be allocated towards the synthesis of efflux pumps, protein repair, and ROS detoxification [24]. The transcriptional activation of these pathways allows the cells to grow and divide under metal stress [24]. These pathways can compensate for the lack of piliation and pilus retraction, as indicated by the ability of acclimated cultures of the Δ*pilB* and Δ*pilT3/4* mutants to grow under metal stress at WT rates (Fig. 4.2). The extensive mineralization along the pili of the hyperpiliated Δ*pilT3/4* strain (Fig. 4.3) suggests that pili-mediated precipitation of Co^{II} outside of the cell minimizes metal diffusion into the cell, as reported for the uranyl cation [13]. The pili are indeed the primary mechanism for the extracellular mineralization of the uranyl cation in *G. sulfurreducens*, a reaction that prevents the toxic cation from traversing the outer membrane and mineralizing in the periplasmic space [13]. As a result, the uranyl cation readily penetrates and gets reductively mineralized into the cell envelope of non-piliated cells while in the resting state and delays their ability to reinitiate growth once in metal-free medium [13]. Similarly, resting cells exposed to Co^{II} for a few hours were able to resume growth in metal-free medium more rapidly when piliated (Fig. 4.4). This fast response is consistent with piliation protecting the cells from metal penetration, which reduces intoxication and facilitates growth recovery in metal-free medium.

The presence of *c*-cytochromes on the cell surface of *G. sulfurreducens* provides an alternative path for the reductive immobilization of Co^{II} in non-piliated cells. These

cytochrome conduits could have contributed to the sparse mineralization of Co observed in TEM images of the non-piliated Δ*pilB* cells (Fig. 4.3). The distribution of mineral particles over the Δ*pilB* cells matches well with the pattern of deposition of Co nanoparticles on the surface of non-piliated WT cells (grown at 30^{o}C). Non-piliated WT cells grown with Co^{II} upregulate cell envelope cytochromes that could provide a pathway for the reductive precipitation of the metal on the outer surface [24]. However, the contribution of the cytochrome pathway to Co^{II} detoxification is likely small compared to that of pili, which provide a more extensive mineralization capacity (Fig. 4.3). The pili-mediated reaction is however not needed once the cells acclimate to metal stress, as alternative detoxification pathways are activated that can support growth and metal detoxification. Notably, non-piliated WT cells produced a thick, protective EPS layer under Co^{II} stress (Fig. 4.3). Such a passive barrier to Co^{II} permeation may offer advantages over the pili to exponentially growing cells. The low reduction potential of the Co^{II}/Co^{0} pair (-0.27 V vs SHE) makes the reductive detoxification of Co^{II} a barely energy-yielding reaction. ATP expenditure on the polymerization and depolymerization of the pili could make the reaction an energy intensive process. By contrast, once synthesized, EPS passively immobilizes Co^{II} before it reaches the cell envelope. Furthermore, the EPS layer of *G. sulfurreducens* anchors outer membrane cytochromes, which could provide some reductive capacity [34]. Importantly, EPS promotes cell-cell agglutination and biofilm formation, a process that enhances tolerance to metals [35] and other biocide compounds [36]. The heterogenous phenotypes of biofilm cells may further increase metabolic rates and catalytic activities that are required for detoxification and survival during metal stress [35-37].

The biomineralization of Co via the conductive pili of *G. sulfurreducens* affords new opportunities for mining and reclaiming this critical metal from environmental and industrial sources. As a strategic resource, Co is a key component of many technologies that society relies on, including rechargeable batteries [38], superalloys [39], and super conductors [40,41]. The biomineralizing properties of *Geobacter* bacteria and their pili could be harnessed to boost Co recovery from metal-impacted sites [42-44]. Microbial electroreclamation technologies may also be developed to recover Co and other metal cations from spent products such as those used in the cathodes of electric vehicle batteries and other consumer electronics [41,45]. The availability of platforms to mass-produce recombinant pilins [15] and assemble them on electrodes [16] or as protein nanowires [46] are also significant, as they provide sustainable solutions for the extraction of metals from a variety of sources and the circularization of manufacturing processes critical to advance the climate economy [15,16].

MATERIALS AND METHODS

Bacterial strains and culture conditions

Cultures of *G. sulfurreducens* strain PCA [47], Δ*pilB* [10], Δ*pilT3/4* and Δ*pilT4* [11] were obtained from our laboratory culture collection. All strains were grown anaerobically in a minimal medium, DB or FW, supplemented with 20 or 15 mM acetate as the electron donor, respectively, and 40 mM fumarate as the electron acceptor [48]. Growth was monitored spectrophotometrically as absorbance at 600 nm (A_{600}) and cultures were routinely grown to late exponential phase (A_{600}, 0.5-0.6) prior to transfer to fresh medium. When indicated, an A_{660} was used to minimize Co^{II} interference with growth measurements.

Co^{II} tolerance assays

Cells of the WT strain were grown in metal-free DBAF medium at 30°C (non-piliated cells) or at 25°C to induce piliation [8,13]. The cultures were then transferred to fresh medium supplemented with 250 μM $CoCl_2$ or an equal volume of anaerobically prepared sterile ddH_2O (untreated controls). The starting A_{600} of the cultures was always 0.05, as previously described [24]. Experiments with the pili-deficient (Δ*pilB*) and pilus retraction-deficient (Δ*pilT3/4*) mutant strains used higher concentrations of $CoCl_2$ (500 μM) and were performed at 30°C. Growth in all cultures was monitored spectrophotometrically at 660 nm (A_{660}) to minimize the influence of Co^{II} on absorbance measurements. Growth phenotypes (length of the lag phase, generation time) were estimated using the Growthcurver R script (https://github.com/sprouffske/growthcurver). Briefly, growth curve data were matched to the sigmoidal curve of best fit to calculate the maximum generation time achieved, the maximum A_{660} achieved (carrying capacity), and initial population density of the culture. The length of the lag phase was defined as the time needed for a culture to rise above A_{660} of 0.05 using the standard equation for logarithmic growth.

Transmission electron microscopy (TEM)

Strains of WT, Δ*pilB* and Δ*pilT3/4* were grown at 30°C to mid-exponential phase (A_{660}, 0.3-0.4) in DBAF media treated with 500 μM $CoCl_2$ and fixed with 2.5% glutaraldehyde prior to deposition for 5 min on Formvar-coated grids (150 square-mesh Ni, Electron Microscopy Sciences). The grids with the samples were washed with double deionized (dd)H_2O three times (30 sec each), side-blotted to remove excess liquid and stored at room temperature until examination using a JEOL 1400 Flash 120kV transmission

electron microscope. A microscopy stain was purposedly omitted to prevent stain and mineral artifacts.

Co^{II} resting cell assay

Resting cell assays were performed as previously described [13] with some modifications. Unless otherwise indicated, all procedures were performed inside an anaerobic chamber (COY Labs). Cultures of WT or Δ*pilT4* cells were grown in FWAF medium at 30°C to mid-exponential phase (A_{600} ~0.4) and dispensed into 50-ml conical tubes. Samples were then pelleted by centrifugation to remove growth medium (10 min, 3,000 *g*), resuspended in a salt wash buffer using a Pasteur pipette, pelleted a second time, and resuspended in wash buffer, as previously optimized for extended viability of *Geobacter* resting cells in metal reduction assays [13,31]. The washed cells were resuspended into 30 ml of reaction buffer to an A_{600} of 0.1 before adding 20 mM acetate as an electron donor and 200 µM of $CoCl_2$ as an electron acceptor and incubating at 30°C. 1 ml samples were taken from resting cell suspensions after 2 h to inoculate 9 ml of untreated FWAF medium to monitor growth (A_{660}) recovery at 30°C after metal exposure [13].

REFERENCES

1 Reguera, G. & Kashefi, K. The electrifying physiology of Geobacter bacteria, 30 years on. *Adv Microb Physiol* **74**, 1-96 (2019). https://doi.org/10.1016/bs.ampbs.2019.02.007

2 Coates, J. D., Phillips, E. J., Lonergan, D. J., Jenter, H. & Lovley, D. R. Isolation of Geobacter species from diverse sedimentary environments. *Appl Environ Microbiol* **62** (1996). https://doi.org/10.1128/aem.62.5.1531-1536.1996

3 Lovley, D. R., Holmes, D. E. & Nevin, K. P. Dissimilatory Fe(III) and Mn(IV) reduction. *Adv Microb Physiol* **49**, 219-286 (2004). https://doi.org/10.1016/S0065-2911(04)49005-5

4 Liu, Y. *et al.* A trans-outer membrane porin-cytochrome protein complex for extracellular electron transfer by Geobacter sulfurreducens PCA. *Environ Microbiol Rep* **6**, 776-785 (2014). https://doi.org/10.1111/1758-2229.12204

5 Santos, T. C., Silva, M. A., Morgado, L., Dantas, J. M. & Salgueiro, C. A. Diving into the redox properties of Geobacter sulfurreducens cytochromes: a model for extracellular electron transfer. *Dalton Trans* **44** (2015). https://doi.org/10.1039/c5dt00556f

6 Esteve-Núñez, A., Sosnik, J., Visconti, P. & Lovley, D. R. Fluorescent properties of c-type cytochromes reveal their potential role as an extracytoplasmic electron sink in Geobacter sulfurreducens. *Environ Microbiol* **10** (2008). https://doi.org/10.1111/j.1462-2920.2007.01470.x

7 Leang, C., Coppi, M. V. & Lovley, D. R. OmcB, a c-type polyheme cytochrome, involved in Fe(III) reduction in Geobacter sulfurreducens. *J Bacteriol* **185** (2003). https://doi.org/10.1128/JB.185.7.2096-2103.2003

8 Reguera, G. *et al.* Extracellular electron transfer via microbial nanowires. *Nature* **435**, 1098-1101 (2005). https://doi.org/10.1038/nature03661

9 Michelson, K., Sanford, R. A., Valocchi, A. J. & Werth, C. J. Nanowires of Geobacter sulfurreducens require redox cofactors to reduce metals in pore spaces too small for cell passage. *Environ Sci Technol* **51**, 11660-11668 (2017). https://doi.org/10.1021/acs.est.7b02531

10 Steidl, R. J., Lampa-Pastirk, S. & Reguera, G. Mechanistic stratification in electroactive biofilms of Geobacter sulfurreducens mediated by pilus nanowires. *Nat Commun* **7**, 1-11 (2016). https://doi.org/doi:10.1038/ncomms12217

11 Speers, A. M., Schindler, B. D., Hwang, J., Genc, A. & Reguera, G. Genetic identification of a PilT motor in *Geobacter sulfurreducens* reveals a role for pilus retraction in extracellular electron transfer. *Front Microbiol* **7**, 1578 (2016). https://doi.org/10.3389/fmicb.2016.01578

12 Cologgi, D. L., Speers, A. M., Bullard, B. A., Kelly, S. D. & Reguera, G. Enhanced uranium immobilization and reduction by *Geobacter sulfurreducens* biofilms. *Appl Environ Microbiol* **80**, 6638-6646 (2014). https://doi.org/10.1128/AEM.02289-14

13 Cologgi, D. L., Lampa-Pastirk, S., Speers, A. M., Kelly, S. D. & Reguera, G. Extracellular reduction of uranium via Geobacter conductive pili as a protective cellular mechanism. *Proc Natl Acad Sci U S A* **108**, 15248-15252 (2011). https://doi.org/10.1073/pnas.1108616108

14 Feliciano, G. T., Steidl, R. J. & Reguera, G. Structural and functional insights into the conductive pili of Geobacter sulfurreducens revealed in molecular dynamics simulations. *Phys Chem Chem Phys* **17**, 22217-22226 (2015). https://doi.org/10.1039/c5cp03432a

15 Cosert, K. M., Steidl, R. J., Castro-Forero, A., Worden, R. M. & Reguera, G. Electronic characterization of Geobacter sulfurreducens pilins in self-assembled monolayers unmasks tunnelling and hopping conduction pathways. *Phys Chem Chem Phys* **19**, 11163-11172 (2017). https://doi.org/10.1039/c7cp00885f

16 Cosert, K. M. & Reguera, G. Voltammetric study of conductive planar assemblies of Geobacter nanowire pilins unmasks their ability to bind and mineralize divalent cobalt. *J Ind Microbiol Biotechnol* **46**, 1239-1249 (2019). https://doi.org/10.1007/s10295-019-02167-5

17 Hamilton, E. I. The geobiochemistry of cobalt. *Sci Total Environ* **150**, 7-39 (1994). https://doi.org/10.1016/0048-9697(94)90126-0

18 Manheim, F. T. Marine cobalt resources. *Science* **232** (1986). https://doi.org/10.1126/science.232.4750.600

19 Krupka, K. M. & Serne, R. J. (ed Pacific Northwest National Laboratory) (Washington, 2002).

20 Backes, C. A., McLaren, R. G., Rate, A. W. & Swift, R. S. Kinetics of cadmium and cobalt desorption from iron and manganese oxides. *Soil Sci Soc Am J* **59**, 778-785 (1995). https://doi.org/10.2136/sssaj1995.03615995005900030021x

21 Shelton, A. N. *et al.* Uneven distribution of cobamide biosynthesis and dependence in bacteria predicted by comparative genomics. *ISME J* **13**, 789-804 (2019). https://doi.org/10.1038/s41396-018-0304-9

22 Osman, D. *et al.* The requirement for cobalt in vitamin B. *Biochim Biophys Acta Mol Cell Res* **1868**, 118896 (2021). https://doi.org/10.1016/j.bbamcr.2020.118896

23 Sokolovskaya, O. M., Shelton, A. N. & Taga, M. E. Sharing vitamins: Cobamides unveil microbial interactions. (2020). https://doi.org/10.1126/science.aba0165

24 Dulay, H., Tabares, M., Kashefi, K. & Reguera, G. Cobalt resistance via detoxification and mineralization in the iron-reducing bacterium *Geobacter sulfurreducens*. *Front Microbiol* **11**, 600463 (2020). https://doi.org/10.3389/fmicb.2020.600463

25 Yan, J., Ritalahti, K. M., Wagner, D. D. & Löffler, F. E. Unexpected specificity of interspecies cobamide transfer from *Geobacter* spp. to organohalide-respiring *Dehalococcoides mccartyi* strains. *Appl Environ Microbiol* **78**, 6630-6636 (2012). https://doi.org/10.1128/aem.01535-12

26 Cologgi, D. L., Lampa-Pastirk, S., Speers, A. M., Kelly, S. D. & Reguera, G. Extracellular reduction of uranium via Geobacter conductive pili as a protective cellular mechanism. *Proc. Natl. Acad. Sci. U S A* **108**, 15248-15252 (2011). https://doi.org/10.1073/pnas.1108616108

27 Courtoy, R., Boniver, J. & Simar, L. Cobalt thiocyanate as a stain for basic proteins and other organic bases on thin sections. *Histochemistry* **55**, 107-115 (1978). https://doi.org/10.1007/BF00493513

28 Mohite, B. V., Koli, S. H. & Patil, S. V. Heavy metal stress and its consequences on exopolysaccharide (EPS)-producing Pantoea agglomerans. *Appl Biochem Biotechnol* **186** (2018). https://doi.org/10.1007/s12010-018-2727-1

29 Konovalova, A. & Silhavy, T. J. Outer membrane lipoprotein biogenesis: Lol is not the end. *Philos Trans R Soc Lond B Biol Sci* **370** (2015). https://doi.org/10.1098/rstb.2015.0030

30 Clark, M. M., Paxhia, M. D., Young, J. M., Manzella, M. P. & Reguera, G. Adaptive synthesis of a rough lipopolysaccharide in *Geobacter sulfurreducens* for metal reduction and detoxification. *Appl Environ Microbiol* **87**, e0096421 (2021). https://doi.org/10.1128/AEM.00964-21

31 Shelobolina, E. S. *et al.* Importance of c-Type cytochromes for U(VI) reduction by Geobacter sulfurreducens. *BMC Microbiol* **7** (2007). https://doi.org/10.1186/1471-2180-7-16

32 Julsing, M. K., Kuhn, D., Schmid, A. & Bühler, B. Resting cells of recombinant E. coli show high epoxidation yields on energy source and high sensitivity to product inhibition. *Biotechnol Bioeng* **109** (2012). https://doi.org/10.1002/bit.24404

33 Kilmury, S. L. N., Graham, K. J., Lamers, R. P., MacNeil, L. T. & Burrows, L. L. Hyperpiliation reduces Pseudomonas aeruginosa pathogenicity by impeding type III secretion. *bioRxiv* (2021). https://doi.org/10.1101/2021.01.28.428742

34 Rollefson, J. B., Stephen, C. S., Tien, M. & Bond, D. R. Identification of an extracellular polysaccharide network essential for cytochrome anchoring and biofilm formation in *Geobacter sulfurreducens*. *J Bacteriol* **193**, 1023-1033 (2011). https://doi.org/10.1128/JB.01092-10

35 Harrison, J. J., Ceri, H. & Turner, R. J. Multimetal resistance and tolerance in microbial biofilms. *Nat Rev Microbiol* **5**, 928-938 (2007). https://doi.org/doi:10.1038/nrmicro1774

36 Mah, T. F. & O'Toole, G. A. Mechanisms of biofilm resistance to antimicrobial agents. *Trends Microbiol* **9** (2001). https://doi.org/10.1016/s0966-842x(00)01913-2

37 Hall-Stoodley, L., Costerton, J. & Stoodley, P. Bacterial biofilms: from the natural environment to infectious diseases. *Nat Rev Microbiol* **2** (2004). https://doi.org/10.1038/nrmicro821

38 Salgado, R. M. *et al.* The latest trends in electric vehicles batteries. *Molecules* **26** (2021). https://doi.org/10.3390/molecules26113188

39 Arjunan, A. *et al.* 3D printed cobalt-chromium-molybdenum porous superalloy with superior antiviral activity. *Int J Mol Sci* **22** (2021). https://doi.org/10.3390/ijms222312721

40 Schwarz, U. *et al.* CoBi3: a binary cobalt-bismuth compound and superconductor. *Angew Chem Int Ed Engl* **52** (2013). https://doi.org/10.1002/anie.201302397

41 Qiao, D., Dai, T., Ma, Y. & Gao, T. Insights into the evolution of cobalt use and implications through dynamic analysis of cobalt flows and stocks and the recycling potential of cobalt from urban mines in China during 2000-2021. *Waste Manag* **163** (2023). https://doi.org/10.1016/j.wasman.2023.03.016

42 Courchesne, B., Schindler, M. & Mykytczuk, N. C. S. Relationships Between the Microbial Composition and the Geochemistry and Mineralogy of the Cobalt-Bearing Legacy Mine Tailings in Northeastern Ontario. *Front Microbiol* **12**, 660190 (2021). https://doi.org/10.3389/fmicb.2021.660190

43 Zhang, K., Zhang, D., Li, X. & Xue, Y. Biomineralization of lead in wastewater: Bacterial reutilization and metal recovery. *J Hazard Mater* **421** (2022). https://doi.org/10.1016/j.jhazmat.2021.126765

44 Gadd, G. M. Metals, minerals and microbes: geomicrobiology and bioremediation. *Microbiology (Reading)* **156**, 609-643 (2010). https://doi.org/10.1099/mic.0.037143-0

45 Dhiman, S. & Gupta, B. Partition studies on cobalt and recycling of valuable metals from waste Li-ion batteries via solvent extraction and chemical precipitation. *J Clean Prod* **225**, 820-832 (2019). https://doi.org/10.1016/j.jclepro.2019.04.004

46 Cosert, K. M., Castro-Forero, A., Steidl, R. J., Worden, R. M. & Reguera, G. Bottom-up fabrication of protein nanowires via controlled self-assembly of recombinant. *mBio* **10** (2019). https://doi.org/10.1128/mBio.02721-19

47 Caccavo, F. *et al.* Geobacter sulfurreducens sp. nov., a hydrogen- and acetate-oxidizing dissimilatory metal-reducing microorganism. *Appl Environ Microbiol* **60** (1994). https://doi.org/10.1128/aem.60.10.3752-3759.1994

48 Speers, A. M. & Reguera, G. Electron donors supporting growth and electroactivity of Geobacter sulfurreducens anode biofilms. *Appl Environ Microbiol* **78**, 437-444 (2012). https://doi.org/10.1128/AEM.06782-11

Chapter 5: Conclusions and Future Directions

The objective of this dissertation was to investigate the mechanisms by which *G. sulfurreducens* tolerates Co^{II} stress to better characterize its role in the biogeochemical cycling of Co. The findings presented provide insight into the many mechanisms used for Co detoxification and the role of reductive pathways in metal tolerance.

In Chapter 2, I described a collaborative effort with lab member Marcela Tabares that revealed a high Co^{II} tolerance by *G. sulfurreducens* cells, comparable to what is typically seen in metal-resistant organisms isolated from highly contaminated sites. The cells underwent an extended lag phase to acclimate to metal stress. During this period, the cells induced multiple pathways to fight Co^{II} intoxication such as efflux pumps for metal extrusion, enzymes for protein repair, and surface chemistry modifications that could mitigate Co^{II} diffusion and promote cell-cell interactions leading to agglutination and biofilm formation. We also saw the downregulation of many genes encoding proteins that Co^{II} could readily infiltrate and inactivate. The upregulation of genes encoding a cytochrome complex (CbcBA) for the reduction of electron acceptors with reduction potentials as low as the Co^{II}/Co^{0} couple is a response only described in *Geobacter*, as of the publication of this thesis. I developed an assay to measure Co^{II} removal by the cells (~25 µM) and used Transmission Electron Microscopy coupled with Energy Dispersive X-ray Spectroscopy (TEM-EDS) to demonstrate the extracellular precipitation of Co on discreet foci over the cell. Additional work to characterize the nanoparticles could be carried out. Techniques such as laser ablation with inductively coupled plasma and mass spectrometry (LA-ICP-MS) could characterize the chemical makeup of the nanoparticles. Furthermore, methods to measure the oxidation state, such as X-ray absorbance spectroscopy (XAS), should be applied to verify the reductive precipitation of Co^{II} as Co^{0}

and quantify the amount of metal reduced as opposed to the amount removed from the medium.

In Chapter 3, I further characterized the role of CbcBA in Co^{II} tolerance using a mutant strain that carried a deletion of the *cbcBA* genes and its genetically complemented strain. The CbcBA deficiency exacerbated some of the phenotypes associated with Co^{II} intoxication. For example, the mutant cells agglutinated more than the wild type (WT) and genetically complemented strains when challenged with non-lethal concentrations of the metal during exponential growth. Yet, when the cells were allowed time to acclimate to the metal before initiating growth, they activated alternative pathways for detoxification and restart growth and cell division at WT rates. Additionally, resting cells of the Δ*cbcBA* mutant removed more Co^{II} from solution and faster, becoming more intoxicated than the WT cells and delaying the recovery of the metal-stressed cells once transferred to metal-free medium. The hypervesiculation of the mutant cells suggested membrane permeability changes that facilitate Co^{II} penetration into the cell envelope and exacerbated intoxication. Membrane permeability assays using dyes that typically cannot permeate the membrane, such as ethidium bromide, may prove useful for testing this proposal. These simple staining procedures use fluorescent stains that can move freely into the membrane, such as fluorescein diacetate, which can be coupled with flow cytometry to identify distinct populations of permeable cells. Notably, the CbcBA deficiency increased vesiculation even in the absence of metal stress, suggesting pleiotropic effects of the mutation on membrane stability. Given the pleiotropic effects of cytochrome mutations in *G. sulfurreducens*, it will be important to rule out compensatory expression of other cytochromes in the Δ*cbcBA* background by using a heme stain. Also

important is performing resting cell suspensions using cells previously grown on a medium that enhances their resistance to osmotic changes during the growth-resting state transitions. In Appendix 1 I describe how subtle changes in the salt content of the growth medium impact the viability of the cells in the resting state and the suitability of the NBAF medium formulation to prepare resting cells for Co^{II} challenge assays for up to 12 h.

In Chapter 4, another collaborative effort with Marcela Tabares, I demonstrated the growth advantage of piliated cells under Co^{II} stress. These experiments used a temperature shift (from 30°C to 25°C) to induce piliation and also compared the Co^{II} tolerance of a non-piliated WT strain to mutants unable to polymerize (Δ*pilB*) or depolymerize (Δ*pilT3/4*) pili. TEM images confirmed the monolateral mineralization of Co in the Δ*pilT3/4* mutant, which is hyperpiliated, and the discreet deposition of the mineral particles on the outer surface in the pili-deficient mutant Δ*pilB*. Spectroscopic analyses of the Co minerals similar to those mentioned above are needed to evaluate the composition of the suspected Co^0 nanoparticles.

Future studies should also strive to further elucidate how the cells regulate the expression of these two reductive pathways (cytochrome and pili) and the adaptive roles that the reductive mineralization of Co^{II} plays in the environment. The role of the cytochrome-loaded Xap exopolysaccharide (EPS) in Co^{II} detoxification also needs to be considered as a contributor to the mineralization reaction. The role of pili dynamics (antagonistic cycles of pilus protrusion and retraction) may also be important for Co^{II} mineralization. However, tools for the study of pilus retraction are limited to retraction-deficient mutants, which are also hyperpiliated. Nevertheless, it is possible to replace

tyrosines of the pilin (Tyr3 mutant) to reduce charge transport along the pili and produce piliated mutant strains unable to reduce metals via this pathway. Ultimately, experiments with mixed Co-Fe oxides will better characterize the role of *Geobacter* as keystone organisms in cobamide dependent ecosystems. Connecting the biomining of Co from these metal oxides to the secretion of cobamides will set the stage for future applications of *Geobacter* as biofertilizers and as drivers of green technologies for the reclamation of Co from spent Co products.

APPENDIX: EFFECT OF GROWTH MEDIA FORMULATIONS ON THE VIABILITY AND CO^{II}-DETOXIFICATION CAPACITY OF RESTING CELLS OF *GEOBACTER SULFURREDUCENS*

ABSTRACT

The many toxic effects of Co^{II} trigger complex cellular responses to overcome intoxication, which may include the activation of repair mechanisms, extrusion pumps, and respiratory chains for reductive mineralization of the metal. Resting cell assays optimized for *Geobacter sulfurreducens* provide great tools to dissect the contributions of respiratory chains to other detoxification pathways. Here I present evidence that subtle changes in the salt content of the growth medium used to harvest cells for resting cell assays can greatly impact the ability of the cells to remain metabolically active while in the resting state. These findings emphasize the need to select growth media formulations with the osmotic balance needed to maintain the viability of the cells under non-growth conditions.

INTRODUCTION

Microbial metal respiration has been a central focus in the study of biogeochemistry, bioremediation, and biotechnology [1-4]. Among metal respiring organisms, *Geobacter* bacteria have been investigated thoroughly for their ability to reduce a broad spectrum of metals such as Fe^{III} and Mn^{IV} oxides [5-8], the uranyl cation (UO_2^{II}) [9-11], and $CuSO_4$ [12] among many others [13]. Techniques have been applied to study metals that support the growth of *Geobacter* bacteria in laboratory cultures with environmentally relevant electron acceptors. For example, the ferrozine assay is used to measure the release of Fe^{II} during the reductive dissolution of Fe^{III} oxides [14]. *Geobacter* bacteria can also use toxic metals and radionuclides as electron acceptors for growth [13]. Energy yields from these reactions

are lower than expected thermodynamically [15], because some of the energy gained from the reduction of the electron acceptors must be diverted towards detoxification [9]. For example, growth of the model representative *Geobacter sulfurreducens* with Co^{II} induces a host of cell responses (repair, extrusion, surface chemistry modifications) that lead to removal of the metal from solution in a non-reductive manner [16]. The poor energy yields predicted for the reduction of Co^{II} to Co^{0} limit cell growth [16] but, nevertheless, provide a pathway for detoxification. Consistent with a reductive mechanism for detoxification, *G. sulfurreducens* cells precipitated Co as nanoparticles on their outer surface and upregulated cytochrome genes involved in extracellular electron transfer to low-potential electron acceptors [16].

The contribution of respiratory chains to the reductive detoxification of Co^{II} is often masked by other pathways used to overcome metal intoxication (chapter 3). Resting cell (RC) assays can help dissect this complex detoxification response. The resuspension of cells in buffers devoid of nutrients allows for the study of enzymatic reactions without the confounding effects of growth and cell division. Depending on the reaction formulation, cells can be maintained in a resting (non-growing) state for various periods of time, as needed to measure specific enzymatic reactions. The concentration of cells in the suspension can also be modified to increase reaction rates and measure reactions that would otherwise be difficult to measure in growing cultures. RC assays have been broadly applied in microbiology [17-19] and are particularly useful to study metal respiration [9,11,20]. By limiting the production of new biomass, RC assays can allow for accurate measurements of metal respiration rates and assess the contribution of individual electron carriers to the measured reaction. Optimal conditions for the reduction of the uranyl cation

(U^{VI} to U^{IV}) by *G. sulfurreducens* resting cells highlighted the need to minimize osmotic stress to cells prepared for the RC assay [9,11]. A stepwise adaptation of fumarate-grown cells to lower osmolarity than in the growth medium is essential for sustained cell viability in the resting state [11]. In the optimized protocol, the cells are first harvested and resuspended in a wash buffer with half the salt (NaCl) content as in the growth medium before being transferred to a reaction buffer containing one-quarter of the growth medium salt content [11]. In chapter 3 and 4, I described the use of the RC assays to investigate the contribution of the CbcBA cytochromes and electrically conductive pili to Co^{II} detoxification. The buffer formulations used for these assays are those optimized for the uranium assays [11].

Similar formulations to the FW medium such as NB (a nutrient broth used for genetic engineering studies [21] and DB (mineral medium used for electrode-reduction studies [22]) are widely used for growth studies with metals. Indeed, we used the DB medium with acetate and fumarate (DBAF) to investigate the detoxification response of *G. sulfurreducens* to Co^{II} (chapter 2). The NB and DB media differ slightly in the type and concentration of some Na^+ and K^+ salts and this, in turn, affects membrane fluidity and vesiculation in *G. sulfurreducens* (Morgen Clark, personal communication). Hence, in this Appendix, I investigated the impact of NB and DB growth media on the ability of resting cells to remain viable and metabolically active in the presence or absence of Co^{II}. For these experiments, I grew *G. sulfurreducens* in either medium with acetate and fumarate (NBAF and DBAF, respectively) and harvested the cells for the RC assay. The results suggest that minor differences in the salt content of the media formulations can greatly impact the ability of *G. sulfurreducens* to overcome the osmotic and metal stress.

RESULTS

Reduced ability of DBAF-grown cells to overcome osmotic and metal stress

The DBAF medium is a mineral medium with acetate and fumarate that was optimized for growth of *G. sulfurreducens* cells used to inoculate microbial fuel cells and build electricity-producing biofilms on anode electrodes [22,23]. This medium was also used to study the tolerance and detoxication response of *G. sulfurreducens* to Co^{II} [16]. For this reason, I harvested cells from mid-exponential phase DBAF cultures and prepared them for a RC assay in the presence or absence of 250 µM $CoCl_2$. Addition of acetate (electron donor) to the cell suspension initiated the reaction (time 0). All of the samples, including untreated controls, required a variable amount of time (lag phase) to resume growth once transferred from the resting cell suspension into the metal-free growth medium (Fig. A.1), a sign of viability loss [9]. Notably, the untreated resting cells taken at the start of the RC assay (0 h) had a delayed restart of growth and, for at least one replicate, only resumed growth after an extended lag phase (Fig. A.1A). This is indicative of an inability of the DBAF-grown cells to overcome osmotic shifts during the preparation of the resting cells. Growth delays were even more pronounced for the untreated cells after 6 h in the resting state (Fig. A.1B) and for all the samples taken from the Co^{II}-treated resting cell reactions (Fig. A.1A-B).

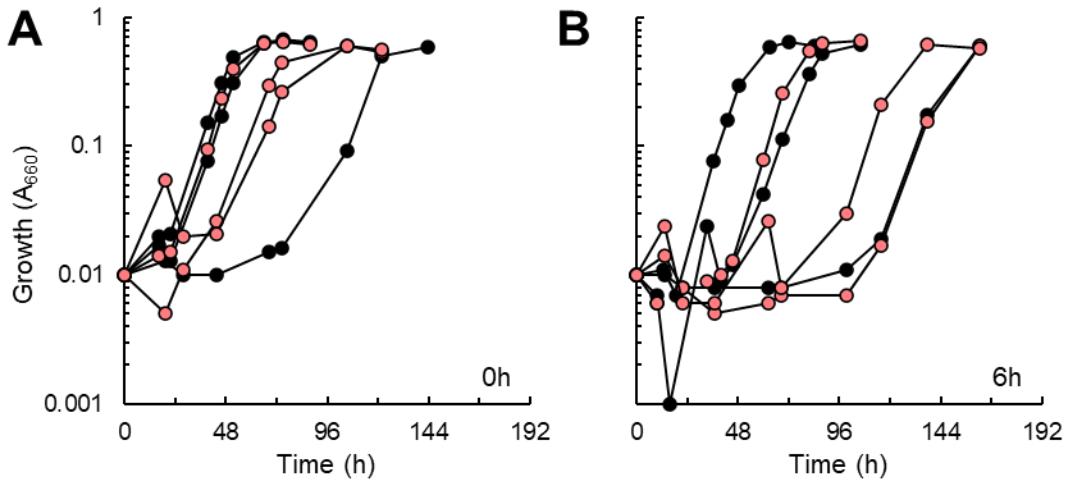

Figure A.1 Growth recovery of DBAF-grown resting cells from Co^{II} stress. Cells were grown and transferred in mid-exponential phase three times in DBAF medium before harvesting mid-exponential cells for the RC assays. Resting cells were challenged with 250 µM $CoCl_2$ for 6 h (pink symbols) or left untreated (black symbols) and recovered in triplicate cultures with metal-free DBAF medium at the beginning **(A)** or end **(B)** of the RC assay (0 and 6 h, respectively).

Enhanced ability of NBAF-grown cells to overcome osmotic and metal stress

NBAF medium is routinely used to recover cells from stressed states, such as during the recovery of cells from frozen stocks and mutants after electroporation [21]. Cells from NBAF cultures also have lower levels of vesiculation (Morgen Clark, personal communication), a phenotype associated with reduced membrane fluidity and permeability [24]. Hence, I harvested mid-exponential cells from NBAF cultures and prepared them for the RC assay, following the same protocol used for DBAF-grown cells. As shown in Fig. A.2A, the resting cell samples resumed growth rapidly independently of the resting cell treatment (with or without Co^{II}) and time in the resting state (0-12 h). The rapid growth restart of the resting cells shows that they remained viable throughout the duration of the assay, in this case for up to 12 h. This timeframe contrasts with the conventional RC assays using FWAF-grown cells, which maintain the viability of the cells in the resting state for approximately

6 h [11]. The DBAF formulation was even worse, reducing the ability of even untreated cells to overcome the osmolarity shifts needed for the preparation of the resting cells.

I also tested the ability of the cells to remain viable in the resting state at $CoCl_2$ concentrations (500 µM) that can be lethal to growing cells [16]. Increasing metal stress on the resting cells did not affect their ability to restart growth once transferred to the growth medium (Fig. A.1B). Hence, not only does the NBAF formulation maintain the viability of resting cells for prolonged periods of time (9-12 h), but it minimizes cell intoxication by Co^{II}. The lower membrane permeability predicted for NBAF-grown cells is expected to reduce metal penetration, providing an effective mechanism to overcome metal stress. These same properties maintain the integrity of the outer membrane through osmotic shifts and during prolonged periods of time in the resting state.

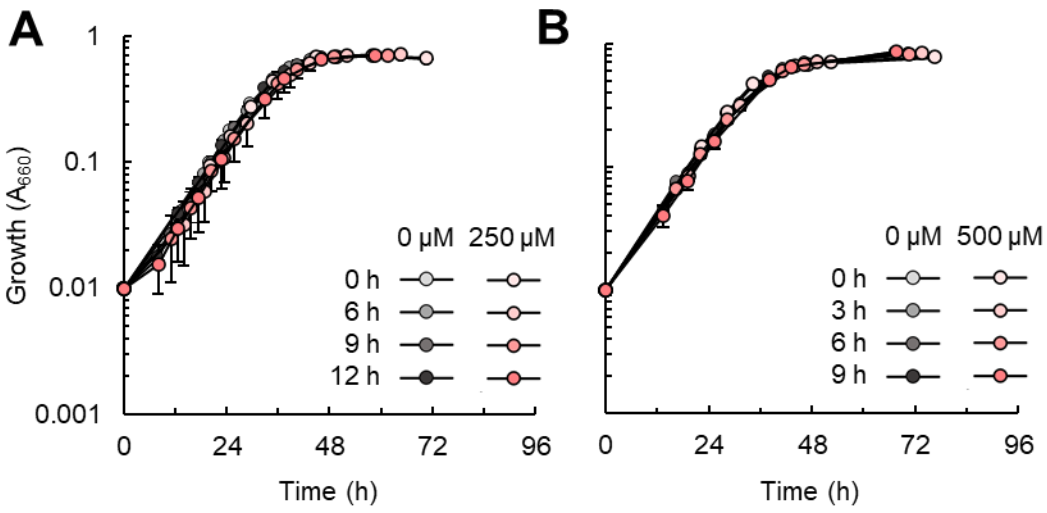

Figure A.2 Growth recovery of NBAF-grown resting cells from Co^{II} stress. Cells were grown and transferred in mid-exponential phase three times in NBAF medium before harvesting mid-exponential cells for the RC assays. Resting cells were challenged with 250 µM **(A)** or 500 µM **(B)** $CoCl_2$ for up to 12 h before being transferred to NBAF medium and incubated at 30ºC to reinitiate growth (A_{660}). Untreated controls (0 µM $CoCl_2$) were also included. Shown are the average of duplicate (untreated) and triplicate (Co^{II}-treated) cultures. Error bars are the standard deviation between replicates.

Comparison of NBAF and DBAF: a matter of salt?

The apparent differences in the ability of NBAF- or DBAF-grown cells to remain viable and metabolically active during and after time in the resting state is surprising. The two media types tested are similar in their composition and there is no clear deviation in the key elements provided [22]. And yet, DBAF-grown cells maintained in the resting state for 6 h needed a much longer lag phase to restart growth than NBAF-grown cells, a sign of media-induced stress (Fig. A.3A). Indeed, the NBAF-grown cells recovered from a 6-h resting state after 17.5 ± 0.1 h. By contrast, DBAF-grown cells maintained for 6 h in the resting state took 75 ± 47 h to restart growth. The presence of Co^{II} did not significantly impact the recovery of the NBAF-grown (20.0 ± 2.5 h lag phase, p = 0.4 vs untreated NBAF cells) or DBAF-grown cells (98 ± 37 h lag phase, p = 0.5 vs untreated DBAF cells) (Fig. A.3A). This suggests that the DBAF cells are more sensitive to osmotic shifts than metal stress.

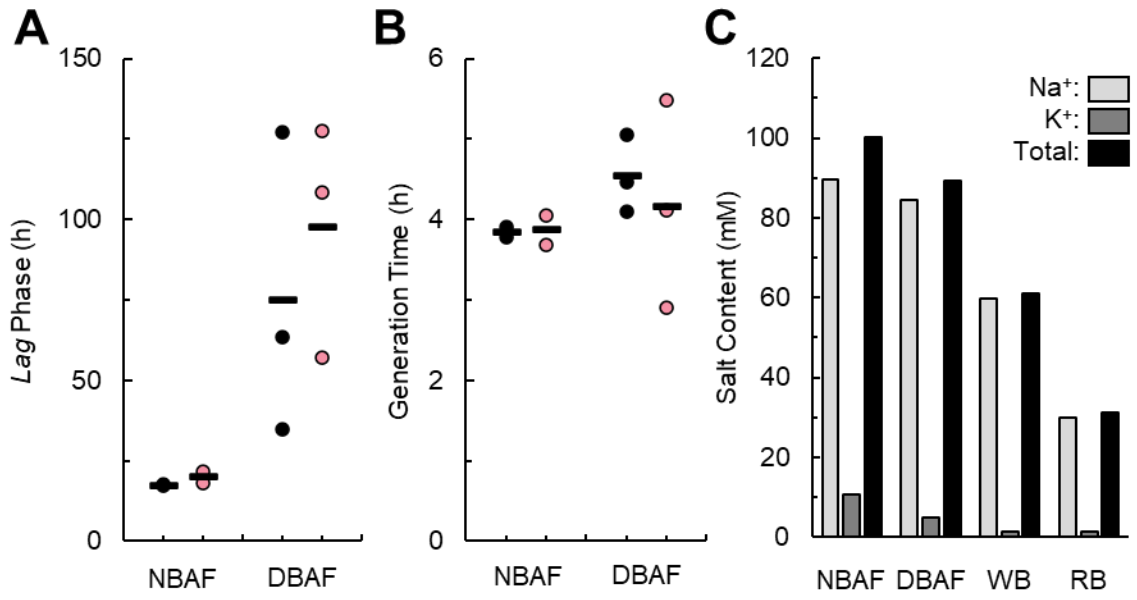

Figure A.3 Comparison of NBAF and DBAF effects on resting cell recovery . (A-B) Growth phenotypes of cells recovered after 6 h in the RC assay treated with 250 µM $CoCl_2$ (pink) or untreated controls (black). The lag phase (**A**) and generation times (**B**) of cells prepared with NBAF or DBAF media are presented as individual replicates (circles) and averages (lines). **(C)** Differences in salt content between the two media as well as the wash (WB) and reaction buffer (RB) used int the RC assay.

Despite the long periods needed for DBAF cells to recover from the resting state, the cells achieved generation times (4.5 ± 0.5 h for untreated cells and 4.2 ± 1.3 h for treated cells, $p = 0.7$) similar to the NBAF cultures (3.8 ± 0.1 h for untreated cells and 3.9 ± 0.3 h for treated cells, $p = 0.9$) (Fig. A.3B). However, these generation times were more variable in the DBAF than in the NBAF cultures (Fig. A.3B), possibly reflecting the activation of different pathways to overcome osmotic stress in each replicate DBAF culture.

The dramatic effect that seemingly similar media formulations have on the viability of cells prepared for the RC assays points to salt differences as the major determinant of whether *G. sulfurreducens* overcomes the stress associated with osmotic shifts. Indeed,

there is a 10.8 mM difference in the Na^+ and K^+ ion content between NBAF (100.2 mM) and DBAF (89.4 mM) (Fig. A.3C). These ions can have broad effects on cell physiology such as alteration of the ionic motive force within the membrane [25,26]. They can also affect membrane fluidity and vesiculation in *G. sulfurreducens* (Morgen Clark, personal communication). These data therefore highlight the importance that growth media formulations have in producing cells suitable for RC assays and the impact that seemingly minor differences in salt content have on cell viability and/or metabolic activity.

DISCUSSION

Suspension in a resting state is a stressful experience for cells and can drastically affect viability [11]. While a lack of nutrients and the washing process can inhibit recovery, the osmolarity of the buffers used is pivotal to survival [11]. Our data show that osmolarity of the medium used to grow the cells for the RC assays also matters. As a result, cells previously grown on NBAF or DBAF media have different sensitivities to the osmotic shifts optimized to prepare resting cells of *G. sulfurreducens* (Fig. A.3). Co^{II} challenge to the resting cells also impacts recovery from the resting state, albeit not as significantly as the osmotic transitions required for the preparation of resting cells. Thus, while NBAF-grown cells readily transitioned between the growth and resting states, DBAF-grown cells experienced significant losses of viability during the transition. This, in turn, reduced the concentration of resting cells that were able to resume growth and produced extended lag phases even in cells that had not experienced metal stress (Fig. A.3). The key difference between these two media formulations seems to be a 10.8 mM higher Na^+/K^+ salt content in the NBAF media compared to DBAF. This difference, though seemingly insignificant, can translate into osmotic pressure differences that may alter the membrane

stability of *G. sulfurreducens* [27]. In support of this, cells grown in the medium with lower salt concentration (DBAF) have a nearly 2-fold increase in OMV production compared to NBAF (Morgen Clark, personal communication). Furthermore, amending the DBAF medium with Na^+ and/or K^+ salts to match the Na^+/K^+ content of NBAF ameliorates OMV levels (Morgen Clark, personal communication). The biogenesis and functions of bacterial OMVs are not fully understood [24] and are just beginning to be explored in *G. sulfurreducens* [28]. It is however well-accepted that some cations can bind and neutralize the negative charge of the LPS that coat the outer membrane of Gram-negative bacteria, relieving the electromagnetic repulsion between the LPS molecules and stabilizing the membrane [29,30]. Hence, the higher salt content in NBAF may stabilize the LPS and provide permeability control and osmoprotection. This is also expected to mitigate Co^{II} permeation and the toxic effects derived from the accumulation of the metal in the periplasm [16].

MATERIALS AND METHODS

Bacterial strains and culture conditions

Cultures of *G. sulfurreducens* strain PCA were obtained from our laboratory culture collection and grown anaerobically in either DB or NB minimal medium as previously described [22]. Media were supplemented with 20 mM of acetate as the electron donor and 40 mM of fumarate as the electron acceptor. Growth was monitored spectrophotometrically as the absorbance at 600 nm (A_{600}) and cultures were routinely grown to late exponential phase (A_{600}, 0.5-0.6) prior to transfer to fresh medium.

Co^{II} resting cell assays

Resting cell assays were performed as previously described [9] with some modifications. Unless otherwise indicated, all procedures were performed inside an anaerobic chamber

(COY Labs). Cultures of *G. sulfurreducens* were grown in either DB or NB media at 30^{o}C to mid-exponential phase (A_{600} ~0.4) and dispensed into 50-ml conical tubes. Samples were then pelleted by centrifugation to remove growth media (10 min, 3,000 *g*), resuspended in WB using a Pasteur pipette, pelleted a second time, and resuspended in WB [11,31]. 10 mL of washed cells were then diluted into 30 ml of RB to an A_{600} of 0.1 before adding 20 mM acetate as an electron donor and treated with 250 or 500 µM of $CoCl_2$ as indicated. RC suspensions were incubated at 30^{o}C and 1-ml samples were taken to inoculate 9 ml of untreated media to monitor growth (A_{660}) recovery at 30^{o}C [31].

REFERENCES

1 Camprubi, E., Jordan, S. F., Vasiliadou, R. & Lane, N. Iron catalysis at the origin of life. *IUBMB Life* **69**, 373-381 (2017). https://doi.org/10.1002/iub.1632

2 Cosert, K. M. & Reguera, G. Voltammetric study of conductive planar assemblies of Geobacter nanowire pilins unmasks their ability to bind and mineralize divalent cobalt. *J Ind Microbiol Biotechnol* **46**, 1239-1249 (2019). https://doi.org/10.1007/s10295-019-02167-5

3 Bopp, C. J. *et al.* Uranium 238U/235U isotope ratios as indicators of reduction: results from an in situ biostimulation experiment at Rifle, Colorado, U.S.A. *Environmental science & technology* **44** (2010). https://doi.org/10.1021/es100643v

4 Lovley, D. R. Electrotrophy: Other microbial species, iron, and electrodes as electron donors for microbial respirations. *Bioresource technology* **345** (2022). https://doi.org/10.1016/j.biortech.2021.126553

5 Reguera, G. & Kashefi, K. The electrifying physiology of Geobacter bacteria, 30 years on. *Adv Microb Physiol* **74**, 1-96 (2019). https://doi.org/10.1016/bs.ampbs.2019.02.007

6 Reguera, G. *et al.* Extracellular electron transfer via microbial nanowires. *Nature* **435**, 1098-1101 (2005). https://doi.org/10.1038/nature03661

7 Aklujkar, M. *et al.* Proteins involved in electron transfer to Fe(III) and Mn(IV) oxides by *Geobacter sulfurreducens* and *Geobacter uraniireducens*. *Microbiology* **159**, 515-535 (2013). https://doi.org/10.1099/mic.0.064089-0

8 Lovley, D. R., Holmes, D. E. & Nevin, K. P. Dissimilatory Fe(III) and Mn(IV) reduction. *Adv Microb Physiol* **49**, 219-286 (2004). https://doi.org/10.1016/S0065-2911(04)49005-5

9 Cologgi, D. L., Lampa-Pastirk, S., Speers, A. M., Kelly, S. D. & Reguera, G. Extracellular reduction of uranium via *Geobacter* conductive pili as a protective cellular mechanism. *Proc. Natl. Acad. Sci. USA* **108**, 15248-15252 (2011). https://doi.org/10.1073/pnas.1108616108

10 Cologgi, D. L., Speers, A. M., Bullard, B. A., Kelly, S. D. & Reguera, G. Enhanced uranium immobilization and reduction by *Geobacter sulfurreducens* biofilms. *Appl Environ Microbiol* **80**, 6638-6646 (2014). https://doi.org/10.1128/AEM.02289-14

11 Shelobolina, E. S. *et al.* Importance of c-Type cytochromes for U(VI) reduction by *Geobacter sulfurreducens*. *BMC Microbiol* **7** (2007). https://doi.org/10.1186/1471-2180-7-16

12 Kimber, R. L. *et al.* Biomineralization of Cu_2S nanoparticles by *Geobacter sulfurreducens*. *Appl Environ Microbiol*, AEM.00967-00920 (2020). https://doi.org/10.1128/aem.00967-20

13 Reguera, G. & Kashefi, K. The electrifying physiology of *Geobacter* bacteria, 30 years on. *Adv. Microb. Physiol.* **74**, 1-96 (2019). https://doi.org/10.1016/bs.ampbs.2019.02.007

14 Sørensen, J. Reduction of ferric iron in anaerobic, marine sediment and interaction with reduction of nitrate and sulfate. *Applied and environmental microbiology* **43** (1982). https://doi.org/10.1128/aem.43.2.319-324.1982

15 Sanford, R. A. *et al.* Hexavalent uranium supports growth of Anaeromyxobacter dehalogenans and Geobacter spp. with lower than predicted biomass yields. *Environ Microbiol* **9**, 2885-2893 (2007). https://doi.org/10.1111/j.1462-2920.2007.01405.x

16 Dulay, H., Tabares, M., Kashefi, K. & Reguera, G. Cobalt Resistance via Detoxification and Mineralization in the Iron-Reducing Bacterium. *Front Microbiol* **11**, 600463 (2020). https://doi.org/10.3389/fmicb.2020.600463

17 Julsing, M. K., Kuhn, D., Schmid, A. & Bühler, B. Resting cells of recombinant *E. coli* show high epoxidation yields on energy source and high sensitivity to product inhibition. *Biotechnol Bioeng* **109** (2012). https://doi.org/10.1002/bit.24404

18 Krishnan, S., Narayan, S. & Chadha, A. Whole resting cells vs. cell free extracts of Candida parapsilosis ATCC 7330 for the synthesis of gold nanoparticles. *AMB Express* **6**, 1-15 (2016). https://doi.org/doi:10.1186/s13568-016-0268-y

19 Li, L., Freier, T. A., Hartman, P. A., Young, J. W. & Beitz, D. C. A resting-cell assay for cholesterol reductase activity inEubacterium coprostanoligenes ATCC 51222. *Applied Microbiology and Biotechnology* **43**, 887-892 (1995). https://doi.org/doi:10.1007/BF02431924

20 Lloyd, J. R. *et al.* Reduction of actinides and fission products by Fe(III)-reducing bacteria. *Geomicrobiology Journal* **19**, 103-120 (2002).

21 Coppi, M. V., Leang, C., Sandler, S. J. & Lovley, D. R. Development of a genetic system for Geobacter sulfurreducens. *Appl Environ Microbiol* **67**, 3180-3187 (2001). https://doi.org/10.1128/AEM.67.7.3180-3187.2001

22 Speers, A. M. & Reguera, G. Electron donors supporting growth and electroactivity of *Geobacter sulfurreducens* anode biofilms. *Appl Environ Microbiol* **78**, 437-444 (2012). https://doi.org/10.1128/aem.06782-11

23 Srikanth, S., Marsili, E., Flickinger, M. C. & Bond, D. R. Electrochemical characterization of Geobacter sulfurreducens cells immobilized on graphite paper

electrodes. *Biotechnology and bioengineering* **99** (2008). https://doi.org/10.1002/bit.21671

24 Avila-Calderón, E. D. *et al.* Outer Membrane Vesicles of Gram-Negative Bacteria: An Outlook on Biogenesis. *Front Microbiol* **12**, 557902 (2021). https://doi.org/10.3389/fmicb.2021.557902

25 Benarroch, J. M. & Asally, M. The Microbiologist's Guide to Membrane Potential Dynamics. *Trends Microbiol* **28**, 304-314 (2020). https://doi.org/10.1016/j.tim.2019.12.008

26 Mulkidjanian, A. Y., Dibrov, P. & Galperin, M. Y. The past and present of sodium energetics: may the sodium-motive force be with you. *Biochim Biophys Acta* **1777**, 985-992 (2008). https://doi.org/10.1016/j.bbabio.2008.04.028

27 Ragoonanan, V., Malsam, J., Bond, D. R. & Aksan, A. Roles of membrane structure and phase transition on the hyperosmotic stress survival of *Geobacter sulfurreducens*. *Biochimica et biophysica acta* **1778** (2008). https://doi.org/10.1016/j.bbamem.2008.06.006

28 Clark, M. M., Paxhia, M. D., Young, J. M., Manzella, M. P. & Reguera, G. Adaptive synthesis of a rough lipopolysaccharide in *Geobacter sulfurreducens* for metal reduction and detoxification. *Appl Environ Microbiol* **87**, e0096421 (2021). https://doi.org/10.1128/AEM.00964-21

29 Sabra, W., Lünsdorf, H. & Zeng, A. P. Alterations in the formation of lipopolysaccharide and membrane vesicles on the surface of *Pseudomonas aeruginosa* PAO1 under oxygen stress conditions. *Microbiology (Reading, England)* **149** (2003). https://doi.org/10.1099/mic.0.26443-0

30 Kadurugamuwa, J. L. & Beveridge, T. J. Virulence factors are released from *Pseudomonas aeruginosa* in association with membrane vesicles during normal growth and exposure to gentamicin: a novel mechanism of enzyme secretion. *Journal of bacteriology* **177** (1995). https://doi.org/10.1128/jb.177.14.3998-4008.1995

31 Cologgi, D. L., Lampa-Pastirk, S., Speers, A. M., Kelly, S. D. & Reguera, G. Extracellular reduction of uranium via Geobacter conductive pili as a protective cellular mechanism. *Proc Natl Acad Sci U S A* **108**, 15248-15252 (2011). https://doi.org/10.1073/pnas.1108616108